Controlled axonal outgrowth and cell reactions to nanostructures

Johansson, Fredrik

2008

Controlled axonal outgrowth and cell reactions to nanostructures

av

Fredrik Johansson

AKADEMISK AVHANDLING
som för avläggande av filosofie doktorsexamen vid
naturvetenskapliga fakulteten, Lunds universitet
kommer att offentligen försvaras i zoofysiologihusets hörsal.

Torsdagen den 23 oktober 2008, kl. 09.00

Fakultetens opponent är Prof. Patric A. Tresco
Department of Bioengineering at the University of Utah,
Salt Lake City, USA

DOKUMENTDATABLAD enl SIS 61 41 21

Organization	Document name
LUND UNIVERSITY Department od Cell and Organism Biology Helgonavägen 3B SE-223 62 Lund Sweden	DOCTORAL DISSERTATION
	Date of issue Oktober, 23th, 2008
	Sponsoring organization
Author(s) Fredrik Johansson	

Title and subtitle
Controlled axonal outgrowth and cell reactions to nanostructures

Abstract
The interface between living cells and artificial surfaces are highly relevant for biomedical applications such as implants and organized cell growth for tissue reconstruction as well as for basic science purposes. In the present thesis, we have studied axonal guidance on various nano-patterned surfaces such as polymethyl-meth-acrylate, porous silicon and on magnetically aligned Ni nanowires. Furthermore, the reaction of macrophages exposed to free nanowires made of Ni, Au, GaP and polystyrene was examined. The impact of porous silicon on the sciatic nerve regeneration was studied in an animal model. The overall aim was to study how neuronal processes grow and extend on nanopatterned surfaces and structures, intended for implantable electrodes or "lab on a chip" devices.

1) Axonal guidance was observed for grooves and ridges with dimensions between 100 nm and 800 nm. The axons were found to grow on the ridge edges and not in the grooves. Axonal guidance and cell guidance was also observed on Ni nanowires with a diameter of 200 nm, magnetically aligned on a glass cover slip.
2) Macrophages exposed to suspensions of nanowires. Nanowires made of Ni, Au, GaP and polystyrene, were studied. We found that the nanowires activated the macrophages, and nanowires composed of metal could induce cell death.
3) Porous silicon with different pore sizes was fabricated. We found that axons preferentially grow on porous silicon as compared to smooth silicon, but only if the pore size is between 150 and 500 nm. The integration with a regenerating nerve on porous silicon in vivo was also found to be better than for smooth silicon. Here, we found the encapsulation to be reduced on the porous silicon surface as compared to a smooth one.

We conclude that axons are guided via contact guidance by structures as small as 100 nm and that magnetic nanowires can serve as such structures. This phenomenon may be used for in vitro applications such as lab on a chip or the creation of neuronal networks with high fidelity. Nanowires in suspension may be toxic to cells and we speculate that this is the case if the wires are too rigid e.g. metal wires, and/or if metal ions are released from the wires. Furthermore, porous silicon is a suitable material at the interface between electronics and living tissue due to its large area to volume ratio resulting in good anchoring of cells and tissue, a favorable situation for electrical recordings. Furthermore, in vivo there is less encapsulation of porous silicon. In vitro, such porous patterned chips supports axonal outgrowth and can be used for attracting axons to specific areas, a useful properties for many applications. Taken together, the present results show that nanomodification of surfaces is a promising avenue, when interfaces to the nervous system are considered.

Key words: peripheral nervous system, axonal guidance, nanoimprint, nanowires, porous silicon, dorsal root ganglia, sciatic nerve, macrophages, contact guidance, fibroblast

Classification system and/or index termes (if any):

Supplementary bibliographical information:		Language English
ISSN and key title:		ISBN 978-91-85067-50-3
Recipient's notes	Number of pages 124	Price
	Security classification	

Controlled axonal outgrowth and cell reactions to nanostructures

Fredrik Johansson

Department of Cell and Organism Biology
Lund University
Lund 2008

LUND
UNIVERSITY

Cover

The background image of the front cover shows porous silicon as it appears in the scanning electron microscope. The inserted images show axons on nano-imprinted polymethyl-methacrylate grooves (left), axons and migrating Schwann cells on stripes of porous silicon (right) and finally two L929 fibroblasts internalizing a Ni nanowire by means of phagocytosis (middle).

Artwork by: Fredrik Johansson, Per Gustavsson, Waldemar Hällström, Patrick Carlberg and Martin Kanje

Printed by Media-Tryck, 2008
ISBN 978-91-85067-50-3

"He who asks a question is a fool for five minutes,
he who does not ask a question remains a fool forever."

-Chinese Proverb

TABLE OF CONTENTS

ABSTRACT

The interface between living cells and artificial surfaces are highly relevant for biomedical applications such as implants and organized cell growth for tissue reconstruction as well as for basic science purposes. In the present thesis, we have studied axonal guidance on various nano-patterned surfaces such as polymethyl-meth-acrylate, porous silicon and on magnetically aligned Ni nanowires. Furthermore, the reaction of macrophages exposed to free nanowires made of Ni, Au, GaP and polystyrene was examined. The impact of porous silicon on the sciatic nerve regeneration was studied in an animal model. The overall aim was to study how neuronal processes grow and extend on nanopatterned surfaces and structures, intended for implantable electrodes or "lab on a chip" devices.

1) Axonal guidance was observed for grooves and ridges with dimensions between 100 nm and 800 nm. The axons were found to grow on the ridge edges and not in the grooves. Axonal guidance and cell guidance was also observed on Ni nanowires with a diameter of 200 nm, magnetically aligned on a glass cover slip.
2) Macrophages exposed to suspensions of nanowires. Nanowires made of Ni, Au, GaP and polystyrene, were studied. We found that the nanowires activated the macrophages, and nanowires composed of metal could induce cell death.
3) Porous silicon with different pore sizes was fabricated. We found that axons preferentially grow on porous silicon as compared to smooth silicon, but only if the pore size is between 150 and 500 nm. The integration with a regenerating nerve on porous silicon in vivo was also found to be better than for smooth silicon. Here, we found the encapsulation to be reduced on the porous silicon surface as compared to a smooth one.

We conclude that axons are guided via contact guidance by structures as small as 100 nm and that magnetic nanowires can serve as such structures. This phenomenon may be used for *in vitro* applications such as lab on a chip or the creation of neuronal networks with high fidelity. Nanowires in suspension may be toxic to cells and we speculate that this is the case if the wires are too rigid *e.g.* metal wires, and/or if metal ions are released from the wires. Furthermore, porous silicon is a suitable material at the interface between electronics and living tissue due to its large area to volume ratio resulting in good anchoring of cells and tissue, a favorable situation for electrical recordings. Furthermore, *in vivo* there is less encapsulation of porous silicon. *In vitro*, such porous patterned chips supports axonal outgrowth and can be used for attracting axons to specific areas, a useful properties for many applications. Taken together, the present results show that nanomodification of surfaces is a promising avenue, when interfaces to the nervous system are considered.

LIST OF PAPERS

This thesis is based on the following papers, which are referred to by their Roman numerals:

I. Axonal outgrowth on nano-imprinted patterns
Fredrik Johansson, Patrick Carlberg, Nils Danielsen, Lars Montelius and Martin Kanje
Biomaterials 2006, 27: 1251–1258

II. Magnetic nanowires for cell guidance
Fredrik Johansson, Malin Jonsson, Kersti Alm and Martin Kanje
Submitted

III. Nanowires induce activation of macrophages
Martin Kanje, Waldemar Hällström, Lars Montelius and Fredrik Johansson
Submitted

IV. Guidance of neurons on porous patterned silicon: is pore size important?
Fredrik Johansson, Martin Kanje, Cecilia Eriksson Linsmeier and Lars Wallman
Physica Status Solidi (C) 2005, 2: 3258-3262

V. The influence of porous silicon on axonal outgrowth *in vitro*
Fredrik Johansson, Martin Kanje, Cecilia Eriksson Linsmeier and Lars Wallman
IEEE Transactions on biomedical engineering 2008, 55: 1447-1449

VI. Porous silicon a potential electrode material in a nerve repair setting - tissue reactions
Fredrik Johansson, Lars Wallman, Nils Danielsen, Jens Schouenborg and Martin Kanje
Submitted

AIMS OF THIS THESIS

The *overall aim was:*

- To study how neuronal processes grow and extend on nanopatterned surfaces and structures, intended for implantable electrodes or “lab on a chip” devices.

The *specific aims* were:

- To establish the extent and perhaps the limitations of contact guidance of regenerating axons on nanometer structures.
- To determine if magnetic nickel nanowires could be used to guide cells and cellular processes.
- To study the effect of nanowires at large using phagocytotic cells (macrophages).
- To determine the attractive or repulsive effect (haptotaxis) of porous silicon surfaces on regenerating axons *in vitro*.
- To study how porous silicon *in vivo* acts as a substrate for regenerating neurons.

1. INTRODUCTION

In all vertebrates, many different cell types such as neurons, muscle cells, epithelial cells and endothelial cells are involved in the organization of different tissue and organs. The behavior and interaction of these cell types during development and wound healing mold and form our bodies to unique individuals. Although unique, we all have the same basic anatomy indicating a common set of intrinsic mechanisms and instructions for migration, division and differentiation among all cell types. For the development of new implants and tissue engineering, scientists are trying to reveal how these sets of intrinsic mechanisms work and utilize the knowledge to create a new generation of implants which are tissue compatible and integrate smoothly with the host. To achieve this, the influence of the implant surface, *i.e.* the topography and chemo-physical properties on which the cells grow is of paramount importance.

Nanotechnology has provided us with tools that allow interaction with cells and sub cellular processes on the appropriate scale [1]. For implants, the surface is what the cells and tissue will experience. It is conceivable that nano-structured implant surfaces can be tuned to interact smoothly with the tissue on the implant site and evoke less of an immune response than would non-structured surfaces. Furthermore, such surfaces could be modified for the organization of the attached cells. They could also be used as sensors and the combination of nanotechnology and biomedicine hold a potential for the development of new types of medical implants.

For several years we have been engaged in projects concerning axonal outgrowth on artificial substrata and one driving force for this thesis was to find suitably nano-modified surfaces for the construction of improved implants in the nervous system which could pave the way for the construction of implantable electrodes with enhanced resolution and biocompatibility.
In this thesis, I have mainly studied how nerve cells interact with artificial nano-structured surfaces.

2. BACKGROUND

2.1. Brain-machine-interface (BMI)

An implantable connection to the nervous system is often referred to as brain machine interface (BMI) [2]. Such devices can also be used on nerves and may help people to restore deficits in neural functions caused by trauma or disease. Some BMIs are already in clinical use like the cochlear implants for hearing [3], pace makers for heart rate control [4] and deep brain stimulators for treatment of neurodegenerative diseases, such as Parkinson's disease [5] (Fig. 1).

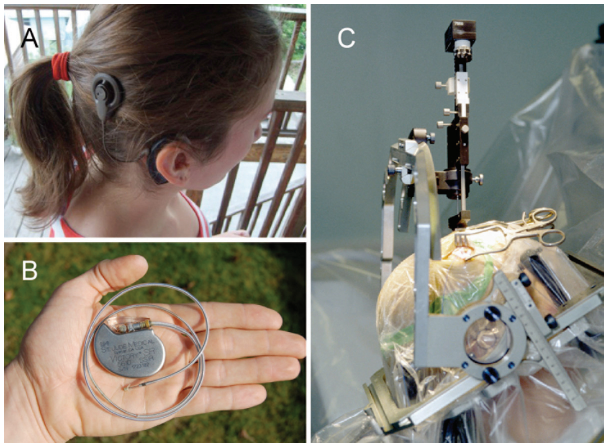

Fig. 1. *The images show three examples of implants in clinical use. A. A cochlear implant for hearing. B. A pacemaker for heart control. C. Electrodes for deep brain stimulation, here is a picture from the implantation operation, where the electrodes are exactly positioned by using a stereotactic instrument. (Images downloaded from "Wikipedia commons" free to use under the GNU Free Documentation Licence.)*

Other BMIs, which include retinal implants and cortical electrode arrays in humans, are still at the experimental stage [2]. The latter which enables control of machinery in the patient´s environment, through their own thoughts, have been developed by Cyberkinetics Neurotechnology Systems [6] using their BMI, the BrainGate™, may be considered the "state-of-the-art" as far as BMIs are concerned (Fig. 2). Well performing BMIs with high resolution would also be new valuable tools for basic science research both *in vitro* and *in vivo*. For *in vivo* studies, they would allow detailed registration of neuronal activity in awake animals. *In vitro* applications of BMIs include high definition neuronal networks and biosensors.

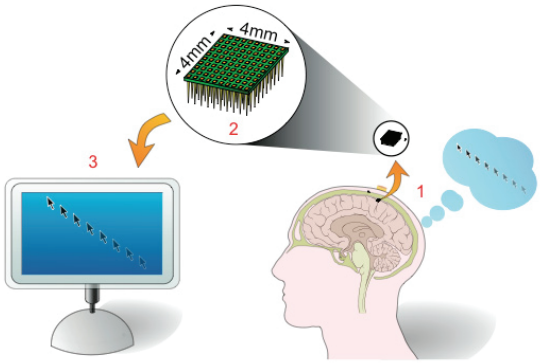

Fig. 2. *This schematic picture shows the basic function of BMIs such as the Braingate™. (1) The patient imagines a motion and (2) the brain-signals are registered by the implanted array of electrodes in the motor cortex (3) the signals are decoded and translated by a computer, resulting in the movement of a cursor on the screen. (Image downloaded from "Wikipedia commons" free to use under the GNU Free Documentation Licence.)*

The BMIs of today are rather primitive with respect to their spatial resolution and their lack of bidirectionality, *i.e.* they usually only work in one direction; cochlea implants only stimulates while the BrainGate™ only register neural activity [6]. The state-of-the-art among implants in regular clinical use is the cochlea implant. This utilizes an external microphone connected via a computer to the auditory nerve (Fig. 3). Deaf children that get an implant after birth can learn to speak in a natural way, demonstrating the excellent function of the implant. However, there is still plenty of room for improvements. Hearing adults that for some reason have lost their hearing and later got a cochlea implant testify that the sound impression is like having their head in a can. In the cochlea implant, the maximum number of electrodes varies between 10 and 100 on an area of a few mm^2 in size, perhaps not an impressive number but obviously enough to interpret sounds [2]. That number, and thereby the resolution, could be increased enormously using nanotechnology. For BMIs this is necessary considering the high cellular and synaptic density in the brain.

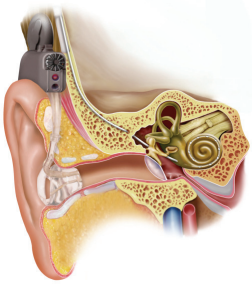

Fig. 3. *This drawing shows that the electrode of the cochlear implant is not in contact with the microphone system outside the head. The signals are transferred from the microphone via a wireless system to the electrode that stimulates the auditory nerve resulting in a sound experience for the patient. (Image downloaded from "Wikipedia commons" free to use under the GNU Free Documentation Licence.)*

There are also other criteria that need to be considered for a BMI. In order to construct a bidirectional neuro-electronic junction in the peripheral nervous system, nerve fibers of different type, *i.e*. motor- and sensory fibers, need to be separated on the BMI surface. This would enable both selective stimulation of different sensory modalities, *i.e*. touch proprioception, temperature and pain, as well as registration of signals from motor neurons. To achieve such a separation, the surface properties are particularly important. In this context, the guidance of axons on surfaces must be studied. Furthermore, an implantable BMI must be biocompatible to survive *in vivo* for years. Thus, it is of most importance to investigate our defense mechanisms, *i.e*. the immuno-response to implanted BMIs. The basic mechanisms of cell reaction to artificial surfaces include events such as cell adhesion and guided locomotion mediated by signal transduction. These mechanisms, together with information on immuno-response are therefore briefly introduced to the reader before the results and discussion of the individual papers are presented.

2.2. Cell adhesion on artificial substrates

Cells in culture usually adhere both to each other and to the substratum on which they grow. When cells collide or approach each other, locomotion is inhibited and tissue formation may start. This phenomenon is called contact inhibition (for review see Takai *et al. 2008* [7]). This thesis concerns mainly the substratum-cell interface and therefore only the adhesion to artificial substratum surfaces will be discussed here. Cell activities such as locomotion, migration and alignment of cells, depend on the formation of firm adhesion to the substratum surface [8]. Hence, the formation of the specialized adhesion points, focal adhesions (FA) will also be discussed briefly.

Cellular adhesion includes several steps: adsorption, attachment and finally, cytoskeletal reorganization. Fibroblasts and epithelial cells have provided most of the current knowledge on how cells adhere to artificial substrates, such as glass or plastic substrates, usually used in tissue culture bottles and Petri dishes. Furthermore, the growth cone that is of special interest in this thesis is another extensively studied object regarding cell-surface interaction.

Initially, there is a nonspecific approach of the cell membrane to the substrate surface. Here cations, such as Ca^{2+} and Mg^{2+} from the medium, help to bridge the gap between the negative cell surface and the usually negatively charged substratum surface [9]. This adsorption is therefore based on electrostatic and van der Waals forces and important for the next step, the

initial precursor contacts. At this point cell adhesion is dependent on the chemical and physical properties of the surface such as; surface charge, hydrophobicity and structure. During the adsorption phase many cells have the potential to produce and prime the surface with proteins including extra cellular matrix (ECM) components. It is possible that such surface-modifications have occurred in our experiments. The released ECM proteins facilitate the initial contact. Then the initial contacts are reinforced by specific binding of transmembrane glycoproteins, integrins, to the surface protein layer. The integrins are receptor dimers (α and β), and many different subunits can be combined in order to recognize different ECM components. Proteins such as fibronectin, collagen I and laminin all share an arginin-glycin-asparagine (RGD) amino acid sequence that nearly half of the over 20 known integrins recognize and bind to. Inside the cell, the microfilaments start moving in a lateral way (parallel to the surface), scanning for suitable attachment sites. When a microfilament reach a precursor contact, this contact is stabilized and more integrins, microfilaments and other proteins such as vinculin and talin, are recruited. Finally, a cluster of integrins and their associated proteins *i.e.* a FA has formed, firmly integrating the surface with the cytoskeleton of the cell (Fig. 4). This enables the creation of tension within the cell, a necessary property for cellular movement and modification of the cell shape.

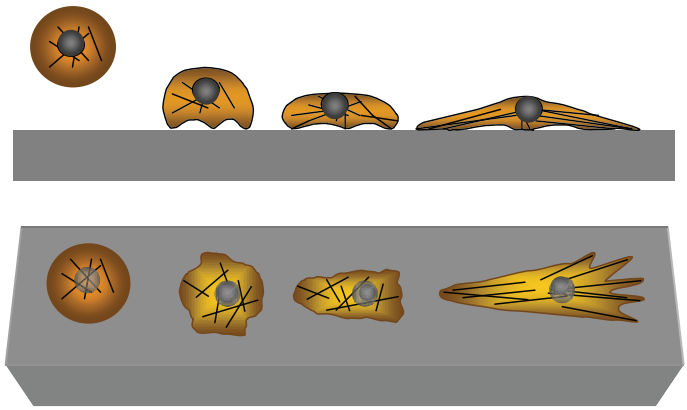

Fig. 4. *The drawing illustrates the processes of cell adhesion seen from the side (upper image) and from above (lower image). From left to right: A cell in suspension is sinking towards the substratum. The initial attachment is mediated by electrostatic forces where ions such as* Ca^{2+} *and* Mg^{2+} *are involved. A few integrins secures the attachment points before connection to the microfilaments via a chain of proteins. Finally, when more integrins and microfilament are recruited to the attachment sites, a focal adhesion forms and the cytoskeleton reorganizes so that the cell may exert tension and crawl.*

In a FA, that is an elongated structure about 0.25-0.5 μm wide and 2.0-10 μm long [10], the gap between cell membrane and the substrata surface is only 10-15 nm, as compared to the "normal" gap of >50 nm. The FAs are dynamic structures that may grow or shrink depending on the tension load applied to them. Finally, due to reorganization of the cytoskeleton, flattening and polarization of the cell may be observed [9,11].

2.3. Cell migration

The FAs and the cytoskeleton are crucial for cell migration. For instance, studies involving toxins that stabilise (phalloidin), or destabilise (cytochalasins) microfilaments, have shown the direct involvment of actin in cell movement [12]. The leading edge of a migrating cell protrudes filopodia, *i.e.* microfilaments surrounded by cell membrane, which attach to the surface via FAs [13] (Fig. 5).

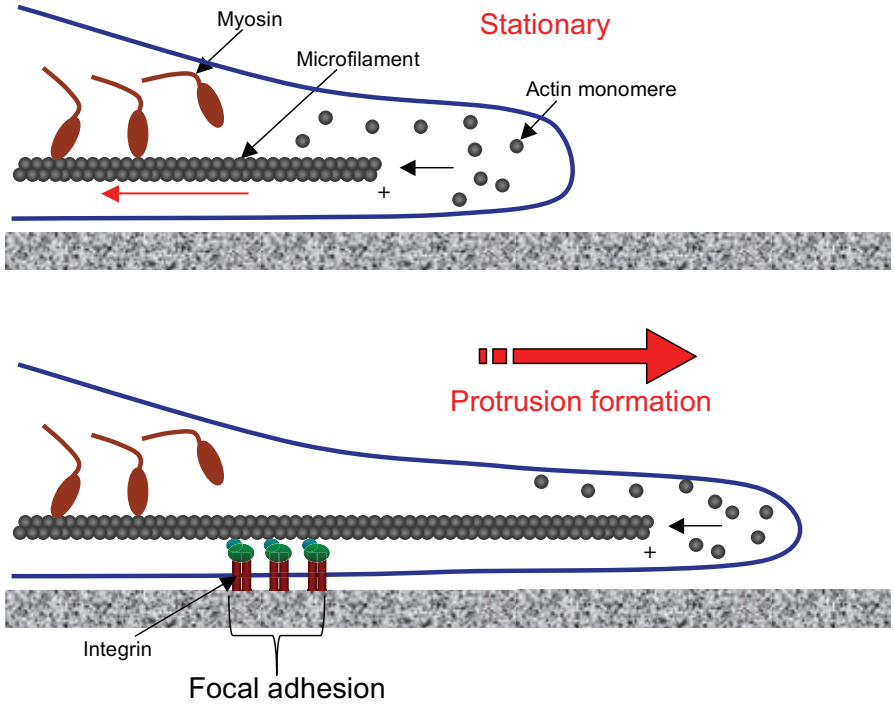

Fig. 5. *The initial steps of cell migration: cell protrusion, attachment and contractile activities. Upper drawing: Plus ends of microfilaments are found at the periphery of a cell. In a stationary cell or cell process, the retrograde flow of microfilaments due to the myosin motor proteins is balanced by the polymerization of microfilaments from actin monomers. Lower drawing: In an advancing cell, or cell process, the binding of the microfilaments to the surface via integrins in a focal adhesion stops the retrograde flow, while the polymerization continues. This results in the formation of a protrusion forward and the myosin motor proteins can pull the cell along the microfilaments.*

The contractile cytoskeleton can anchor filaments and then pull most of the cell body forward until the tension at the trailing edge rip off the FAs, or even break off a part of the cell itself, leaving a track of integrins and membranes behind. The contractive ability of the cytoskeleton is due to the motor protein myosin. Myosin work closely associated with actin (micro) filaments, in a sliding, ATP dependent, fashion although the exact details of the mechanism by which this occurs in non-muscle cells remain elusive [14].

2.4. Guidance of cells and cell processes

Guidance of migrating cells is necessary during embryogenesis and wound healing, where different cell types and extending cell processes are directed to the correct site in an organism. There are many cues, or taxes, that work by them selves or in combinations to guide cells. A taxis is usually described as an innate behavioral response by a freely motile organism (or cell) to a stimulus (light, chemicals etc.) from a particular direction, whereby an organism moves either towards (positive taxis) or away from (negative taxis) the stimulus. A taxis differs from a turning response or tropism. Tropism is the growth movement towards or away from a stimulus exhibited by plants or sessile animals [15]. However, concerning axonal growth cones the term tropism is sometimes used, probably because the axon exhibits a growth movement while the cell body is more or less stationary. The two terms are often used interchangeable. I will hereafter use the term taxis for both cells and axons.

By using different types of taxes, chemical, topographical or electrical, on nerve cell projections or other cells of interest, it is possible to design a chip surface so that cells grow and proliferate in a predicted way. Grooves, ridges, chemical tracks or surface roughness could be exploited to force cells to grow in a desired spatial pattern [11,16,17]. This enables the development of improved lab-on-a-chip applications such as biosensors, grafts for nerves or tendons, neural networks etc. where ordered cell arrangement is of great importance. Neurons are especially interesting in this context, since they send out long guidable extensions, axons, and use electrical signals for communication. Such signals could be integrated in neuro-electronic systems [18,19]. In this thesis mainly three taxes are discussed: chemotaxis, contact guidance and haptotaxis.

2.4.1. Chemotaxis

In chemotaxis a single-cell or multicellular, motile organisms direct their movements according to certain chemical gradients in their environment. Eucaryotic cells are large enough to detect gradients over their cell body, while prokaryotic cells need to move in order to detect a gradient. Chemotaxis is defined as positive if the movement is in the direction of a higher chemical concentration and negative if the direction is the opposite [15].

2.4.2. Contact guidance

Already in 1911, R. G. Harrison reported that cells grown on treads from a spider's web followed the fibers [20]. In 1945, the American developmental neurobiologist Paul Weiss named this behavior "contact guidance" [21] but it was not until the early 70´s that biologists seriously tested the idea of contact guidance again, starting with growing cells on grooved substrata and on spheres [22,23]. Since then, the cellular responses to topographical cues of many different kind have been tested, including curved surfaces, single steps, angled planes, pillars, pits, pores, cylinders, spheres and finally the most studied structure, parallel grooves and ridges [24]. The explosion of research in this area was mainly due to the rapid development of techniques in the computer industry. Hence, structures with micrometer- and the last 10-15 years even sub-micrometer sized objects have become available for biomedical research. Today, it is clear that structures as small as 5-10 nm change the morphology of some cells, *i.e.* macrophages [25] and some of the molecular components of the guiding system have been identified [26,27] (see below).

A problem when trying to deduce a general mechanism for guidance from the studies mentioned above is that the cellular response depends not only on the surface topography, but also on the substratum material and type of cells used. The molecular mechanism responsible for contact guidance is not yet altogether elucidated but several mechanisms have been proposed:

Firstly, one group of theories is based on the mechanical properties of the cytoskeleton and the probability to extend a process, *i.e.* polymerize actin filaments in a particular direction. The assumption is that the stiffness of the cytoskeleton prevents bending over sharp edges so that the only way to find a solid surface to adhere to would be to extend along a ridge, or stay on the planar surface. This assumption that cytoskeletal elements are unable to bend more than a few degrees [28-33], have also been used to explain the guidance along fibers. In 1976,

Dunn *et al*. proposed that pseudopodia could only bend a few degrees so that if the surface curvature was to sharp, the pseudopodium would not be able to attach [34]. In agreement, Smeal and colleagues 2005 showed the same thing for neurites and also constructed a theoretic Bolzmann model. The model called "A bending stiffness model" illustrates how a filopodia, grown on fibers with low curvature radius, may not be flexible enough to curve around the fiber. Therefore, the filopodia elongate along the fiber (± a few degrees, determined by the fiber radius) [35].

Another group of theories concerns the probability of FA formation at certain sites. Here it is assumed that ECM proteins preferentially adsorbed to the discontinuities, *i.e*. edges, present on grooved substrates. The adsorbed proteins should then be responsible for the subsequent alignment of FA and hence the contact guidance [21-23,36-38].

A third theory is based on the restriction of the area available for the elongated FAs to adhere when ridges are small enough. In order to fit on a small ridge, the FAs are forced to align along the ridges, thereby inducing the alignment of the entire cell due to the tension of the actin filaments that exert force mainly along the FAs´direction. That theory may explain the large effect of ridge width found in many studies [10,34,39-41].

Finally, a forth strictly mechanical "tensegrity-theory" (from tensional + integrity) has been suggested. This theory, introduced by Ingber [42] who was inspired by the field of engineering, is based on the concept of minimizing the energy in a system, *i.e*. to balance the forces in the cytoskeleton so that a biomechanical steady state is reached when attached to a surface via FAs [43].

2.4.3. Haptotaxis

Haptotaxis, (Greek: haptein, to fasten; taxis, arrangement) was first described and named in 1965 by S. B. Carter. He defined it as: "movement of a cell is controlled by the relative strengths of its peripheral adhesions, and that movements directed in this way, together with the influence of patterns of adhesion on cell shape, are responsible for the arrangement of cells into complex and ordered tissues." In simple words: cells preferentially move onto surfaces with higher adhesion (Fig. 6). Carter also, in the same article, explained contact inhibition based on the haptotaxic theory [44].

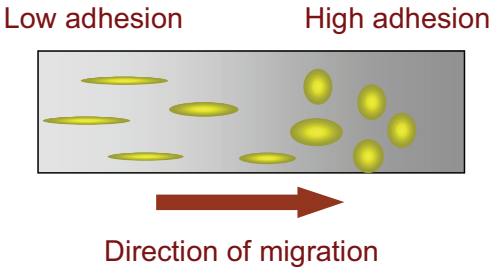

Fig. 6. *The drawing illustrates the phenomenon called Haptotaxis. Cells growing on a substratum with an ahesion gradient, move from less adhesive substrata to more adhesiv substrata where the migration stops.*

2.4.4. Axon guidance

The delicate task of axonal path finding, during embryogenesis or after a peripheral nerve injury, is performed by a specialized cellular structure, the growth cone (Fig. 7). In many ways a growth cone resembles of a hand, where filopodia (the fingers) consist mainly of ordered microfilaments surrounded by membrane. Lamellipodium, the web-like structure between the filopodia, have a more random system of microfilaments surrounded by the cell membrane. The axon mainly have neurofilaments and microtubuli that ends approximately at the center of the growth cone, although some dynamic microtubuli are present in the peripheral parts of the growth cone as well.

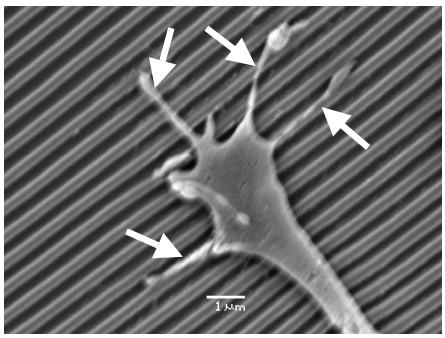

Fig. 7. *This Scanning electron microscope (SEM) image illustrates a growth cone, resembling a human hand, with obvious filopodia (arrows) that sense the surroundings, in this case grooves. Between the filopodia, the lamellipodia, a web like structure can be seen. The image is reprinted from paper I.*

The idea that growth cones are involved in axonal path finding was suggested by Ramon y Cajal, already in the 1890s´ and R. G. Harrison, as mentioned before, also studied axonal elongation in the 1910s´, deducing that growth cones are indeed involved in axonal outgrowth [45]. The growth cone behaves much like a migrating cell (with an extending axon attached to it) and sends out filopodia to probe the surroundings while lamellipodia secures the attachment to the surface. Filopodia may be very long (several micrometers) and can therefore sample the surroundings far ahead of the central core of the growth cone. When a filopodium finds and attaches to a suitable part of the surface via integrins, the dynamic actin filaments stop the "tread milling" movement and thereby initiate an elongation of the filopodium. The elongation of an axon demands more building material such as membrane and cytoskeleton sub units. These are mainly synthesized in the cell body and must therefore be transported via axonal transport along the microtubules to the growth cone [45].

The guidance of growth cones, and thereby the axons, depend on two major signals: non-diffusible (short range) and diffusible (long range). The first one includes cues like binding with integrins or cadherins *i.e.* haptotaxis and contact guidance, while the latter is the classical chemotaxis, often mediated by nerve growth factor (NGF), brain derived neurotrophic factor (BDNF) or neurotrophin 3 (NT3). (Note that NGF was always included in the culture medium in our axonal guidance studies.) The cues can be both positive and negative and work together in order to orchester the correct path finding of all different axons. In studies *in vivo*, the guidance has been found to occur stepwise, in a “stop-and-go” fashion, with many guidepost cells (often immature neurons) along the way. Different axons, intended for different sites, respond to cues in different ways, *i.e.* are attracted or repelled. Once the pioneering axons have found their way, other axons may use them as scaffolds and exhibit fasciculation via contact guidance [45].

In simplified systems, like *in vitro* cultures, cells can be exposed to one single cue at a time. Tracks of laminin or fibronectin is of special interest since integrins, that mediate bindings to ECM-like surfaces bind readily to such tracks, promoting axonal outgrowth. There are also inhibitory proteins, such as collapsin that causes the collapse (hence the name) of the growth cone at very low concentration [46].

2.4.5. Signal transduction

Knowledge about the guidance mechanisms described above is useful for predicting the response of a cell to a certain structure. However, they do not show the complete picture since also the biochemical signaling due to the topographic cues play an important role in the guidance. Over the recent years, several important signaling molecules have been identified and some mechanisms responsible to the observed rearrangement of the cytoskeleton have been revealed.

All cell movement and alignment described above depend on well coordinated assembly and disassembly of the cytoskeleton and in particular microfilaments. The intracellular signaling pathways arising from the extracellular cues, which lead to the rearrangement of the cytoskeleton, involve a cascade of reactions referred to as signal transduction.

For migrating cells hydrolase enzymes such as the small GTPases: Rac, Cdc42, Ras and Rho have been shown to be important for organizing the cytoskeleton during migration. Rac is essential for the protrution of lamellipodia and thereby forward movement, Cdc42 is necessary for keeping the cell polarity while Ras regulates the FAs and associated actin fibers [26]. The last one, Rho has been reported necessary for cell adhesion during movement and thereby contact guidance [26,47]. The guidance of axons depends on the same molecules, Cdc42 and Rac that mediate growth cone attraction and elongation while Rho mediates repulsion and growth cone collapse [27]. The alternating activation GTPases of by the external cues via the membrane receptors can thus guide the axon in a stop and go fashion, reflected in the wandering behavior of axonal outgrowth found in our studies.

2.5. The nervous system

In our experiments, we used neurons and in particular sensory neurons from the peripheral nervous system (PNS). PNS connects the central nervous system (CNS) that include the brain and spinal cord, with the rest of the body, *e.g.* muscles, glands, intestines, skin and sensory receptors. In the studies presented in paper I, II, IV-VI, we used regenerating axons from sensory neurons. The sensory neurons are found in the dorsal root ganglia (DRG), which contribute axonal processes into the spinal nerves. In a mouse such a ganglion contain several thousand neurons (Fig. 8). In the first study (paper I) we also used superior cervical ganglia that contain the cell bodies of the post ganglionic sympathetic neurons.

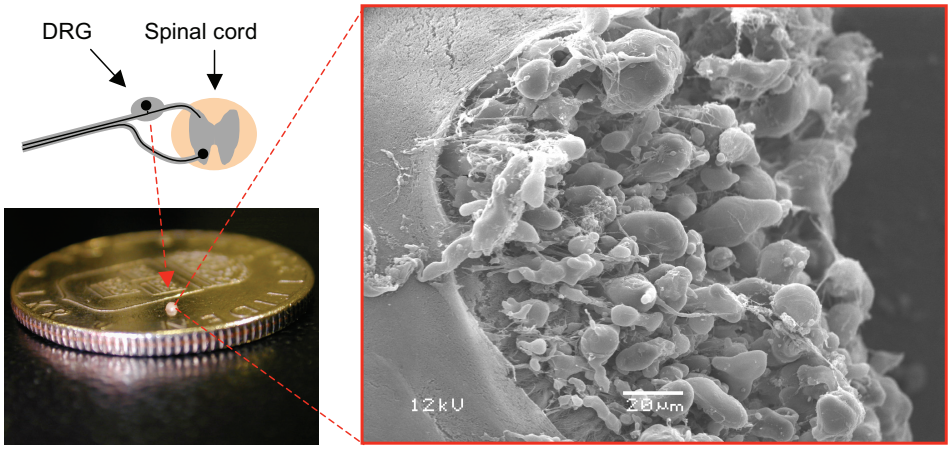

Fig. 8. *The cell bodies of sensory neurons are found in the dorsal root ganglia (DRG), just outside the spinal cord. In a DRG from a mouse there are thousands of sensory neurons.*

A typical nerve is organized into several fascicles, containing thousands of axons of different sensory modalities, motor axons and autonomous axons that may be visualized by immuno-staining for the structural proteins including neurofilament. Glial cells, called Schwann cells, surround the axons of the PNS. They are responsible for the formation of myelin, an insulating lipid layer around the axon. Fibroblasts, endothelial cells and resident macrophages are also parts of a functional nerve. All these cell-types are present in the dissociated cultures prepared from the DRG and they may secrete proteins, which may affect both the growth of neurons and the substratum.

The dissociated neurons regenerate their axons in tissue culture. It shall be born in mind that we have here studied guidance of regenerating adult sensory neurons in two settings. The experiments in paper I, II, IV and V were performed *in vitro*, in an environment which is quite different from that in paper VI, where regeneration was initiated *in vivo* by a transection of the sciatic nerve, followed by a tube repair. In the latter case, a fibrin matrix forms in the tube (see next section) and is utilized as a substrate for the regenerating nerve fibers [48]. Notably, in the *in vivo* situation there are also inflammatory cells present.

2.6. *In vivo* response to implants

The studies presented within this thesis are conducted with the intention of constructing a new type of a neuro-electric implant. Anything alien that is inserted into an organism will be attacked by the immune system and inflammatory cells will try to phagocyte the foreign object. If this is not possible the object will be encapsulated by fibroblasts that secrete fibrous ECM components [49]. For an electrode, encapsulation is problematic since it insulates the electrode, resulting in low signal to noise ratios. Therefore, control of the inflammatory response to an implant is essential.

The biological response to an implanted object can be divided into an acute inflammation phase and a chronic inflammation phase that finally is manifested as granulation tissue. The first phase, lasting from minutes to days is due to the tissue trauma caused by the implantation procedure and is manifested by exudation of fluid and plasma proteins (edema), platelets and recruitment of white blood cells such as neutrophils. The plasma proteins released, immediately adsorb on the implant surface, and soon a fibrin matrix, reinforced by collagen is formed around the implant, although there is usually a thin liquid filled pocket close to the implant surface. This initial matrix enables further migration of cells such as macrophages/monocytes and fibroblasts. The invading cells are guided by chemotaxic cues. In this context, macrophages, that originate from specific white blood cells called monocytes are of special interest since they are involved in all stages of the immune reaction and are therefore one of the most central cell types within the immune system. There are two groups of macrophages: one is circulating and one is resident. These two sub-populations of macrophages can be distinguished using antibodies to the ED1 and ED2 antigen, respectively.
The macrophages main task is to phagocytose. This is performed both in a non-specific manner as scavenger cells or in an initial defense after infection, and later the phagocytosis may be more specific when antibody-tagged pathogens are attacked. Macrophages also serve as antigen-presenting cells and can thereby initiate antibody production against a pathogen. They also function as secretory cells with a broad arsenal of substances including cytokinesis. A macrophage can be further activated by signals such as lymphokines and then turn into a more aggressive form with directed phagocytosis. If the invading particle/object is too large to engulf, such as an implant, the macrophages may end up in a state called frustrated phagocytosis. This stage includes extreme flattening of the cells and release of reactive oxygen species and granules to the extra cellular space. The macrophage may then finally loose its ability to phagocytose [50].

The invasion of the monocytes/macrophages and fibroblasts, represent the start of the next inflammation phase, which is characterized by the presence of macrophages, monocytes, foreign body giant cells, blood vessels and connective tissue. This phase may evolve into a chronic state due to the persistent stimulus from the implant where the fibrin matrix is gradually exchanged for a more collagen rich network (fibrosis) by the invading fibroblasts, enhancing the tensile strength [49]. The collagen-reinforced network finally becomes a fibrous capsule surrounding the implant, an unwanted feature for most types of implants (Fig. 9). This stage lasts for the entire lifetime of the implant or the organism [50]. In paper VI, we suggest that nano-modifications of the surface can be used to control the inflammatory response.

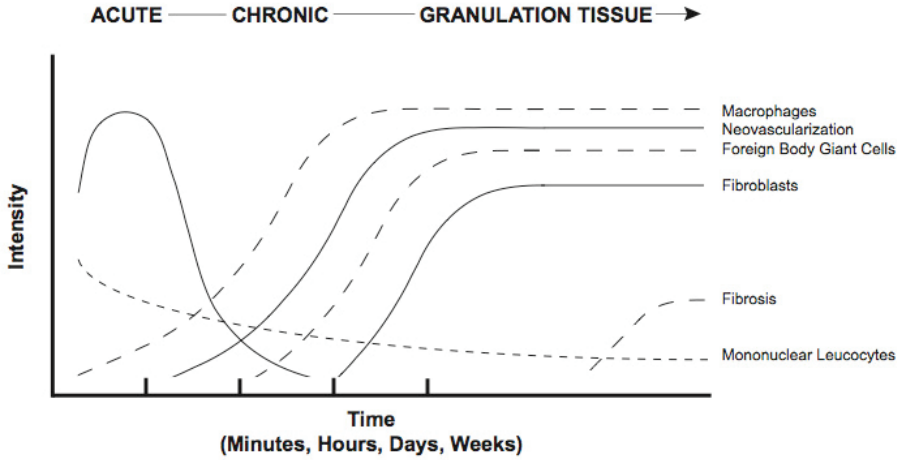

Fig. 9. *The diagram schematically shows the different stages of tissue response to an implant. The image is adapted from Andersson, "Mechanism of Inflammation and Infection With Implanted devices" 1993).*

2.7. Nanotechnology

Nano, the Greek word for dwarf, corresponds to 10^{-9} in the SI system. The term nanotechnology has however not yet been properly defined. Often spatial dimensions of 100 nm or less, in at least one direction is mentioned as limit. The structures used in this thesis are usually 100 nm or more, and some would perhaps call these sub-micrometer structures rather than nanostructures. I will use a less strict interpretation and everything smaller than a micrometer is here considered as nano-scale structures.

Nanostructures are either produced "bottom-up", or "top-bottom". In the bottom-up approach that has emerged from chemistry, nanometer structures are built by putting atoms and molecules together, much like using LEGO-bricks. This can be very elegantly done if working along with nature, *i.e.* minimizing the energy within the structure creating for instance self assembled monolayers. The other approach, top-bottom, has emerged from the field of physics. Here the procedure starts with a large bulk material, and the desired structures are carved out by different etching procedures. The two techniques can be combined to make, for example patterns of nanowires with e-beam lithography and epitaxy.

2.7.1 Topography with high definition, UV-lithography and EBL

The fabrication of micro and nanometer sized features with well-defined patterns is one of the crucial step in topographical experiments. The technique is directly adopted from the computer industry where different photolithographic methods have been used for many years.

The first step is usually to cover or the substrate *e.g.* a silicon wafer, with a light sensitive polymer, a photoresist. The photoresist is sensitive to irradiation and becomes either more soluble (positive resist) or less soluble (negative resist). A pattern can be defined by illuminating certain areas and then chemically remove the soluble parts of the resist layer. At this stage the topographic pattern of the resist itself can be used, but in most cases the wafer is etched, either with chemicals or with an ion gas (reactive ion etch – RIE). The remaining resist protects the substrate so that etching will only affect the bare parts of the substrate, resulting in a controlled etch process. Since the depth of the structures does not depend on the irradiation used, but rather on the etch parameters, this dimension is easily made very small. In contrast, the lateral dimensions of the patterns are limited by the wavelength-dependent scattering of electromagnetic radiation. To define small structures we need shorter wavelengths. The most common technique so far is UV-lithography, where ultraviolet light is

used. A mask put in front of the light source define the pattern in the photo resist. This enables mass production since entire wafers can be exposed within seconds in a parallel fashion. The limitation of this method is the wavelength of UV-light. The size of structures made by this method is usually in the micrometer-domain. To fabricate smaller structures shorter wavelengths must be adopted. Accelerated electrons, an electron beam, where the de Broglie wavelength is below the wavelength of UV-light suites this purpose. Using Electron Beam Lithography (EBL) we can produce structures down to about 10 nm [51]. The drawback of EBL is that the entire structure cannot be exposed simultaneously, as in the case with UV-lithography. Instead the electron beam work in a serial manner, without a mask, and illuminates the substrate pixel by pixel to define the pattern. This process is slower than UV-lithography, and complicated structures might require exposure times of hours. It is therefore a trade off between spatial resolution and exposure time.

The UV-lithography in paper IV, V and VI, was carried out at the Department of Electrical Measurement while the EBL used in paper I, was made at the Nanometer laboratory of the Department of Solid State Physics.

2.7.2. Soft lithography - nanoimprint

A fast way to produce high-resolution topographical pattern *en masse* is to use soft lithography. Soft lithography is a summarizing name for many different techniques by which polymer replicas can be made from a single master. The soft lithography methods have become very popular not at least among biologists, since clean room facilities and expensive machines are not necessary once the master has been fabricated [52]. Nanoimprint lithography (NIL) was first described by Chou *et al.* in 1995 [53] and was the soft lithography technique chosen for this thesis. The technique is described in Figure 10. Briefly, a patterned stamp, here manufactured by EBL is used and the topography of the stamp is transferred into a smooth layer of polymer under high pressure and temperature above the glass transition temperature (Tg) for the polymer. When the resist is cooled below the Tg, it becomes rigid resulting in a stable pattern that can be separated from the stamp. This procedure can be repeated several times, using the same stamp, enabeling parallel production of many high definition patterns. Furthermore, the choice of polymer is almost arbitrary. This is the strength of using NIL. Another advantage of using NIL for testing cell reaction to topography, is that the different parts of the structures, *i.e.* wall, top and bottom of a groove/ridge are more similar in roughness than such structures made with etching. The reason for this is the

isotropic property of the imprinted polymer combined with the imprinting procedure, where all surfaces are made simultaneously and in the same way.

2.7.3. Nanowires

Nanowires are structures with high aspect ratios, *i.e*. length/diameter. Most research today is concentrated on very thin nanowires with diameters of only a few nm. Such thin wires can be considered one-dimensional and quantum mechanical effects are dominating. The intended applications of these wires are mainly within electronics. Natural "nanowires" are readily found in nature. For instance, the cytoskeleton can be regarded as a matrix of different dynamic nanowires and nanotubes *i.e*. microfilaments, microtubules and intermediate filaments, with diameters of 5-9 nm, 25 nm and ~10 nm, respectively. Artificial nanowires can be constructed by several methods and the nanowires employed in the present studies were made using three different techniques:

Vapor-Liquid-Solid (VLS) synthesis method (epitaxy) is used for the production of semiconductive nanowires. Here a feed gas deposits atoms, layer by layer exclusively at sites prepared with a catalyzing material on the surface. The catalyst is usually colloidal gold and the diameter of the growing wire is determined by the diameter of the gold particle (for details, see Fig. 12, chapter 3).

Template based electrodeposition for metallic or conducting polymer wires is a second method of nanowire production. In this method, a porous membrane is used as template for the wires, grown by electrodeposition from an electrolyte. The diameter of the wires formed, is determined by the pore size of the template. The template is dissolved in order to set the produced nanowires free (for details, see Fig. 13, chapter 3). In this method as well as for epitaxy, the deposited material of the electrolyte, or feed gas for epitaxy can be changed during synthesis. This means that nanowires with a striped appearance of alternating materials is possible to synthesis.

A third method for the production of polymer nanowire synthesis is "template based molding" (for details, see Fig. 14, chapter 3). Here a liquid polystyrene solution is molded in a template as above. When the solvent evaporates, the polymer solidifies and the template can be removed.

2.7.4. Porous silicon (pSi)

In 1953 Arthur and Ingeborg Uhlir at Bell telephone laboratories discovered porous silicon (pSi). It was during electro polishing of a P-type silicon crystal in aqueous HF that something odd happened; hydrogen evolved and instead of a shiny polished surface, a brown crust was formed. This was the first recorded observation of porous silicon although the true morphology could not be determined since there was no electron microscope in the laboratory at the time [54]. The true structure was clarified first in 1972 [55]. After the discovery, scientists showed little interest in the material until 1990, when Canham found that pSi could emit visible light [56], photoluminescence [57], as well as electro- and chemiluminescence [58]. Since this indicated that a new generation of light emitting semiconductor components was possible within a near future, the research increased explosively.

The mechanism responsible for the optical features of pSi is not clear, but is believed to originate from nanometer-sized disruptions in the silicon lattice. Due mainly to stability problems of the pSi layers, no commercial devices using the optical properties of pSi are yet available and much of the attention is now directed to another characteristic feature of pSi; the large area to volume ratio. This enables applications such as enzyme reactors, but also the use of pSi as an electrode surface for biological systems [59,60]. The area of interest has thereby changed from engineering and physics to chemistry and biology. The main applications for pSi in biology are as biosensors [61] and support for biochemical reactions and proteomics [62]. At the end of the 20th century the cell supporting properties of pSi were demonstrated [63]. We studied the cell interaction with pSi as substratum both *in vitro* in paper IV and V and *in vivo*, in paper VI.

The formation of the pores in pSi is a stochastic electro chemical process. Even though the process of forming the pores is stochastic, this is only true for the initial phase of the electro chemical etch. Once the pore formation is initiated, the etching is easily controlled so that average pore sizes can be controlled in a reproducible fashion. The diameters of the pores range from a few nanometers up to some micrometers depending on etch parameters such as: etching solution, current density, doping level, irradiation etc. (Fig. 11).

3. EXPERIMENTAL PROCEDURES

3.1. Nanoimprinting process (paper I)

Round silicon wafers with a diameter of 25 mm (SILTRONIX, France), were spin coated with PMMA-950 resin (Micro-chem corp, USA). The wafers were hard baked and subjected to nanoimprinting using a silicon master stamp that was made with the Electron Beam Lithography (EBL) and lift off technique. The imprinting was carried out at 50 bar / 180° C using a prototype imprinting machine (Nanoimprint 2,5 TOM). After cooling, the master and replica were separated with a scalpel (Fig. 10).

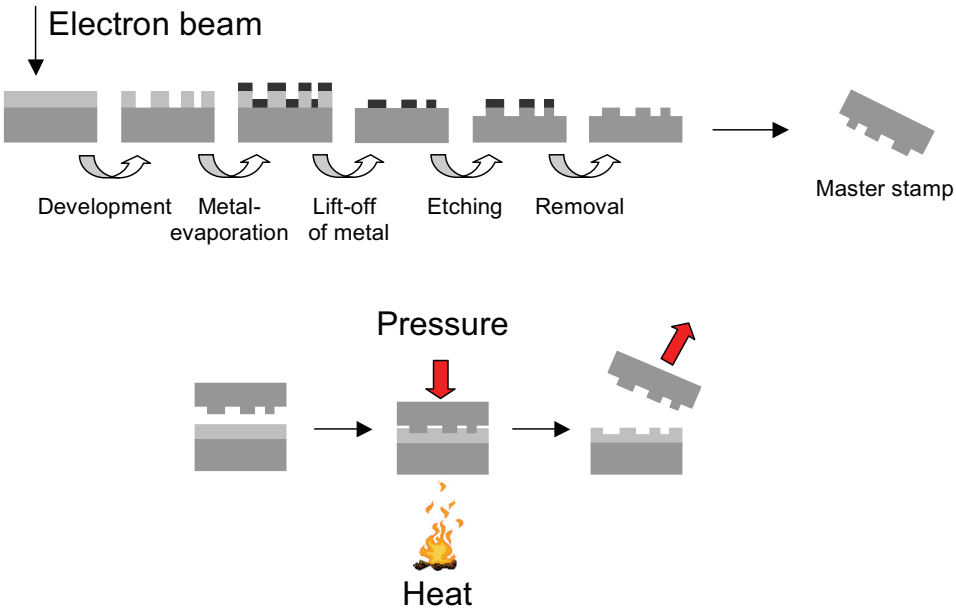

Fig. 10. *This is a simplified drawing illustrating the steps in the production of the imprinted nano-patterns. Upper row: Electron beam lithography with lift off technique was used for the manufacturing of the master silicon stamp. Lower row: A silicon wafer was spin coated with PMMA and the stamp made by EBL, was used for the following nanoimprinting into the PMMA layer.*

3.2. Porous silicon chips (paper IV, V and VI)

Oxidized 3" <100> p-doped (1-20 Ω/cm) Si wafers were patterned using standard UV-lithography and etching of the SiO_2 layer, before diced into chips. The chips were mounted with gaskets between two chambers containing a mixture of HF and dimethylformamide (DMF). One electrode was placed in each chamber and a 100 W lamp was used to illuminate the back of the wafer (the side with no defined pattern) (Fig. 11). Current densities between 2.5 and 20 mA/cm^2 were used to create different pore sizes. The etching time varied between 2 and 20 min. After the electrochemical etch, the wafers were submerged in HF for 25 min to remove the remaining SiO_2. The chips were finally rinsed in ethanol and distilled water before storage in distilled water.

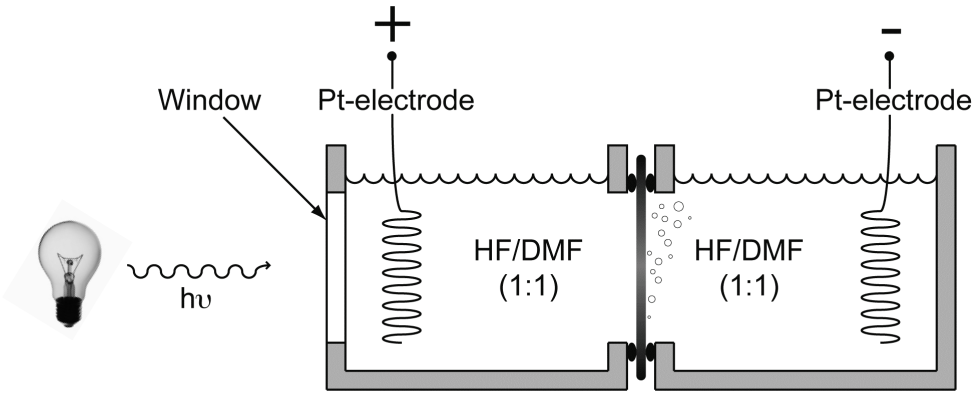

Fig. 11. *This schematic drawing shows the setup for electrochemical etching to obtain porous silicon (pSi). The light creates electron-hole-pairs where the holes are driven towards the cathode, facilitating the stochastic etch-process that results in the porous morphology of pSi. (HF=hydrofluoric acid, DMF=dimethylformamide and Pt=platinum)*

3.3. Synthesis of nanowires (paper II and III)

Wires were produced by: epitaxi for GaP-wires, template based electro-deposition for metallic wires and template based molding of polystyrene wires.

3.3.1. GaP nanowires (paper III)

The 2.5 μm long GaP nanowires were grown by epitaxi on GaP samples with a (111)B surface orientation. Prior to growth, the GaP samples were etched in a mixture of HCl, H_2O and HNO_3 in a 2:2:1 ratio. Then, aerosol deposition of 50 nm gold particles with a density of

approximately 1 particle/μm^2 was performed, followed by the epitaxy. The details of nanowire growth and sample preparations for epitaxy have been described in detail by Svensson *et al.* 2005 [64]. After growth, the wires were scraped into a solution of 3% Triton X in water and separated by gently sonication. The wires were then pelleted by centrifugation, washed in water and finally diluted in 1 ml sterile PBS before use.

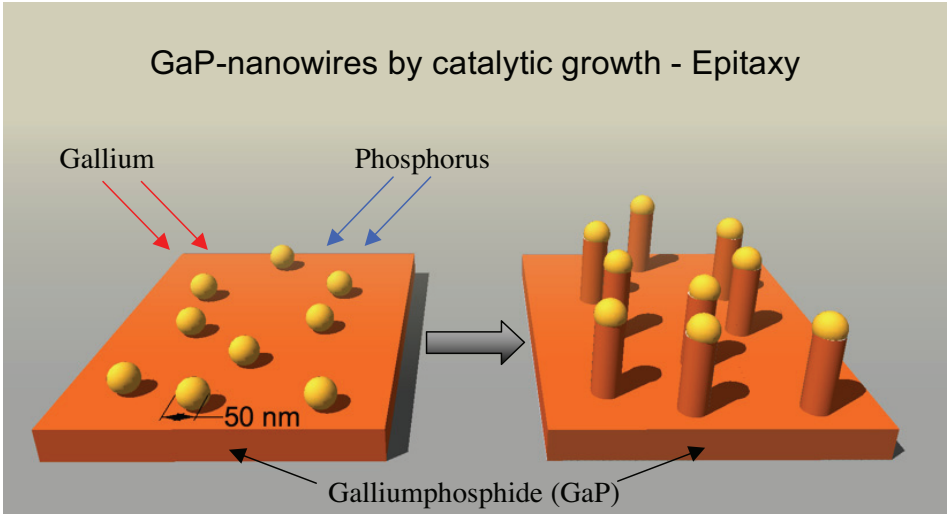

Fig. 12. *The catalytic growth of GaP nanowires from a GaP substrate is facilitated by aerosol deposition of gold particles that catalyze the formation of GaP nanowires from the feed gases. The wires grow at the Au/GaP interface so that the Au particle is always at the top of the wire. The wires used in this study were approximately 2.5 μm long and had an aspect ratio of 1:50.*

3.3.2. Metallic nanowires (paper II and III)

For the synthesis of Ni and Au nanowires commercially available 60 μm thick alumina membranes (Anodisc, Whatman Inc, England) with Ø=200 nm pores were used as templates (fig. 13). One side of the Anodisc filter has a thin layer (~1 μm) of smaller pores (Ø=20 nm) that merge into the larger pores. This side of the membrane was covered with Ga/In eutectic (Alfa Aesar®, Germany) to form a conductive layer that was used as cathode during the electrodeposition. The filter was placed on a copper electrode with the conducting layer in contact with the electrode. A reservoir, sealed with gaskets and secured by clippers was placed atop of the filter. The reservoir was filled with aqueous Ni plating solution (1M $NiCl_2$, pH 1) or Au plating solution (0.02 M $HAuCl_4$ and 1M NaCl (1:3 v/v), pH 1.5). A Ni or carbon electrode was placed in the solution and served as anode. The electro-deposition voltage was held constant at 1.5 V (DC), 40 min for the Ni deposition and 2 h for the Au deposition. After

the electro deposition, the Ga/In coating on the Anodisc membrane was removed by concentrated nitric acid using a pad of cotton wool. The filter was then dissolved in 3 M NaOH during 30 min. The free nanowires were rinsed in 96% ethanol or PBS depending on the study.

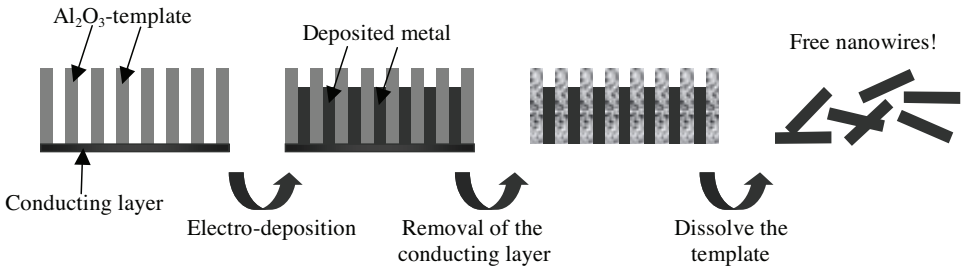

Fig. 13. *The metal nanowires were made by electro-deposition in an Al_2O_3 Anodisc template. The conducting layer (Ga/In eutectic), necessary for the electro-deposition, was removed by HNO_3 before the template was dissolved in NaOH.*

3.3.3. Fluorescent plastic nanowires (paper III)

Alumina membranes (Anodisc, Whatman Inc) with Ø=200 nm pores penetrating the entire membrane, was used as template for the plastic nanowire production. Polystyrene (PS) (Mw=100000) was chosen as polymer for the plastic nanowires that were produced as follows (Fig. 14). Approximately 0.5 ml polystyrene/xylol solution (5g PS in 15 ml xylol) was mixed with 40 μl of 3,3'-dioctadecylindocarbocyanine (DiI) solution comprised of a few DiI (Invitrogen-Molecular probes™, USA) crystals that had been dissolved in 40 μl xylol. Two drops of this fluorescent mixture was put on an objective slide. An Anopore filter was placed atop of the fluorescent polystyrene. The filter was then covered with a protection paper and another glass objective slide. Clamps were used to compress the preparation while the xylol evaporated over night in a low-pressure exicator. The preparation was dismounted and further dried in air until no smell of xylol could be detected. The filter was then dissolved in 3 M NaOH for 60 minutes leaving standing PS nanowires on a thin PS support. The fluorescent PS nanowires was thoroughly washed in water, sprayed with ethanol and dried. The plastic nanowires were then scraped from the PS support into a solution of 3% Triton X-100 in water and separated by gently sonication. The wires were then pelleted by centrifugation, washed in water and finally diluted in 1 ml sterile PBS before use.

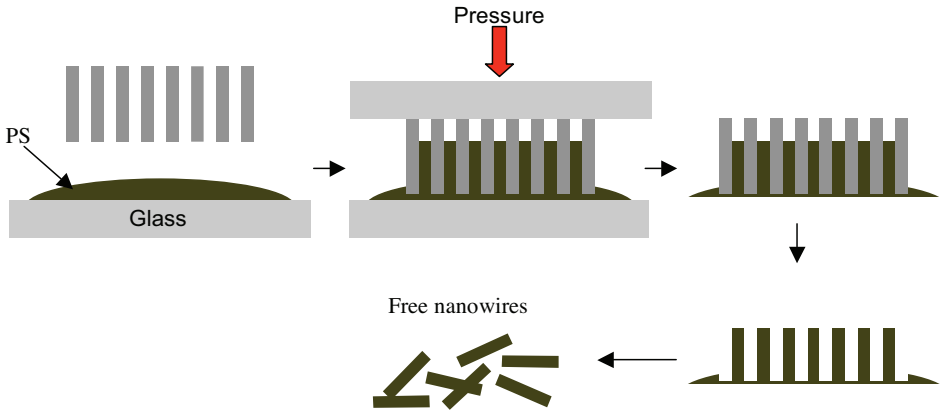

Fig. 14. *The drawing shows the production of fluorescent polystyrene (PS) nanowires. An Al_2O_3 template was pressed into the DiI/PS/Xylol-solution between two glass slides. After evaporation of the Xylol, the nanowires could be scraped off from the thin plastic surface.*

3.4. Animals

Adult female NMRI mice (Taconic-Møllegard Breeding Centre, Denmark) or female Sprague Dawley rats (Taconic-Møllegard Breeding Centre, Denmark) were used for the experiments. In addition, transgenic mice carrying the reporter gene for GFP were utilized. All animal-related procedures were approved by the Malmö/Lund Animal Ethics Committee on Animal Experiments.

3.5. Organ cultures

The lumbar (L4-L6) dorsal root ganglia (DRG) and in some cases the superior cervical ganglion (SCG) from mice were dissected and kept in serum free culture medium (RPMI-1640, Sigma, USA) until mounted on the nano-structured surfaces. The nano-structured chips were sprayed with ethanol (70%) for sterilization before use. The ganglia were dipped in Matrigel® and placed on the chips. The Matrigel® acted to glue the ganglia to the silicon chip and facilitate axonal outgrowth onto the chip surfaces. Two ml of serum free culture medium (RPMI-1640, Sigma, USA), containing 20 ng/ml NGF (Peprotech, USA) was added to each dish to further stimulate axonal outgrowth and the whole-mounted preparations were incubated at 37°C in a humidified atmosphere of 93.5% O_2 and 6.5% CO_2.

3.6. Cell cultures

3.6.1. Macrophages

Resident peritoneal macrophages were obtained from NMRI- and GFP mice. The animals were anaesthetised and decapitated. Then a portion of PBS was injected intraperitoneally. Macrophages were "forced" into the injected PBS by belly massage during 2 min before approximately 1.5 ml intraperiotoneal fluid was withdrawn with a syringe. The sample was centrifuged, and the cell-containing pellet was resuspended in 1 ml ice-cold erythrocyte lysis buffer (NH_4Cl 8.3 gram /l, $NaHCO_3$ 0.84g/ l and EDTA 29.3 mg/l, pH 7.4) for 5 min. The samples were then centrifuged and washed twice in serum free medium RPMI 1640, 1 ml each time. The cell suspension was resuspended in 1 ml medium and the cell concentration estimated using a haemocytometer. The samples were then diluted to ~1 million cells/ml. 200 μl of the cell suspension was seeded onto each 18 x 18 mm^2 glass cover slips (Menzel Gläser, Germany) in plastic Petri dishes. For time-lapse confocal microscopy, 200 μl cell suspension was seeded directly into plastic Petri dishes equipped with a glass window bottom. After two hours non-adherent cells were removed by washing in PBS before 2 ml of RPMI 1640 containing 2 % fetal calf serum was added. The cultures were maintained at 37°C in a humidified atmosphere of 93.5% O_2 and 6.5% CO_2.

3.6.2. Fibroblasts

Cells of the fibroblast cell line L929 were seeded onto nanowire-coated 18 x 18 mm^2 glass cover slips (Menzel Gläser, Germany) in plastic Petri dishes while control cells were grown directly in standard Petri dishes. The cell concentration was determined in a haemocytometer and diluted to 35 000 cells/ml in RPMI 1640 medium complemented with 0.5% fetal calf serum and antibiotics (50 IU/ml penicillin and 50 μg/ml streptomycin). The cells were cultured for 24 h at 37°C in a humidified atmosphere of 93.5% O_2 and 6.5% CO_2.

3.6.3. Dissociated DRG neurons

NMRI mice were anaesthetized and killed by heart puncture. The lumbar L6 –thoracic Th10 DRGs, were removed by dissection, and dissociated in a solution of 0.25% collagenase, in serum-free RPMI 1640 medium before suspended in serum-free RPMI 1640 culture medium supplemented with nerve growth factor (20 ng/ml). Two ml of the cell suspension was seeded onto nanowire coated 18 x 18 mm^2 glass cover slips (Menzel Gläser) in plastic Petri dishes. The cells were cultured for 72 h at 37°C in a humidified atmosphere of 93,5% O_2 and 6,5% CO_2.

3.7. Fixation

All fixation (see Table 1) was performed at room temperature (RT) and the fixatives used were:

- Paraformaldehyde (PFA), 4% in 0.1 M PBS, pH 7.2.
- Stefanini's fixative, 2% formaldehyde and 15% of a saturated aqueous picric acid solution in 0.1 M PBS, pH 7.2.
- Glutaraldehyde (GA), 2.5% in 0.15 M sodium cacodylate buffer, pH 7.2.
- Osmiumtetroxide (OsO_4), 2% in 0.15 M sodium cacodylate buffer, pH 7.2, for post fixation in transmission electron microscopy preparations.

After fixation all preparations were washed at least 3 x 5 min in the buffer used in the fixative.

Paper	Cell or tissue	Fixative	Fixation time
I	DRG	Stefanini´s + GA	2 h for both
II	Fibroblasts + dissociated DRGs	PFA	10 min
III	Macrophages	PFA	1 h
IV	DRG	GA	1 h
V	DRG	GA	1 h
VI	Sciatic nerve and DRG	Stefanini´s + GA + OsO_4	2 h, 5 h or 1 h

Table 1. *Overview of the fixatives and fixation times used in the respective papers*

3.8. Immunocytochemistry

All antibodies used in this thesis were diluted in PBS with 0.25% Triton-X and 0.25% bovine serum albumin (BSA). The primary antibodies were incubated with the preparations over night in at 4°C while the secondary antibodies were incubated at RT for different periods of time, see table 2 for details on antibody staining protocols.

Paper	Cells or tissue	Primary antibody	dilution	Secondary antibody	dilution	time
I	DRG	Rabbit-NF 200 (Sigma, USA)	1:200	Alexa 488 Goat-anti-rabbit (Molecular Probes, USA)	1:200	35 min
II	Dissociated DRGs	Rabbit-NF 200 (Sigma, USA)	1:200	Alexa 594 goat-anti-rabbit (Invitrogen, USA)	1:200	2h
III	Macrophages	F4/80 or IB4	1:200	Alexa goat anti rat	1:50	2h
IV	DRG	Rabbit-NF 200 (Sigma, USA)	1:200	Alexa 488 Goat-anti-rabbit (Molecular Probes, USA)	1:200	35 min
V	-	-	-	-	-	-
VI	Sciatic nerve and DRG	Rabbit-tubulin III (Santa Cruz, USA) mouse-ED1 (Serotech, England) rabbit-ATF3 (Santa Cruz, USA)	1:400	Alexa 488 goat-anti-rabbit Alexa 488 goat-anti-mouse (Invitrogen, USA)	1:400	2h

Table 2. *Overview of all Immunostaining including specimens, antibodies, concentration and incubation times used in respective paper*.

3.9. Cytochemistry

In paper II the microfilaments of the fibroblasts were stained using the fluorescent dye phalloidin. After fixation and rinsing, the cells were extracted with 0.1% Triton X-100 in PBS for 3-5 min. After additional rinsing in PBS containing 1% BSA, 200 µL of phalloidin (5 µL, 6.6 μM methanolic stock solution diluted in 200 µL PBS with 1% BSA, Alexa Fluor® 488 phalloidin, Invitrogen - Molecular probes™) was added to each cover slip. The cultures were incubated for 20 minutes at RT, washed once with PBS and incubated with bisbenzimide (1 mg/ml in PBS) during 10 minutes for nuclear counter staining. The preparations were finally washed twice with PBS.

In paper VI, all sections were counterstained with bisbenzimide. In paper III, the cultures

were stained for dead cells by propidium iodide (PI) (SigmaAldrich P-4170, Sweden). PI stains the nucleus of cells that have a disrupted cell membrane leaving healthy cell unstained. In this study, the macrophages were treated with PI at a final concentration of 5 μg/ml during 10 minutes.

3.10. Scanning electron microscopy (SEM)

After fixation and rinsing, the cultures were dehydrated in a graded series of ethanol (50%, 70%, 96% and 100%) before critical point drying. Finally the preparations were sputter coated with gold-palladium (~15 nm) before studied and photographed in a SEM (JEOL, JSM-5600 LV).

3.11. Transmission electron microscopy (TEM)

After fixation and post fixation, the tissue was separated from the chips and dehydrated in a series of ethanol (50%, 70%, 96% and 100%) and finally in acetone. The tissue was embedded in epon resin (epoxy based resin) over night, trimmed and sectioned on a microtome. The sections were mounted on copper grids and studied in the TEM (JEOL, JEM-1230).

3.12. Quantifying the guidance of cells and axons

Regarding guided single cells, as partly in paper II, the elongation of the cell gives a clear axis indicating the guiding direction. In paper II, I used the free software “ImageJ” for Mac OS X that may be downloaded at: http://rsb.info.nih.gov/ij/. The aligned fibroblasts at different areas on the patterned substratum and control surfaces, were analyzed using the fit ellipse function in ImageJ. This function replace each cell with an ellipse and give the lengths of the major and minor axis in addition to the angle of the major axis. Cells with a major/minor axis ratio <1,5 were considered round, and no direction could be measured. Such round cells were omitted in the alignment analysis, although counted. The deviation from the expected orientation (along the pattern of the substrate) was calculated and statistically tested against the control cells.

In paper I, we present a simple Fast Fourier Transform (FFT) analysis in order to quantify the guidance on different patterns. The FFT analysis was made using NHI-Image (version 1.63) equipped with a FFT-macro.

3.13. Statistics

When necessary, a two-way ANOVA was used for statistical analysis, followed by the Fisher PSLD *post hoc* test. The ANOVAs were performed on a Macintosh computer using the software "Statview 5.0.1", while the t-tests were performed directly with the Microsoft software "Excel". A p-value less than 0.05 was considered significant.

4. RESULTS AND DISCUSSION

Paper I. Axonal outgrowth on nanoimprinted patterns

In paper I, we investigated if axonal outgrowth was affected by nano-patterns (grooves and ridges) made in polymethyl-meth-acrylate (PMMA) covered silicon chips, manufactured by nano-imprint technology. The use of NIL has many advantages for biological purposes since it is cost- and time efficient so that many test surfaces can be produced. The resolution is not dependent on scattering or diffraction, therefore structures smaller than 10 nm are easily reproduced [51]. PMMA is a well-characterized polymer for NIL in our laboratory and a pilot study of axonal outgrowth (not shown) on PMMA indicated good growth rate for DRG axons. Therefore PMMA was chosen as substrate material.

To evaluate axonal outgrowth, adult mouse sympathetic (SCG) and sensory (DRG) ganglia were mounted on the chips close to the nano-patterns that were of two types, parallel grooves or ridges. The spatial features were: 300 nm deep grooves with varying widths of 100-400 nm. The pitch of the grooves was 200-1600 nm. Ridges (the inverted pattern) with the same sizes as the grooves were also tested. Seventeen different striped patterns with variable distances (pitch) between grooves or ridges were produced on the same chip in order to simultaneously test several dimensions. The seventeen testing areas were 200 x 200 μm squares with grooves or ridges in the polymer material (PMMA) (Fig. 15).

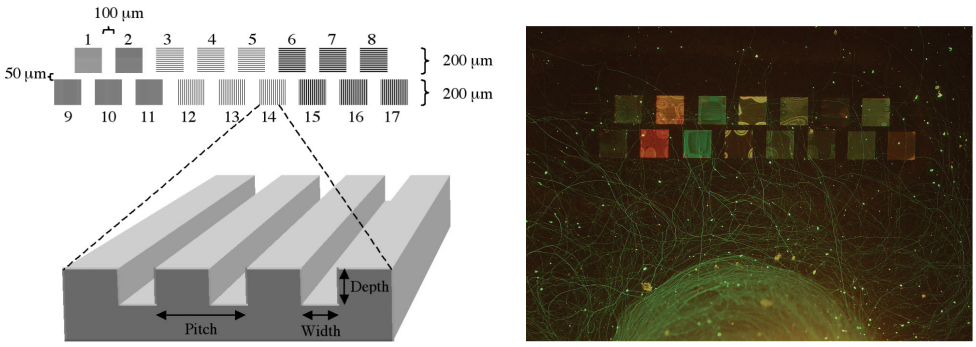

Fig. 15. *Left: The seventeen test areas had different pitches (200-1600 nm) and widths (100-400 nm) but the same depth (300 nm). Right: The different gratings resulted in interference patterns and hence different colors in light microscopy. The ganglion with fluorescently stained axons is clearly visible.*

The ganglia were cultured for 5-7 days on the chips, in medium containing 25 ng/ml of nerve growth factor to stimulate axonal outgrowth. Apart from sterilization in ethanol, the surfaces were not treated in any way before cell culturing. The aim was to study how topographical cues affected axonal outgrowth. After one week of incubation, axonal outgrowth was investigated using immunocytochemistry or SEM. At this time point an extensive outgrowth had occurred. The regenerating axons displayed contact guidance on all patterns, where most axons (diameter < 1μm) except for the thickest ones (diameter > 1μm) were found to align along the imprinted nanopatterns and consequently turned up to 90° as they entered the "testing squares" (Fig. 16).

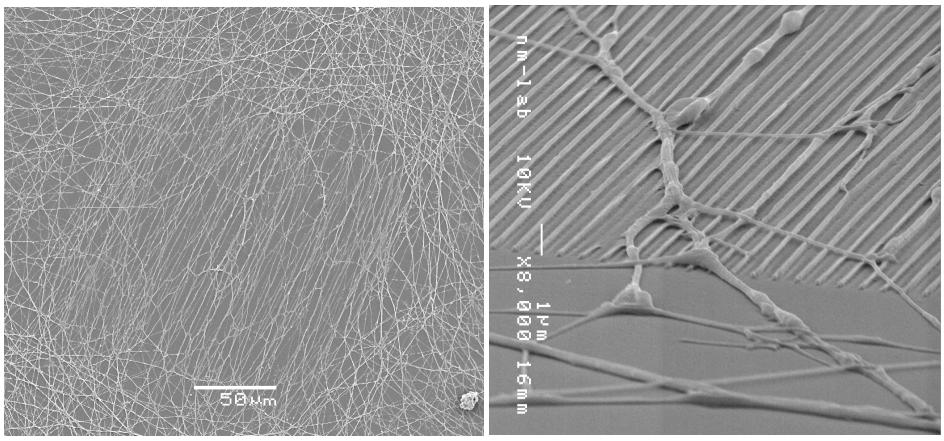

Fig. 16. *The regenerating axons aligned along the grooves and ridges (left and right respectively). The axons were also found to grow on the ridges rather than in the grooves (right).*

The efficiency of guidance appeared to be related to the diameter of the axons. One explanation to this behavior may be that larger growth cones, that may be somewhat related to the axon diameter, easily traverse the grooves. Furthermore, we found that the nerve cell processes preferred to grow on ridge edges and elevations in the patterns rather than in grooves, a seemingly claustrophobic behavior. This behavior has been reported before, but only for single cells (fibroblasts) on microstructures [65]. Our study is, to our knowledge, the first on axons. The finding that axons and whole cells behave in the same way when guided by substrate topography is interesting, although not surprising, and indicates a common mechanism for guidance. Thus, hypotheses regarding contact guidance of cells may also apply to axons. Previous studies have shown that cells prefer negative or zero radius curvature rather than positive ones, *i.e.* cells prefer to grow uphill rather than downhill [34,35]. This may explain why we did not observe any axons in the grooves; axons, like cells, thus seem to

refrain from turning downwards, even on nanometer sized structures. We also found that sensory nerve fibers (DRG) were guided by the nanopatterns in the same manner as the axons from autonomic ganglia (SCG), indicating that this may be a general behavior among neurons.

We cannot entirely exclude that other cues, in addition to topography, affect the guidance. The question is if, in this type of studies, guidance is solely due to the surface topography or if there is any influence of protein released from the ganglia or the gel used to mount them. Notably, we used no serum in the culture medium in order to minimize such chemical effects, and PMMA was in part chosen as substatrum material since it has been shown to adsorb proteins 5-10 times less that polystyrene [66].

We conclude that axons of peripheral neurons thrive on PMMA and extend axons, which can be guided by nano-patterns in the PMMA when the lateral features are 100 nm or larger. These findings could be taken advantage of for the construction of neuronal networks where ordered outgrowth, and connections to other neurons, can help understanding the signaling patterns between neurons within such networks.

Paper II. Magnetic nanowires for cell guidance

Paper II concerns contact guidance induced by magnetically aligned Ni nanowires *in vitro*. Here a new way to induce guidance of cells or cell processes using magnetic nanowires is presented. In paper I it was clear that square shaped grooves and ridges a few hundred nm wide, deep or high, induced contact guidance. The next question was whether cylindrical structures such as wires, in the same size range as the ridges studied in paper I had the same guiding effect.

Although the phenomenon of contact guidance on thin fibres has been known since the beginning of the 20th century [20] there are few studies on growth on nano-meter-sized fibres. In the previous studies, polymer-fibre matrices were mainly manufactured with the electro-spinning technique [67], and to our knowledge no studies concerning axonal and cell growth on magnetic metal nanowires have been presented before. Since magnetic nanowires can be maneuvered by magnetic fields, they have been suggested as connectors in microelectronic

systems [68]. Such wires are interesting for electrode purposes since their positions can be controlled and they are conducting, a characteristic that most polymer nanowires lack.

Magnetic Ni-nanowires (200 nm in diameter and 40 μm long) were manufactured using a template based electro-deposition method (Fig. 13 and 17). Drops, of a nanowire/ethanol suspension, were placed at glass cover slips. The nanowires were aligned in an external magnetic field (110-115 mT), and adhered by electrostatic forces such as van der Waals forces to the cover slips after evaporation of the ethanol. After the wires had adhered, the magnetic field was removed. L929 fibroblasts and dissociated dorsal root ganglia (DRG) neurons from mice were cultured on the nanowire-coated cover slips for 24 h and 72 h, respectively.

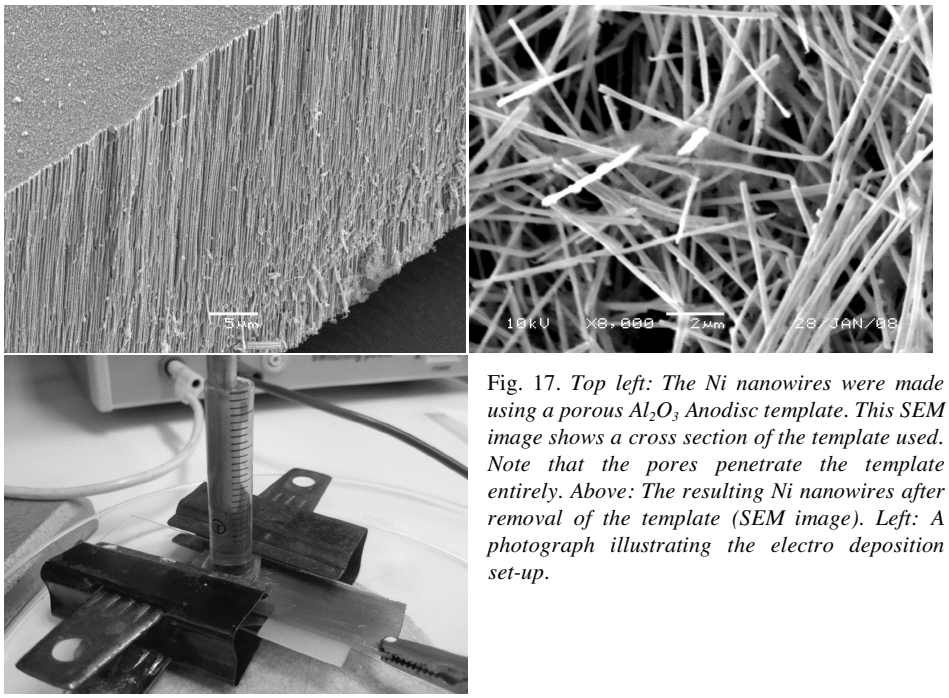

Fig. 17. *Top left: The Ni nanowires were made using a porous Al_2O_3 Anodisc template. This SEM image shows a cross section of the template used. Note that the pores penetrate the template entirely. Above: The resulting Ni nanowires after removal of the template (SEM image). Left: A photograph illustrating the electro deposition set-up.*

The fibroblasts were affected by the aligned nanowires and displayed contact guidance, *i.e.* they had an elongated morphology stretching along the nanowires. The fibroblasts cultured on smooth control surfaces or the ones found on areas outside the nanowires, had a flattened irregular shape. In addition, the regenerated axons displayed contact guidance on the wires (Fig. 18). In this case the axons aligned with the nanowires although the effect was most

clearly observed on densely packed nanowires rather than on dispersed ones. The guidance was quantified for the fibroblast cultures, using the software ImageJ, and found to be significant ($p<0.001$). It was clear that wires, in the same size range as the ridges studied in paper I, had a guiding effect on both axons and fibroblasts.

There were no overt signs of toxicity due to the Ni-wires. Although no toxic effect was apparent, Ni may be released from the nanowires, and thus the question of Ni toxicity was raised and is further discussed in paper III.

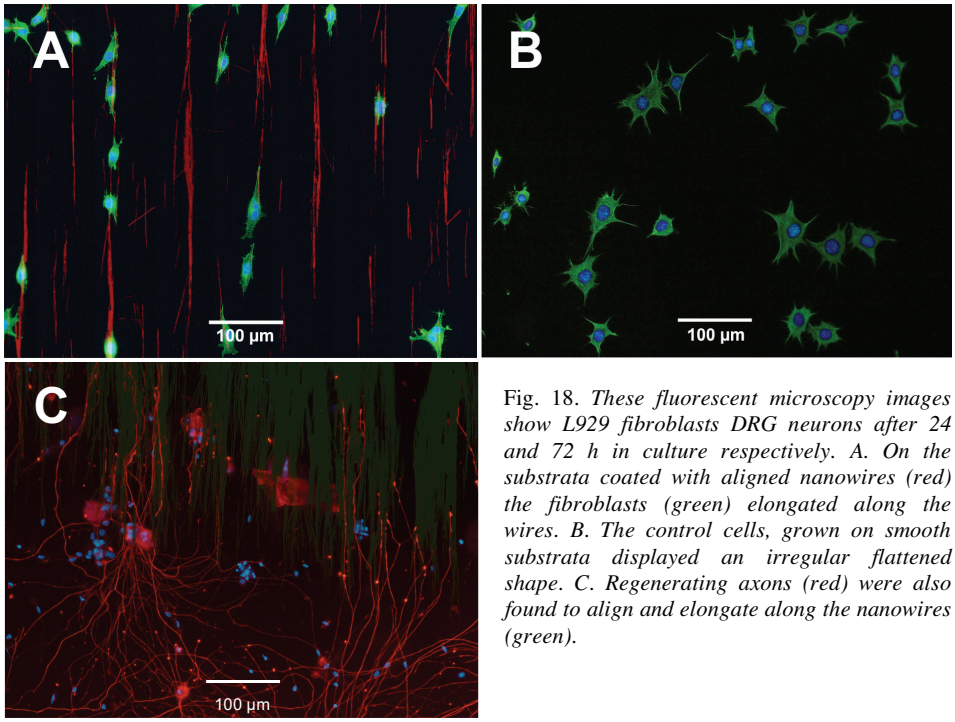

Fig. 18. *These fluorescent microscopy images show L929 fibroblasts DRG neurons after 24 and 72 h in culture respectively. A. On the substrata coated with aligned nanowires (red) the fibroblasts (green) elongated along the wires. B. The control cells, grown on smooth substrata displayed an irregular flattened shape. C. Regenerating axons (red) were also found to align and elongate along the nanowires (green).*

The nanowires aligned in the magnetic field, but alignment was not perfect. To optimize the cell-guidance on the wire patterns, the alignment of the wires could be improved. Parameters affecting the alignment have been extensively studied by others [69,70]. The alignment of wires is affected by the liquid flow during evaporation if the drag force exceeds the magnetic force of the external field. Furthermore, we found that an excess of nanowires resulted in aggregation due to magnetic interactions among the wires, resulting in alignment disturbances. The introduction of micro magnet arrays [71,72] may facilitate the production of highly complicated

although ordered, guiding patterns in real time without any predetermined lithographic patterning. This would enable a more dynamic way of testing guidance phenomenon on nanowires *in vitro* and would be valuable for the production of neuronal networks and cell patterns. Guidance of cells by externally controlled structures could find applications in many different fields, *e.g.* "lab on a chip" devices, medical nerve grafts or for the construction of tissue or organ like structures in vitro, including neuronal networks. Moreover, the possibility to combine different metals along the wire, *e.g.* Au-Ni-Au, and also chemically functionalize the different parts of the wire, makes magnetic nanowires highly interesting for nanobiotechnology approaches [71,73,74]. One could imagine systems with differently functionalized and aligned wires that attract different sub-populations of axons within a nerve and guide them to spatially separated electrodes. This would enable stimulation of axons of different modalities a possibility highly attractive for a new generation of prosthesis with built in receptors for *e.g.* heat and pressure. Magnetic nanowires could also be used to direct an implant with ordered cells to a specific location in the body.

Paper III. Nanowires induce activation of macrophages

In paper III, the macrophage reaction to nanowires made of different materials and was tested both *in vitro* and *in vivo* in an attempt to unravel how the innate immune system was affected by free nanowires.

Resident intraperitoneal macrophages from mouse in explant cultures were exposed to nanowires made of polystyrene (PS), nickel, gold and gallium phosphide (GaP). The PS, Ni and Au nanowires were all produced by a template-based method, using commercially available porous alumina membranes and had a diameter of approximately 200 nm and lengths in the range 5-60 μm. The nanowires produced via epitaxi, had a diameter of 50 nm and an approximate length of 2.5 μm.

All types of nanowires activated the explanted macrophages as visualised by changes in morphology after explantation. However, the degree of activation was different. The macrophages tried to engulf the wires and some perished in these attempts, reducing the number of macrophages in the exposed cultures and increasing the number cells which accumulated PI. Plastic wires however, had no significant effect on cell death.

Injections of both the plastic and the metallic nanowires intraperitoneally increased the number of macrophages, which could be harvested from the animals three days later, a classical sign of macrophage activation.

Taken together, the results show that large aspect ratio nanostructures like nanowires cause activation of an inflammatory response *in vivo*, but the response is dependent on the type of nanowires used. Furthermore, from time-laps movies (not shown) we have observed that the cells react quickly to the nanowires and begin to phagocytose them within minutes from exposure (Fig. 19).

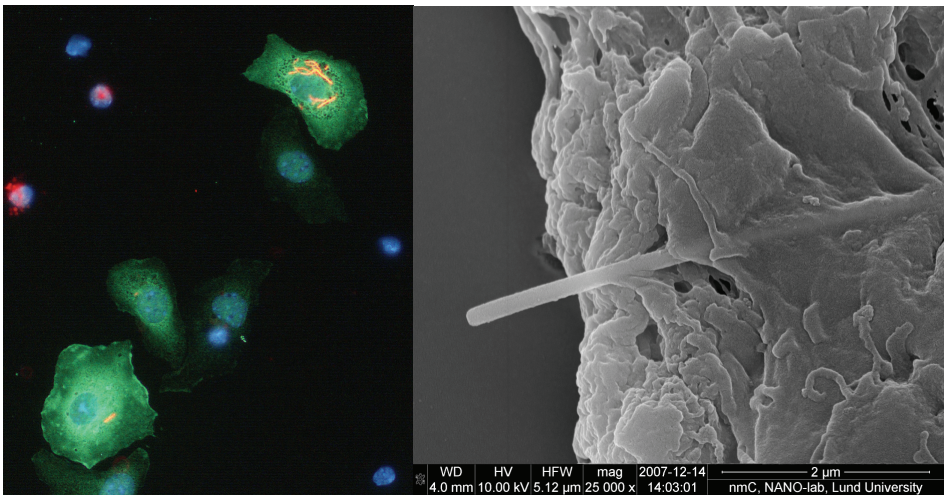

Fig. 19. *Left: Macrophages from GFP mice were green fluorescent and the DiI labeled polystyrene nanowires can be easily detected, also after phagocytosed by the cells. Right: Often the nanowires were found to penetrate the membrane. Here is a Ni nanowire pointing out from a macrophage (SEM image).*

The least activating wires were the plastic ones, perhaps this is a combination of their chemistry and the Young´s Modulus of Elasticity for PS. PS is much softer than metals or crystal materials (~$3x10^9$ Pa for PS as compared to >$7x10^{10}$ Pa for metals and crystalline materials) and can, as observed in the microscope and in time-laps movies, be bent by the phagocytosing cells.

Ni was found to induce cell death to a larger extent than the other wires. This might be due to the release of Ni from the wires, manifested as a toxic effect on the cells. It may also be explained by the very high Young´s Modulus of Elasticity, *i.e.* the stiffness of Ni (Ni is ~20 times stiffer than Au). Such hard and sharp materials may be difficult for the cells to

internalize during phagocytosis, a phenomenon observed in the time-laps movies. We often observed wires penetrating the cells after phagocytosis. This is an observation that indicates that the extremely elongated shaped wires in combination with an inflexible material may be harmful for phagocyting cells.

Our finding that nanowires activate macrophages is important and pertinent to health hazard issues. The wires are similar in size and structure, at least the metallic ones, to asbestos fibers, a known stimulator of inflammation and a carcinogen. Considering the increased industrial use and production of nanostructures, health hazard posed by nanostructures should be regarded as an area of major concern.

Paper IV. "Guidance of neurons on porous patterned silicon is pore size important?" and **Paper V. "The influence of porous silicon on axonal outgrowth *in vitro*"**

These studies started with a pilot study (paper IV) strongly indicating that pore size of porous silicon (pSi) is a crucial feature for axonal outgrowth and guidance. Paper V was designed, based on the findings in the pilot study, and hence both papers are discussed together.

We quantified the haptotaxic effect of different pore sizes (diameters from 100 nm to 1500 nm) on axonal outgrowth (Fig. 20). To this end DRG explants were cultured on alternating stripes of porous and smooth Si without any previous priming with proteins. The stripes were wide, 20-50 μm, so that the discontinuities between smooth and porous areas, that might induce contact guidance, would not be a significant factor. Serum free RPMI-1640 culture medium, containing 20 ng/ml NGF in order to stimulate axonal outgrowth, was used and the whole-mounted preparations were incubated for 7 days (Fig. 21).

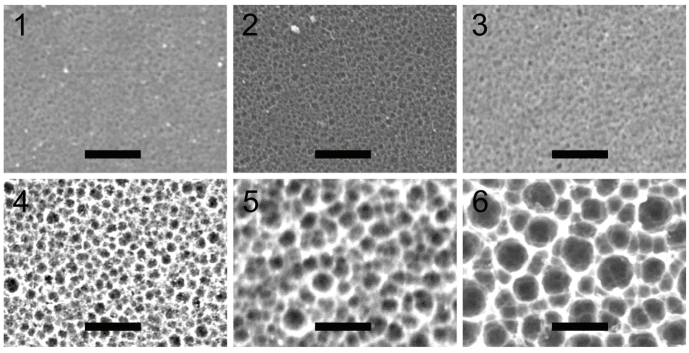

Fig. 20. *These SEM images show the porous morphology of the surfaces used in paper V. The average pore sizes are: 100, 150, 200, 500, 1000 and 1500 nm respectively. Scale bar 2 µm.*

The goal of the study was to determine if there was an optimal pSi pore size, for axonal guidance and elongation. The main finding was that axons exhibit a haptotaxic behavior and preferentially elongate on porous silicon within a limited range of pore sizes. Axons are attracted to 150-500 nm sized pores while larger and smaller pores have no such effect (Fig. 22). Thus, there is both a lower and an upper, topographically determined, haptotaxic limit. The optimal pore size for axonal outgrowth is therefore suggested to be in this interval.

Interestingly, Karlsson *et al.* 2004 found a lower activation of adherent neutrophils on Al_2O_3 with 200 nm wide pores as compared to 20 nm wide pores [75]. This suggests that cells, other than neurons, also display a change in reaction to porous topographies when grown on pore sizes similar as ours and therefore porous surfaces with right pore sizes may be considered biocompatible.

The mechanism responsible for this different haptotactic behavior is not yet known. Our hypothesis is that on "large pore" surfaces, fewer edges are available for protein adhesion (different physical chemical properties) as compared to small pore surfaces (although still better that smooth bulk surface). Since proteins are essential for strong cell adhesion, less protein coverage offers fewer axonal attachment points, and therefore axonal outgrowth is crippled. This idea points in a direction where smaller pores are always better, but at some point this larger edge area may not be available to more proteins. Large proteins, *e.g.* laminin that is around 50 nm wide, may simply sterically prevent more than a few molecules to adsorb onto the edge of a small pore, even though the attractive edge area could have more possible anchor sites.

A more geometrical hypothesis is that, longer distances between possible adhesion areas make it less probably for axons (filopodia) to find suitable anchor places. However (as in the hypothesis above), since small pores exhibit more edges, why are not the smallest pores the best? This may be due to the fact that these pores are small enough to be geometrically considered as a flat surface by the regenerating axon. Further experiments are required to reveal the mechanism responsible this behavior.

It has previously been shown that cells prefer pSi and show better viability as compared to smooth Si [16,76,77], but the pore size influence has not been investigated in detail and the majority of studies are made on pores smaller than 150 nm, *i.e.* smaller than our smallest

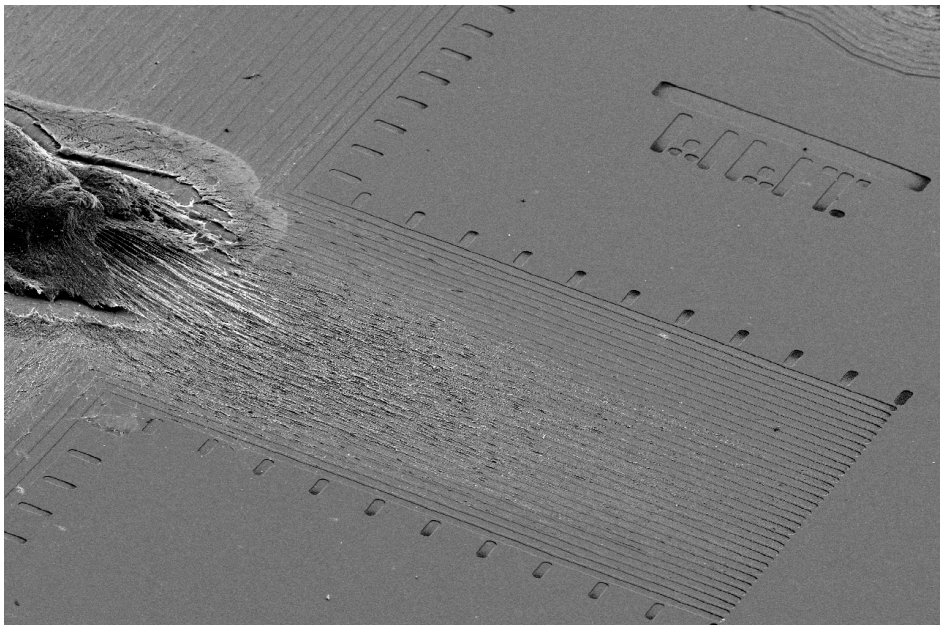

Fig. 21. *In this SEM image, the DRG with extending axons, the matrigel edge and the patterned substrate are clearly visible, illustrating the experimental set-up. Note the etched scale bar representing 1 mm.*

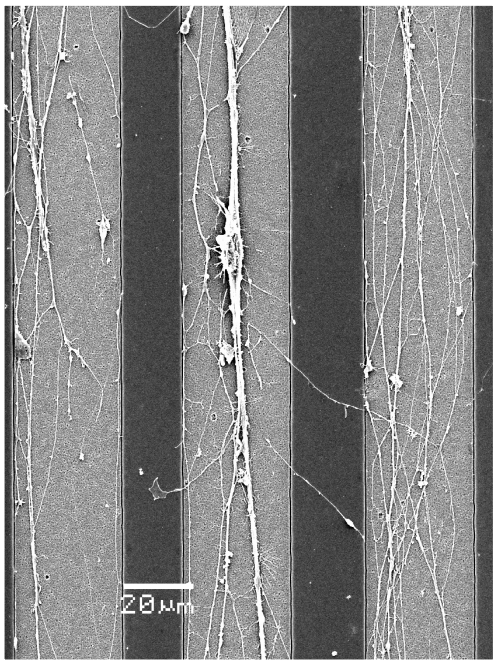

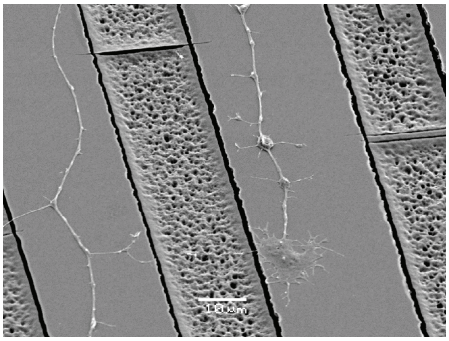

Fig. 22. *The generating axons were attracted to porous surfaces with dimensions of 150-500 nm (left) while larger and smaller pore sizes were not as attractive (right). Note that in the left picture, there is also a migrating, elongated cell that might be a Schwann cell or a fibroblast.*

pores. Interestingly, Sapelkin *et al*. 2006 [78] reported that cell bodies of the neuronal B50-cell line showed clear adhesion preference on porous (50-100 nm average pore size) areas as compared to smooth Si surfaces. Our report indicates that axons have no such selectivity, or even the reverse, for pSi with pore size around 100 nm. It may therefore be hypothesized that the mechanism that make cell bodies attach to surfaces in an acute adhesion phase differs from the way axons attach during regeneration. However, there may be different cellular responses on pores <100 nm and pores >100 nm and with no overlap, it is difficult to make any conclusions.

We conclude that, for pSi there is a certain pore size range (150-500 nm) that is optimal for regenerating axons, *i.e*. the axons prefer to elongate on these structures as compared to smooth surfaces such as bulk silicon. PSi is a suitable electrode material [60], can be used for drug delivery [79] and the finding that it also can be utilized also for guidance, propose pSi as a candidate for a multifunction bio-implant.

VI. Porous silicon a potential electrode material in a nerve repair setting - tissue reactions

Paper VI describes nerve regeneration across pSi and smooth Si, and how the inflammatory response develops to pSi when implanted in a nerve repair setting *in vivo*. A silicon chip, with one smooth (control side) and one porous side, inserted into a silicone tube was used to bridge a 5 mm defect in the rat sciatic nerve (Fig. 23). Thus, a kind of entubulation repair was used. Six or twelve weeks later, new nerve structures surrounded by a perineurium like capsule, had formed on each side of the chip. The pore size chosen was approximately the same (~1 μm) as those used in a similar study outside the nervous system, where the tissue reaction to different structured surfaces implanted subcutaneously was investigated [80,81].

Fig. 23. *This picture from the implantation of the chip display the silicone tube with the pSi chip visible inside. The tube connects the cut ends of the sciatic nerve of the rat. Note the sutures that fixate the nerve ends in the tube.*

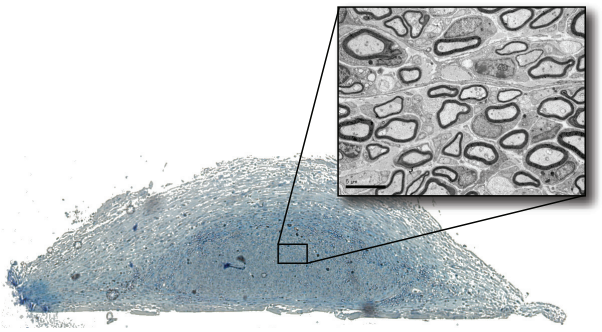

Fig. 24. *This cross section, stained with toloudine blue, shows the typical dome-shaped appearance of the new nerve from one side of the chip. Note the area with regenerated axons (dark blue) and the connective tissue surrounding the axons. The width of this section is approximately 1,8 mm. The inserted transmission electron microscope image illustrates the normal looking axons within the new nerve. Note the myelinisation of several axons.*

The regenerated nerve looked "normal" with both myelinated and unmyelinated axons (Fig. 24), it also contained blood vessels, macrophages, fibroblasts and connective tissue. The number of regenerated nerve fibers did not differ on either side of the chip as shown by immuno-staining for neurofilaments. However, the capsule of fibroblasts that had formed in contact with the chip was significantly thinner on the porous side than on the smooth side. Such a difference has also been observed for implants of pSi and smooth Si subcutaneously [80]. The thickness of the capsule around the nerve structure decreased over time, probably due to the maturation of the dense fibrous capsule.

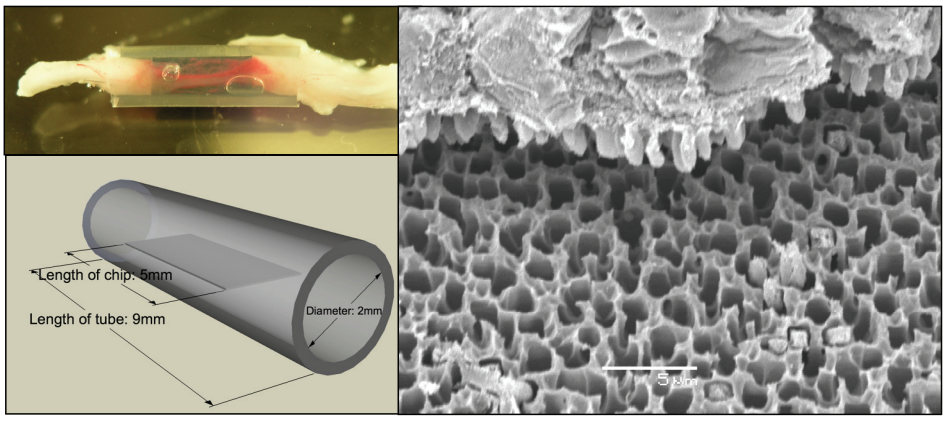

Fig. 25. *After 6 or 12 weeks, the tube where dissected out from the rat (top left). The tissue that had attached very firmly to the porous surface was removed from the chip (right). The chip and tube sizes are illustrated in the drawing (lower left).*

Interestingly, cellular protrusions and/or extra cellular matrix had formed on the pSi side and the nerve structure was found to attach firmly to this surface (Fig. 25). As contrast, on the smooth silicon surface the tissue did hardly attach at all and was very easy to remove.

We also studied the capsule formation where the tissue where in contact with the silicone tube. Here we also found differences in capsule thickness. The capsule opposite to the porous side was found to be thicker than the one on the smooth side. We suggest that this may be due to the friction and shear forces induced by movements of the chip within the silicone tube. On the porous side of the chip where the tissue was firmly attached (Fig. 25), the friction and shear forces are concentrated at the silicone tube interface resulting in more encapsulation as compared to the smooth side. On the smooth side the friction and shear forces are more evenly distributed to both the chip and the silicone tube interface resulting in less encapsulation towards the tube.

Immuno-staining for invading macrophages (ED1) showed a foreign body reaction mainly within the 40 μm thick interface layer in contact with the chip surface (Fig. 26). Macrophages were however also present in the entire tissue, although in lower numbers. The number of macrophages decreased over time perhaps due to formation of a more rigid capsule that reduced the stimuli from the implanted chip.

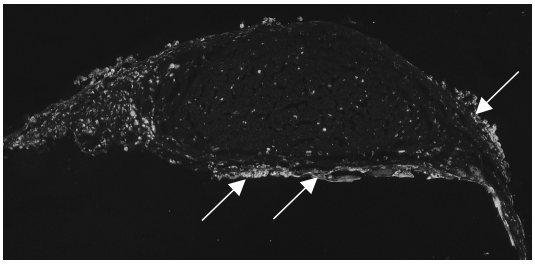

Fig. 26. *The Immunostaining of the invading macrophages (ED1 positive cells) revealed a higher number of macrophages at the interfaces toward the silicon chip and the silicone tube (arrows), as compared to the interior of the new nerve structure. The width of this section is approximately 1,5 mm.*

We conclude that a pSi surface, due to its large surface area, diminished inflammatory response and promoting firm adhesion to the tissue, should be a good material for the development of new implantable electronic nerve devices. It has been demonstrated that electrodes in the brain, tethered to the skull induce more glial scar tissue than untethered electrodes [82]. A part of this problem may be due to movements at the tissue/chip interface and the use of structured implants such as pSi could overcome this problem.

5. GENERAL DISCUSSION

5.1. Differences between *in vitro* and *in vivo*

Most of the work performed in this thesis, have been performed *in vitro*. As one would expect, the results from studies in such reduced systems may not apply in an *in vivo* setting where the interactions between different cell types and the chemical environment is more complicated. This was for instance obvious in paper VI. Here the regenerating axons did not grow in direct contact with the pSi chip surface as in the *in vitro* experiments. This could be due to several mechanisms such as fibrin matrix assembly, extensive adhesion of serum proteins on the chip surface and invasion of macrophages, events that are not present *in vitro*. Even in CNS incapsulation is relevant, with astrocytes shielding implanted electrodes as reported by Biran *et al.* 2007 [82]. For future experiments it cannot be excluded that manipulation of the inflammatory response would allow axons to grow on the chip surface also *in vivo*. The advantage with an in vitro system is that the environment can be controlled so that molecular mechanisms can be studied using pharmacological means.

Despite the difference between *in vitro* and *in vivo*, we have indeed demonstrated that pSi can be a suitable implant material *in vivo,* based upon the finding with the firm interaction with regenerating tissue resulting in low immune response. At the same time, pSi has nice cell adhesion and guiding properties for applications *in vitro*.

5.2. Quantifying alignment of cells and axons

Quantifying the alignment of cells is usually easy since they change their morphology according to the topography, and become elongated as in paper II. Then the direction of alignment for each cell is usually very clear and can be measured.

In the case of guided axons, the length scale is much different and the axons have a wandering behavior. Even if an axon shows clear contact guidance, it may sometimes change to an adjacent ridge. This wandering behavior, makes it difficult to quantify the alignment of individual axons and a more macroscopic, overall method must be adopted. In paper I, a Fourier transform was used to analyze large areas with aligned axons.

The basic idea of Fourier analysis is that any graph, or pattern, can be described as a sum of sinus and cosinus functions. This means that when scanning a pattern of different intensities, *i.e.* axons growing on a surface, the frequency of finding an axon can be described by a mathematical function. On a perfectly aligned pattern (straight lines) one would find a set of discrete frequencies when scanning perpendicular to the lines while scanning along the axons would generate no frequencies at all, since the intensity is not changing along the pattern (Fig. 27). In this way the axons growing on the nanopatterns in paper I were scanned in all directions looking for discrete frequencies. The most prominent frequency found was used as a measurement of the total alignment on the pattern in question, although the direction of the axons will of course be perpendicular to the scanning direction (Fig. 28).

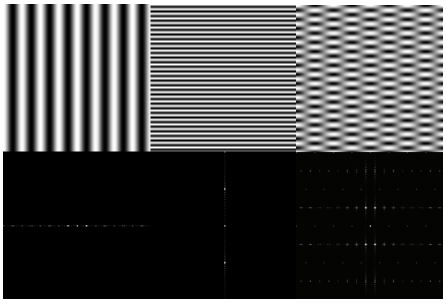

Fig. 27. A Fast Fourier Transform (FFT) was used for alignment analysis. For illustration, regular cosinus-patterns (top) result in discrete frequency peaks after the FFT (bottom). Note the frequencies that are found in two dimensions in the right images.

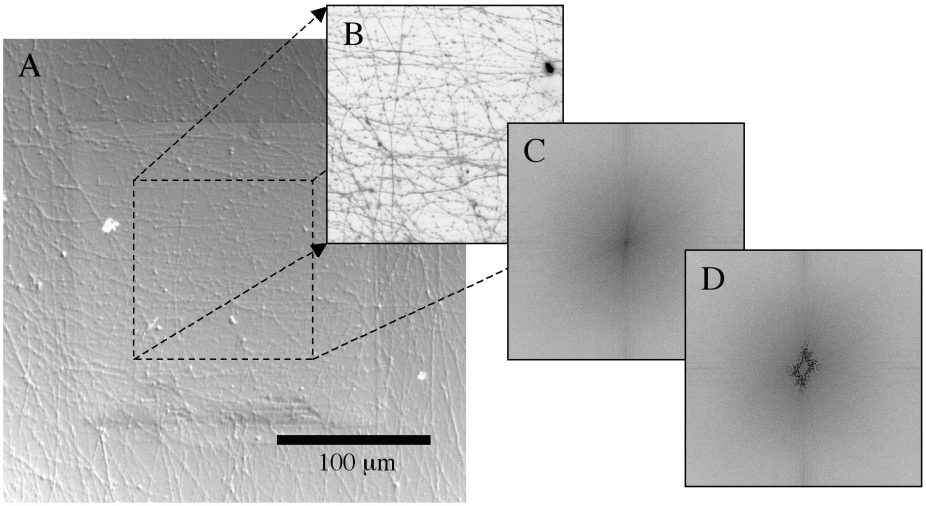

Fig. 28. For axons on a surface (A and B), analyzed by Fast Fourier Transform (C), a regular pattern such as guided axons along grooves can be detected. An ellipse shaped pattern in the frequencies space (D) will be a measurement of the average alignment in the image. A more elongated shape would indicate better alignment and thereby better aligned outgrowth.

5.3. Brief summary of cell reaction to nanostructures

Our results in paper I, II, IV and V, add novel knowledge as to that found in the literature regarding guidance of axons and cells by nanostructures. We have shown that sensory and autonomic axons from mice and L929 fibroblasts detect and align along nanometer-sized grooves, ridges and nanowires. We have furthermore demonstrated that the pore size of porous silicon is important for the outgrowth of axons on such structures.

The cell responses to alterations in surface topography, down to the micrometer scale have previously been documented especially for grooved topographies [20,24,83,84]. Most cells follow the discontinuities of grooves and ridges, and attain an elongated shape due to surface induced rearrangements of the cytoskeleton [24,26,47]. Grooved surfaces also induce changes in transcription and the up and down regulation of several genes [85], but the explicit mechanism for cell guidance has yet to be clarified.

The development of techniques to produce surface structures in the nanometer range has revealed that cells respond also to such surfaces. Macrophage-like cells can react to steps in the single nanometer range [25] and endothelial and fibroblast cells are sensitive to patterns with features down to 10 nm [86,87]. Cell extensions such as fibroblast filopodia have been found to respond to nano-topographies [87,88]. The importance of symmetry or discontinuity of the nanometer patterns has also been pointed out [89]. However, few studies have so far been performed on neurons and their axons to nano-patterned substrata although Rajnicek et al [90] reported that CNS neurites were guided by shallow (14 nm deep and 1 μm wide) grooves. Contact guidance of chicken DRG neurons on single scratches (0.1-0.2 μm wide), has also been reported by Stepien and coworkers [91]. *In vitro* studies off cultured cells on pSi have shown good cell adhesion and viability [16,77] and Ni nanowires for cell separation studies, with internalized wires, have been demonstrated [72,73,92,93] although no guiding properties have been investigated before.

5.4. Choise of substrate materials

For an implant like a BMI, not only the topography but also the chemical composition of the implant is important. This is true also for *in vitro* experiments where toxicity and transparency have to be considered.

5.4.1. Polymer for nanoimprinting

For biological purposes polyesters have many desirable features. Polyesters are relatively hydrophilic as compared to the standard Petri dish material polystyrene, where surface manipulation *i.e.* addition of oxygen by plasma treatment, must be conducted before cell culturing. Furthermore, polyesters are transparent, and therefore well suited for microscopy using inverted microscopes [9]. The polymer chosen for paper I, is a polyester called polymethyl-meth-acrylate (PMMA) commonly known as bone cement for orthopedics or plexi glass. The use of PMMA in orthopedics and as contact lenses (Fig. 29) encouraged us to use PMMA in this study. Furthermore, it is a common photo resist in lithographic processes and has well documented features and compatibility with most lithographical processes.

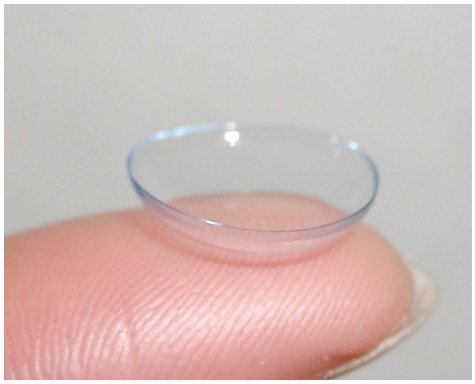

Fig. 29. *Polymethyl-meth-acrylate (PMMA) is commonly used in contact with the human body. Examples are hard contact lenses (left) and bone cement in orthopedics. (Image downloaded from "Wikipedia commons" free to use under the GNU Free Documentation Licence.)*

In contact guidance studies on grooves and ridges it is believed that some edge effects due to geometrical restrictions of the polymer, *e.g.* concentration of charges, may be present. This should occur even if the material is perfectly isotropic. Therefore, chemical interactions through biochemical patterning can never be excluded, but perhaps minimized by choosing a substrate that adsorbs small amounts of proteins. PMMA is therefore a reasonable choice since it has been shown to adsorb proteins 5-10 times less that polystyrene [66]. The drawback of PMMA and most other polymers (except for conducting polymers) is that they are insulators and therefore not useful as electrode material.

5.4.2. Porous substratum

Finding a suitable surface for an interface between cells and electronics was one of the driving forces for this thesis. Silicon is still the "working horse" in electronics and microfabrication and most processing techniques are suited for Si. Planar Si is not intended for cell culturing or implantation why a surface modification is necessary. The use of pSi may therefore enhance the biological interfacing properties with Si and the biocompatibility of pSi have also been shown to be good, as compared to smooth Si [80]. Therefore pSi was chosen as substrate in paper IV, V and VI.

The drawback of pSi and Si for *in vivo* applications is the rigidity of the material with an E-modulus of ~10^{11} Pa as compared to *e.g.* rubber that have an E-modulus of 10^7 Pa. For implant applications, mimicking the mechanical properties of the surrounding tissue is usually a good idea. Since soft tissue in an organism is much softer than soft artificial materials such as rubber, Si would probably be too rigid to mimic any biological tissue. Still, in combination with other materials it may be interesting for *in vivo* applications. The advantages of pSi are in particular the anchoring ability, the large surface area and the ability of making it electrical conducting.

5.4.3. Nanowire materials

In paper II and III, nanowires were used, either bound to a surface or in suspension with the cells. In paper II the nanowires were made of Ni that was chosen for its ferromagnetic properties. Other ferromagnetic elements such as Co were considered, but were ruled out due to processing techniques and possible negative effect on cell viability [94].

In paper III we used Au, polystyrene (PS) and GaP nanowires in addition to the ones made of Ni. Au was chosen because it is regarded an inert metal that could serve as control to the Ni nanowires. Polystyrene that is used in Petri dishes for cell cultures is a polymer, and softer than metals and could therefore be used to test if there was any effect due to rigidity. Furthermore, it is non-toxic and compatible with the processing technique and was therefore used. Finally GaP, that is a III/IV semi conducting material, was picked since there have been studies on the interaction of GaP-nanowires and neuronal cells [95,96], and the production technique narrows the materials of choice.

6. GENERAL CONCLUSIONS

- Neurons extend processes on nanostructured surfaces and such structures can be used for axonal guidance. Nanoimprint lithography is a suitable technique for preparing such nano-structured cell culture substrates. Axons from the peripheral nervous system of mice, detect and align along nanometer-sized grooves and ridges imprinted in PMMA *in vitro*.
- Magnetically aligned Ni nanowires can be used to guide axons from the peripheral nervous system of mice and L929 fibroblasts *in vitro*.
- Nanowires of different materials and sizes activate macrophages both *in vivo* and *in vitro*. *In vitro*, Ni-, Au-, PS- and GaP-nanowires in suspension are phagocytosed by macrophages within minutes. Metallic nanowires cause cell death.
- Porous silicon *in vitro* can induce a haptotactic response of axons from the peripheral nervous system of mice. The haptotactic response is related to the pore size of the surface so that a range of pore sizes attracts, and thereby guides axons.
- Porous silicon *in vivo* appears to be a good material for nerve implants, generating less of an inflammatory response than smooth silicon in a nerve repair setting.

7. ACKNOWLEDGEMENTS

The work presented in this thesis was carried out mainly at the division of animal physiology and zoology, at the department of Cell and Organism Biology, but also at the department of Electrical Measurement and the department of Solid State Physics. I wish to acknowledge a few persons that have made my time as PhD student fun and memorable on a more or less every day basis:

Martin Kanje, my supervisor who is always enthusiastic and sees the good things in life. Thanks for all scientific guidance and good times along the road to finish this tiny little book. **Lars Montelius**, supervisor during my diploma work, who one day a long time ago, asked if I wanted to grow some cells on imprinted surfaces instead of doing a more traditional physics project, thank you! **Nils Danielsen**, my co-supervisor who always has something wise to say. He has also given me a different angle to many medical issues. **Marie Adler-Maihofer** and **Inger Antonson** for helping me with all the difficult animal related work, I could have done nothing without you. I am also grateful for your company in the lab. **Erik Hallberg** and **Rita Wallén,** who has taught me everything regarding electron microscopy. Especially thanks to Rita for the company during the lab-work. **Marianne Andersson** and **Margaret Payne Sykes** who make sure everything work as it should regarding contracts and economy. A special thank you to **Eva Dahlberg**, who takes care of everyone and bring cake! All my old and new colleagues: **Anna**, **Hamid, Martina, Cicci, Johanna, Lisa, Shahram, Sofia** and **Kersti,** thank you and good luck. My roommates over the years: **Charlotta**, **Louise**, **Veronica**, **Erica** and **Catja** for your kindness and all the fun moments! **Per**, my old roommate and friend, It would not have been such a nice journey without your sense of humor, caring manner, and the fact that you are a living dictionary. Also thanks to **Bodil**, **Johan**, **Leif**, **Anders**, **Stina**, **Björn**, **Stefan** and last but not least **Lasse** for interesting discussions. At the department of electrical measurement my greatest appreciations are to **Walle**, who showed and helped me with all clean room techniques, also **Anton**, **Martin**, **Mikael**, **Andreas**, **Marcus** and everyone else who have joined me in the lab and on the floor-ball court shall not be forgotten. I would also like to express my gratitude to the people at solid stat physics, **Christelle** and **Waldemar** for all science and non-science discussions, **Patrick** for all the fun we had in the lab and elsewhere. Also thanks to **Sara**, **Mariusz**, **Ivan**, **Richard** and especially **Jonas**, who came up with the FFT analysis idea, something he has not got enough credit for. Friends outside the lab, no names none forgotten.

For all help and support, not least during the writing of this thesis, I want to thank my and Ulrica´s relatives and especially my mother, father and brothers who always support me – I love you.
Finally, I wish to express my endless love for my wife **Ulrica** my daughter **Filippa** and my son **Fabian**. You are the joy of my life!

8. POULÄRVETENSKAPLIG SVENSK SAMMANFATTNING

De medicintekniska framstegen har under de senaste decennierna varit stora, inte minst utvecklingen av olika implantat som pacemakers, höftproteser och cochlea implantat. För alla implantat är gränsytan mot kroppsvävnaden, det vill säga våra celler, helt avgörande för hur implantatet kommer att uppfattas av kroppen. Om implantatet inte är vävnadsvänligt kommer det att stötas bort eller kapslas in, vilket försämrar dess funktion avsevärt, inte minst för olika typer av sensorer, som till exempel elektroder avsedda för kontaktering av nervsystemet.

Inom ramen för denna avhandling, som består av sex delarbeten, har jag studerat hur nervcellsutskott uppför sig när de odlas på nanostrukturerade ytor. Storleksmässigt rör vi oss i området 100 till 1500 nanometer. Ett typiskt hårstrå är cirka 70 mikrometer, en cell 10-20 mikrometer och det går 1000 nanometer på 1 mikrometer som jämförelse. Jag har också studerat hur makrofager, en del av kroppens immunförsvar, reagerar på nanostrukturer i suspension och undersökt hur en nanostrukturerad yta påverkar läkning/regeneration av Ischiasnerven i en råtta.

Avsikten med avhandlingen var att förstå vilka topografiska faktorer som styr nervceller och deras utskott och samtidigt finna optimala ytor för bioimplantat, speciellt sådana som kan implanteras i nervsystemet. Sådana ytor kan även användas för att konstruera konstgjorda, odlade neurala nätverk.

Jag har använt olika tekniker för att framställa de nanostrukturer på vilka jag sedan odlat nervcellerna. I första arbetet trycktes nanostrukturerna (åsar och diken) i en plastyta med motsvarande teknik som CD/DVD skivor framställs. På dessa plastytor odlades sedan sensoriska nervceller. Det visade sig att nervcellernas utskott linjerade upp sig längs med åsarna eller dikena som var så små som 100 nanometer. Vi visade därmed för första gången att nervcellsutskott kan guidas av topografiska strukturer på nanometernivå det vill säga att celler reagerar på strukturer i storleksordningen 100-800 nanometer. I arbete nummer II, tillverkade jag magnetiska nickelnanopinnar med en diameter av 200 nanometer. Dessa orienterades med hjälp av en extern magnet och då pinnarna torkat in på en glasyta, odlades nervceller men också fibroblaster, en typ av celler som normalt tillverkar bindväv i kroppen på ytor med Ni-pinnarna. Även här linjerade nervcellsutskotten och fibroblasterna upp sig

längs med nanopinnarna. Detta är en ny intressant tillämpning. Med hjälp av magnetiska nanopinnar kan man alltså styra både celler och axoners utväxt. En ny teknik som kan finna tillämpningar inom flera grenar av bioteknikområdet.

Då konstgjorda nanopartiklar av olika slag blir allt vanligare, och de pinnar vi använde är nålformade och liknar asbestfibrer på många sätt, frågade vi oss hur celler reagerar på lösa nanopinnar. För att testa detta (arbete III) tillverkade vi, förutom nickelpinnar, även nanopinnar av guld, plast och galliumfosfid, ett ämne som förekommer i lysdioder. Dessa pinnar tillsattes till en odlingsskål med makrofager, som är en del av vårt försvar mot främmande kroppar. Makrofagerna reagerade genom att skyndsamt äta upp pinnarna, en helt adekvat och normal reaktion mot något främmande. Makrofagerna hade alltså aktivetrats på ett sätt som liknar reaktionen vid en bakterieinfektion. Sedan visade det sig att de hårda metallpinnarna var så svårsmälta för makrofagerna att många av dem dog i sina försök att oskadliggöra pinnarna. Detta var inte fallet med nanopinnar av plast. Vi drog slutsatsen att styvhet och form kan påverka skadligheten (graden av makrofagaktivering) hos en partikel, och att nanopinnar i den storleksordning som vi använde, dvs. 200 nanometer i diameter och några mikrometer långa, bör hanteras försiktigt tills de exakta skademekanismerna är fastslagna.

Resten av arbetena (IV, V och VI) inriktades på kisel och framför allt på poröst kisel. Kisel är det absolut vanligaste materialet för integrerade kretsar då det går att dopa, det vill säga ändra den elektriska ledningsförmågan, och kan därför även vara ett lämpligt material för implanterbara elektroder ämnade för forskning eller medicintekniska tillämpningar. Ytan hos kisel som används för integrerade kretsar är helt slät, vilket visat sig vara ofördelaktigt för levande celler och vävnad. Därför etsades kiselskivorna så att vissa områden fick en porös, tvättsvampsliknande yta, vilket innebär att man får en ytförstoring, en fördel för till exempel elektroder.

På sådana kiselchips odlades sedan nervceller som tidigare. Det visade sig att utskotten från nervcellerna föredrog att växa på de porösa områdena, men främst då porstorleken var mellan 150 och 500 nanometer (arbete IV och V). För att undersöka materialets biokompatibilitet i en nerv opererades porösa chips in i avklippta nerver hos råttor (arbete VI). Efter en tids läkning (6 eller 12 veckor), inklusive regeneration av nervcellsutskott, avlivades råttorna och implantaten togs ut. Kapseln som bildats runt implantatet mättes och befanns vara tunnare

mot poröst kisel än mot slätt kisel, ett tecken på bättre integration av materialet hos värddjuret.

Sammanfattningsvis visar studierna att det är möjligt att med nanoteknologi modifiera ytor så att man kan styra nervcellsutskott dit man önskar på en chipyta, till exempel till stimulerande eller registrerande elektroder. Vidare förefaller vissa stavformade nanostrukturer vara skadliga för celler då de exponeras för fria sådana pinnar. Slutligen framstår nanostrukturerat poröst kisel som en kandidat för nya implanterbara elektroder då det erbjuder god vidhäftning till celler och vävnad, är elektriskt ledande, har stor kontaktyta och minskar inkapsling.

9. References

1 E. K. Yim, R. M. Reano, S. W. Pang, A. F. Yee, C. S. Chen, and K. W. Leong, Biomaterials 26, 5405-13 (2005).
2 J. P. Donoghue, Nat Neurosci 5 Suppl, 1085-8 (2002).
3 A. Rivas, A. L. Marlowe, J. E. Chinnici, J. K. Niparko, and H. W. Francis, Otol Neurotol 29, 639-48 (2008).
4 K. Mortensen, V. Rudolph, S. Willems, and R. Ventura, Expert Rev Med Devices 4, 321-33 (2007).
5 P. Limousin and I. Martinez-Torres, Neurotherapeutics 5, 309-19 (2008).
6 http://www.cyberkineticsinc.com, (2008).
7 Y. Takai, J. Miyoshi, W. Ikeda, and H. Ogita, Nat Rev Mol Cell Biol 9, 603-15 (2008).
8 M. S. Ridyard and E. J. Sanders, Anat Embryol (Berl) 199, 1-7 (1999).
9 V. Kielberg, Cellodling - En praktisk handbok i odling av mammalieceller (AB Labassco förlag, 1994).
10 P. T. Ohara and R. C. Buck, Exp Cell Res 121, 235-49 (1979).
11 X. F. Walboomers and J. A. Jansen, Odontology 89, 2-11 (2001).
12 J. A. Cooper, J Cell Biol 105, 1473-8 (1987).
13 W. M. Becker, L. J. Kleinsmith, J. Hardin, and G. P. Bertoni, The world of the cell, 7 ed. (Pearson/Benjamin Cummings, 2008).
14 L. K. Wayne Becker, Jeff Hardin, The world of the cell, 6:th ed. (Pearson Education, 2004).
15 I. F. I. F. Henderson, Henderson´s dictionary of biological terms., 10:th ed. (Longman Scientific & Technical, 1989).
16 S. C. Bayliss, L. D. Buckberry, P. J. Harris, and M. Tobin, Journal of Porous Materials 7, 191-195 (2000).
17 P. Gustavsson, F. Johansson, M. Kanje, L. Wallman, and C. E. Linsmeier, Biomaterials 28, 1141-51 (2007).
18 P. Fromherz, Ann N Y Acad Sci 1093, 143-60 (2006).
19 W. L. Rutten, Annu Rev Biomed Eng 4, 407-52 (2002).
20 R. G. Harrison, Science 34, 279-281 (1911).
21 P. Weiss, Journal of Experimental Zoology 100, 13 (1945).
22 N. G. Maroudas, Exp Cell Res 74, 337-42 (1972).
23 Y. A. Rovensky, I. L. Slavnaja, and J. M. Vasiliev, Exp Cell Res 65, 193-201 (1971).
24 R. G. Flemming, C. J. Murphy, G. A. Abrams, S. L. Goodman, and P. F. Nealey, Biomaterials 20, 573-88 (1999).
25 B. Wojciak-Stothard, A. Curtis, W. Monaghan, K. MacDonald, and C. Wilkinson, Exp Cell Res 223, 426-35 (1996).
26 C. D. Nobes and A. Hall, J Cell Biol 144, 1235-44 (1999).
27 B. N. Patel and D. L. Van Vactor, Curr Opin Cell Biol 14, 221-9 (2002).
28 G. A. Dunn and A. F. Brown, J Cell Sci 83, 313-40 (1986).
29 C. Oakley and D. M. Brunette, Biochem Cell Biol 73, 473-89 (1995).
30 X. F. Walboomers, H. J. E. Croes, L. A. Ginsel, and J. A. Jansen, Biomaterials 19, 1861-1868 (1998).
31 X. F. Walboomers, W. Monaghan, A. S. Curtis, and J. A. Jansen, J Biomed Mater Res 46, 212-20 (1999).
32 B. Wojciak-Stothard, A. S. Curtis, W. Monaghan, M. McGrath, I. Sommer, and C. D. Wilkinson, Cell Motil Cytoskeleton 31, 147-58 (1995).
33 B. Wojciak-Stothard, Z. Madeja, W. Korohoda, A. Curtis, and C. Wilkinson, Cell Biol Int 19, 485-90 (1995).
34 G. A. Dunn and J. P. Heath, Exp Cell Res 101, 1-14 (1976).
35 R. M. Smeal, R. Rabbitt, R. Biran, and P. A. Tresco, Ann Biomed Eng 33, 376-82 (2005).
36 D. M. Brunette, Int J Oral Maxillofac Implants 3, 231-46 (1988).
37 J. Meyle, H. Wolburg, and A. F. von Recum, J Biomater Appl 7, 362-74 (1993).
38 X. F. Walboomers, H. J. Croes, L. A. Ginsel, and J. A. Jansen, J Biomed Mater Res 47, 204-12 (1999).
39 E. T. den Braber, J. E. de Ruijter, L. A. Ginsel, A. F. von Recum, and J. A. Jansen, Biomaterials 17, 2037-44 (1996).
40 E. T. den Braber, J. E. de Ruijter, L. A. Ginsel, A. F. von Recum, and J. A. Jansen, J Biomed Mater Res 40, 291-300 (1998).

41 A. J. Maniotis, C. S. Chen, and D. E. Ingber, Proc Natl Acad Sci U S A 94, 849-54 (1997).
42 D. E. Ingber, J Cell Sci 104 (Pt 3), 613-27 (1993).
43 M. J. Dalby, Med Eng Phys 27, 730-42 (2005).
44 S. B. Carter, Nature 208, 1183-7 (1965).
45 S. J. H. Kandell E R, Jessell T M, Principles of neuroscience, 4th ed. (McGraw-Hill companies New York, USA, 2000).
46 S. X. Jiang, J. Kappler, B. Zurakowski, A. Desbois, A. Aylsworth, and S. T. Hou, Eur J Neurosci 26, 801-9 (2007).
47 A. M. Rajnicek, L. E. Foubister, and C. D. McCaig, Biomaterials 29, 2082-95 (2008).
48 N. Danielsen, H. L. Vahlsing, M. Manthorpe, and S. Varon, Experimental Neurology 99, 622-635 (1988).
49 A. Rosengren, Thesis, Lund University, 1997.
50 M. Karlsson, Thesis, Uppsala University, 2004.
51 S. Y. Chou, P. R. Krauss, W. Zhang, L. J. Guo, and L. Zhuang, Journal of Vacuum Science & Technology B 15, 2897-2904 (1997).
52 I. Maximov, E. L. Sarwe, M. Beck, K. Deppert, M. Graczyk, M. H. Magnusson, and L. Montelius, Microelectronic Engineering 61-2, 449-454 (2002).
53 S. Y. Chou, P. R. Krauss, and P. J. Renstrom, Applied Physics Letters 67, 3114-3116 (1995).
54 I. U. Arthur Uhlir, in Dawn of porous semiconductor research, 50th Anniversary Lecture, Cullera, Spain, 2004, p. 1-2.
55 Theuniss.Mj, Journal of the Electrochemical Society 119, 351-& (1972).
56 L. T. Canham, Applied Physics Letters 57, 1046-1048 (1990).
57 A. Halimaoui, C. Oules, G. Bomchil, A. Bsiesy, F. Gaspard, R. Herino, M. Ligeon, and F. Muller, Applied Physics Letters 59, 304-306 (1991).
58 P. Mccord, S. L. Yau, and A. J. Bard, Science 257, 68-69 (1992).
59 J. Drott, Porous silicon : an enzyme coupling matrix for micromachined reactors (Univ., Lund, 1997).
60 J. Persson, N. Danielsen, and L. Wallman, J Biomater Sci Polym Ed 18, 1301-8 (2007).
61 F. P. Mathew and E. C. Alocilja, Biosensors & Bioelectronics 20, 1656-1661 (2005).
62 M. Bengtsson, S. Ekstrom, G. Marko-Varga, and T. Laurell, Talanta 56, 341-353 (2002).
63 S. C. Bayliss, P. J. Harris, L. D. Buckberry, and C. Rousseau, Journal of Materials Science Letters 16, 737-740 (1997).
64 C. P. T. Svensson, W. Seifert, M. W. Larsson, L. R. Wallenberg, J. Stangl, G. Bauer, and L. Samuelson, Nanotechnology 16, 936-939 (2005).
65 E. T. den Braber, H. V. Jansen, M. J. de Boer, H. J. E. Croes, M. Elwenspoek, L. A. Ginsel, and J. A. Jansen, Journal of Biomedical Materials Research 40, 425-433 (1998).
66 J. A. Alaerts, V. M. De Cupere, S. Moser, P. Van den Bosh de Aguilar, and P. G. Rouxhet, Biomaterials 22, 1635-42 (2001).
67 J. M. Corey, C. C. Gertz, B. S. Wang, L. K. Birrell, S. L. Johnson, D. C. Martin, and E. L. Feldman, Acta Biomater 4, 863-75 (2008).
68 M. Tanase, D. M. Silevitch, A. Hultgren, L. A. Bauer, P. C. Searson, G. J. Meyer, and D. H. Reich, Journal of Applied Physics 91, 8549-8551 (2002).
69 C. M. Hangarter and N. V. Myung, Chemistry of Materials 17, 1320-1324 (2005).
70 C. M. Hangarter, Y. Rheem, B. Yoo, E. H. Yang, and N. V. Myung, Nanotechnology 18, - (2007).
71 D. H. Reich, M. Tanase, A. Hultgren, L. A. Bauer, C. S. Chen, and G. J. Meyer, Journal of Applied Physics 93, 7275-7280 (2003).
72 M. Tanase, E. J. Felton, D. S. Gray, A. Hultgren, C. S. Chen, and D. H. Reich, Lab Chip 5, 598-605 (2005).
73 A. Hultgren, M. Tanase, E. J. Felton, K. Bhadriraju, A. K. Salem, C. S. Chen, and D. H. Reich, Biotechnol Prog 21, 509-15 (2005).
74 S. Kim, K. L. Shuford, H. M. Bok, S. K. Kim, and S. Park, Nano Lett 8, 800-4 (2008).
75 M. Karlsson, A. Johansson, L. Tang, and M. Boman, Microsc Res Tech 63, 259-65 (2004).
76 S. C. Bayliss, L. D. Buckberry, I. Fletcher, and M. J. Tobin, Sensors and Actuators a-Physical 74, 139-142 (1999).
77 S. C. Bayliss, R. Heald, D. I. Fletcher, and L. D. Buckberry, Advanced Materials 11, 318-321 (1999).
78 A. V. Sapelkin, S. C. Bayliss, B. Unal, and A. Charalambou, Biomaterials 27, 842-6 (2006).
79 K. Zhang, S. L. Loong, S. Connor, S. W. Yu, S. Y. Tan, R. T. Ng, K. M. Lee, L. Canham, and P. K. Chow, Clin Cancer Res 11, 7532-7 (2005).

[80] A. Rosengren, L. Wallman, N. Danielsen, T. Laurell, and L. M. Bjursten, IEEE Trans Biomed Eng 49, 392-9 (2002).
[81] L. Wallman, (Lund, 2006).
[82] R. Biran, D. C. Martin, and P. A. Tresco, J Biomed Mater Res A 82, 169-78 (2007).
[83] A. Curtis and C. Wilkinson, Biomaterials 18, 1573-83 (1997).
[84] A. I. Teixeira, G. A. Abrams, P. J. Bertics, C. J. Murphy, and P. F. Nealey, Journal of Cell Science 116, 1881-1892 (2003).
[85] M. J. Dalby, M. O. Riehle, S. J. Yarwood, C. D. Wilkinson, and A. S. Curtis, Exp Cell Res 284, 274-82 (2003).
[86] M. J. Dalby, M. O. Riehle, H. Johnstone, S. Affrossman, and A. S. Curtis, Biomaterials 23, 2945-54 (2002).
[87] M. J. Dalby, M. O. Riehle, H. Johnstone, S. Affrossman, and A. S. Curtis, Cell Biol Int 28, 229-36 (2004).
[88] M. J. Dalby, N. Gadegaard, M. O. Riehle, C. D. Wilkinson, and A. S. Curtis, Int J Biochem Cell Biol 36, 2005-15 (2004).
[89] A. S. Curtis, N. Gadegaard, M. J. Dalby, M. O. Riehle, C. D. Wilkinson, and G. Aitchison, IEEE Trans Nanobioscience 3, 61-5 (2004).
[90] A. Rajnicek, S. Britland, and C. McCaig, J Cell Sci 110 (Pt 23), 2905-13 (1997).
[91] E. Stepien, J. Stanisz, and W. Korohoda, Cell Biol Int 23, 105-16 (1999).
[92] A. Hultgren, M. Tanase, C. S. Chen, G. J. Meyer, and D. H. Reich, Journal of Applied Physics 93, 7554-7556 (2003).
[93] A. Hultgren, M. Tanase, C. S. Chen, and D. H. Reich, Ieee Transactions on Magnetics 40, 2988-2990 (2004).
[94] K. S. Kasprzak, F. W. Sunderman, Jr., and K. Salnikow, Mutat Res 533, 67-97 (2003).
[95] W. Hallstrom, T. Martensson, C. Prinz, P. Gustavsson, L. Montelius, L. Samuelson, and M. Kanje, Nano Lett 7, 2960-5 (2007).
[96] C. Prinz, W. Hallstrom, T. Martensson, L. Samuelson, L. Montelius, and M. Kanje, Nanotechnology 19, - (2008).

I

Available online at www.sciencedirect.com
SCIENCE DIRECT®
Biomaterials 27 (2006) 1251–1258
Biomaterials
www.elsevier.com/locate/biomaterials

Axonal outgrowth on nano-imprinted patterns

Fredrik Johansson[a,*], Patrick Carlberg[b], Nils Danielsen[c], Lars Montelius[b], Martin Kanje[a]

[a]Department of Cell and Organism Biology, Lund University, Helgonavägen 3b, SE-223 62 Lund, Sweden
[b]The Nanometer Structure Consortium, Solid State Physics, Department of Physics, Box 118, Lund University, SE-221 00 Lund, Sweden
[c]Department of Experimental Medical Science, BMC F10, Lund University, SE-221 84 Lund, Sweden

Received 14 March 2005; accepted 25 July 2005
Available online 6 September 2005

Abstract

Nanotechnology has provided methods to fabricate surface patterns with features down to a few nm. If cells or cell processes exhibit contact guidance in response to such small patterns is an interesting question and could be pertinent for many applications. In the present study we investigated if axonal outgrowth was affected by nano-printed patterns in polymethylmethacrylate (PMMA)-covered silicon chips. To this end adult mouse sympathetic and sensory ganglia were mounted in Matrigel® on the chips close to the nano-patterns. The patterns consisted of parallel grooves with depths of 300 nm and varying widths of 100–400 nm. The distance between two adjacent grooves was 100–1600 nm. The chips were cultured in medium containing 25 ng/ml of nerve growth factor to stimulate axonal outgrowth. After 1 week of incubation, axonal outgrowth was investigated by immunocytochemistry or scanning electron microscopy. Axons displayed contact guidance on all patterns. Furthermore, we found that the nerve cell processes preferred to grow on ridge edges and elevations in the patterns rather than in grooves, a seemingly claustrophobic behavior. We conclude that axons of peripheral neurons might be guided by nanopatterns on PMMA when the lateral features are 100 nm or larger. The present results can be utilized for nerve regenerating scaffolds or the construction of a stable, high-resolution electronic interface to neurons, which is required for future brain machine interfaces.

Keywords: Cell culture; Nanotopography; Nerve guide; Nerve regeneration; Polymethylmethacrylate

1. Introduction

Extensive efforts are made to construct a junction between neurons and electronic chips i.e. a brain machine interface (BMI) [1,2]. The potential impact of such devices is enormous since they can be used to compensate for both sensory and motor deficits in the nervous systems e.g. they could be used to restore vision, hearing and motor impairments as well as impaired autonomic functions. This feat is however not trivial since the number of nerve cell processes and neurons are counted in the millions and efficient neuro-electronic junctions must be small. Thus they must have a high-spatial resolution; here nanotechnology may offer a solution. In this study we tested whether neuronal processes, axons, could be guided by nanopatterns (grooves and ridges), and if these nanopatterns possess the spatial resolution required to contact thousands of nerve fibers on a small silicon/polymer-based chip surface.

For single cells, the cellular response to alterations in surface topography, down to the micrometer scale has been well documented especially for grooved topography [3–6]. Most cells follow the discontinuities of grooves and ridges, and attain an elongated shape due to surface-induced rearrangements of the cytoskeleton [4]. Grooved surfaces also induce changes in transcription and the up and down regulation of several genes [7], but the explicit mechanism for cell guidance has yet to be clarified. The development of techniques to produce surface structures in the nanometer range has revealed

*Corresponding author. Tel.: +46 46 2229354; fax: +46 46 2224539.
E-mail address: per_fredrik.johansson@cob.lu.se (F. Johansson).

0142-9612/$ - see front matter © 2005 Elsevier Ltd. All rights reserved.
doi:10.1016/j.biomaterials.2005.07.047

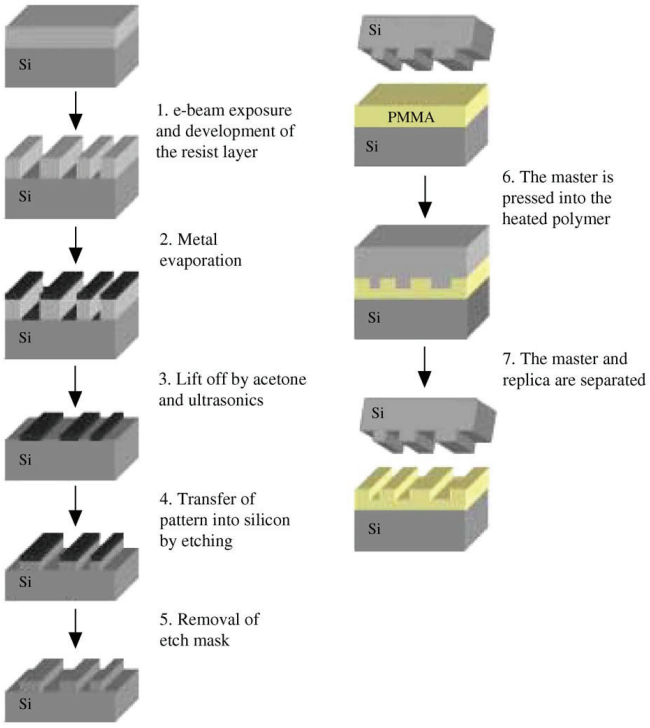

Fig. 1. Master fabrication by electron beam lithography (EBL), left column and nanoimprint lithography (NIL), right column: EBL: First a silicon wafer is spin coated with a lift off layer (LOL). The resist is exposed with an e-beam and developed to give the desired pattern. A thin layer of chrome is evaporated onto the pattern. In the lift-off step, the LOL dissolves and leaves a chrome etch mask behind. After etching in KOH, the chrome is removed and the silicon master is ready. NIL: The silicon master is pressed (50 bar) into a layer of polymethylmethacrylate (PMMA) under heating (180 °C). When cooled, the master is peeled away and the imprinted pattern remains, supported by the silicon chip.

that cells also respond to such nanostructures. Macrophage-like cells can react to steps in the nanometer range [8]. Endothelial and fibroblast cells are sensitive to patterns with features down to 10 nm [4,9,10]. Furthermore the importance of symmetry or discontinuity of the nanometer patterns was pointed out [4]. However, the response of neurons and their axons, to nanopatterned substrata, have not been studied in detail. Rajnicek et al [11] reported that central nervous system (CNS) neurites were guided by shallow (14 nm deep and 1 μm wide) grooves. Furthermore, contact guidance for chicken dorsal root ganglion (DRG) neurons on single scratches (0.1–0.2 μm wide), was reported by Stepien and coworkers [12]. Fibroblast filopodia have also been found to respond to nanotopographies [10,13], whether or not, axonal or growth cone filopodia also respond to submicron structures have hitherto not been determined.

In this study we used nanoimprint lithography (NIL), on polymer (polymethylmethacrylate—PMMA) covered silicon wafers (Fig. 1), to test the reaction of neuronal processes to grooves and ridges smaller than 1 μm. The purpose of the study was to investigate if axons could be guided by nanometer sized patterns. The study of axonal guidance differs from studies of single cell guidance. When dealing with guided single cells, the elongation of the cell gives a clear axis indicating the guiding direction. In the case of axons, the length scale is much different and the axons have a wandering behavior. Even if an axon shows clear contact guidance, it may change to an adjacent ridge. This makes it difficult to compare the guiding properties of different patterns and a more macroscopic method must be adopted (Figs. 5 and 6). In this study we present a simple fast Fourier transform (FFT) analysis in order to quantify the guidance on different patterns.

2. Materials and methods

2.1. Materials

2.1.1. Fabrication of substrata: Nanoimprinted negative pattern

Standard, 25 mm diameter, round silicon wafers (SILTRONIX, France) with one side polished were rinsed in trichloroethylene (5 min), acetone (5 min) and isopropanol (5 min) before drying in a nitrogen flow. The wafers were then spin coated (3000 rpm, 30 s) with PMMA-950 (diluted in anisol 8%) (Micro-chem corp, USA). The wafers were hard baked in oven (180 °C, 30 min), and then subjected to nanoimprinting using a silicon master stamp (made with the electron beam lithography (EBL) and lift off technique, [15,16]). The imprinting was carried out at 50 bar/180 °C (using a prototype imprinting machine: "Nanoimprint 2,5 TOM"). After cooling, the master and replica were separated with a scalpel. The features of the replica are depicted in Fig. 2 and Table 1.

2.1.2. Fabrication of substrata: Nanoimprinted positive (inverted) pattern

When fabricating the inverted pattern, an (oxidized) imprinted wafer was used. The pattern was transferred into the SiO_2 layer of the silicon wafer by reactive ion etch (RIE), and the resist material was removed. After silanization [16], in order to make the separation of master and replica easier, the silicon wafer could be used as master stamp for the inverted patterns, i.e. free standing walls (Fig. 3).

Table 1
The nanopatterned squares (number 1–17) hold grooves with different widths and pitch but all grooves have the same depth (300 nm)

Pattern no.	1, 9	2, 10	3, 11	4, 12	5, 13	6, 14	7, 15	8, 16	17
Width (nm)	100	100	100	200	200	200	400	400	400
Pitch (nm)	200	300	500	400	600	1000	800	1200	2000

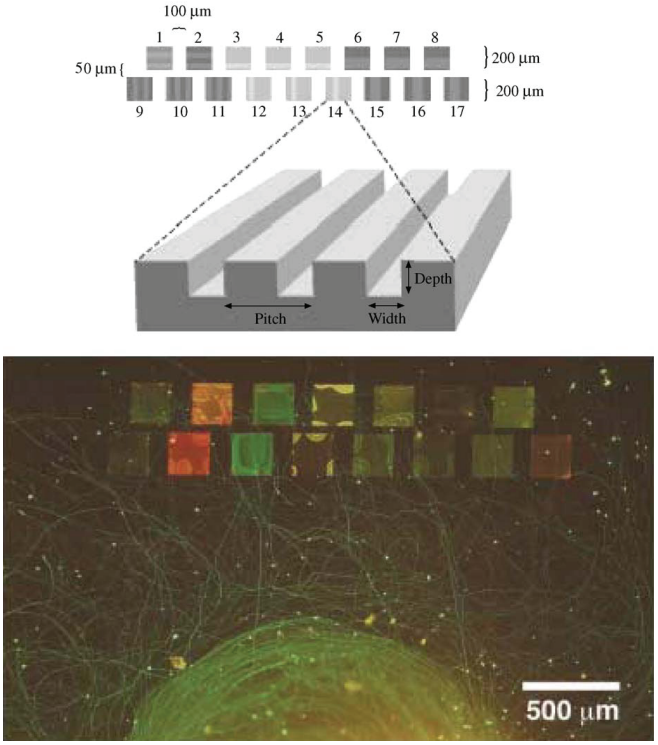

Fig. 2. Upper panel: The nanoimprinted wafers were ordinary round 25 mm silicon wafers covered with a polymer (PMMA 950). The patterns consisted of 17 squares (200 µm × 200 µm) with grooves oriented horizontally and vertically and with different width and pitch, Table 1. Lower panel: Axonal outgrowth from mouse superior cervical ganglion after 7 days of culture on the nanopatterned areas. Axons are fluorescently green. The printed squares were visualized by white light and the colors of the different patterns are due to interference, reflecting the dimensions of the grooves.

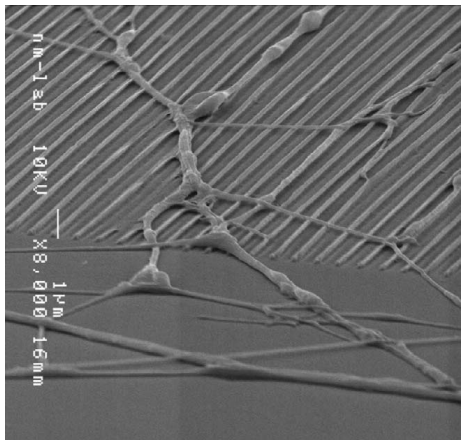

Fig. 3. Scanning electron microscopy picture showing axons (on a positive pattern) that after a few μm align to the ridges. Here the ridges (100 nm high and 100 nm wide) are of the same dimensions as the axons: Note especially that all axons are growing on top of the ridges and not in the grooves between the ridges.

2.2. Cell culture

All animal-related procedures were conducted in accordance with local ethical guidelines and approved animal care protocols. The nanoimprinted wafers were placed in (32 mm) Petri dishes and sterilized using ethanol (70%). Sympathetic (superior cervical ganglion—SCG), or sensory ganglia (DRG) from adult female NMRI mouse (B&K, Sweden) were dissected. The ganglia were mounted on the wafers using small drops (~1 μl) of Matrigel® (Collaborative Research, USA) as glue. The ganglia were positioned around 1 mm from the nanoimprinted patterns on the wafers. In order to prevent the ganglia from being washed off when adding the medium, the preparations were incubated at 37 °C for 2 min to allow the Matrigel® to polymerize before 2 ml of the culture medium was added; (RPMI 1640, Biocrome AG, Germany), containing 25 ng/ml nerve growth factor (Pepro Tech, UK). The cultures were incubated at 37 °C in an atmosphere of 6.5% CO_2 and 93.5% O_2 for 5–7 days before fixation.

2.3. Immunocytochemistry and florescence microscopy

The cultures were fixed with Stefanini's fixative (2% paraformaldehyde and 15% saturated aqueous picric acid solution in 0.1 M phosphate buffer, pH 7.2) for 2 h at room temperature (RT) and then rinsed 3 times in phosphate buffered saline (PBS). The axons were then immunostained (over night at 8 °C) using the primary antibody directed against the heavy subunit of neurofilaments, Rabbit NF 200 (Sigma, USA), diluted in a mixture of Triton X-100 (0.25%), bovine serum albumin (0.25%) in PBS. After repeated rinses in PBS, the cultures were further incubated with an Alexa 488 conjugated secondary antibody detecting rabbit IgG (35 min, dark, RT, 1:200, Molecular Probes, Eugene USA), rinsed in PBS and coverslipped using glycerol-PBS (1:1). The preparations were then observed and photographed using a fluorescence microscope (Olympus AX 70 equipped with an Olympus DP50 camera). To visualise the axons and the nanopatterns at the same time, two lamps (striking white light) oriented perpendicular to each other and at some angle to the sample, made the nanopatterns visible in the microscope.

2.4. Scanning electron microscopy (SEM)

The cultures were fixed with 2.5% gluteraldehyde buffered in 0.15 M sodium cacodylate (pH 7.2, 20 °C, 1 h). After fixation, the cultures were repeatedly rinsed in cacodylate buffer. The cultures were dehydrated in a graded series of ethanol (50%, 70%, 96% and 100% alcohol) prior to critical point drying. The preparations were sputter coated with gold-palladium before examination in the SEM (JEOL JSM-5600 LV).

2.5. FFT analysis for axon guidance quantification

FFT analysis was made using NHI-Image (version 1.63) equipped with a FFT macro. NHI-Image is a public domain image processing and analysis program that can be downloaded at: http://rsb.info.nih.gov/nih-image/.

For the FFT, digital images (fluorescence microscopy) of axonal outgrowth were used. The images were inverted and changed to greyscale using Adobe® Photoshop 7.0, before transferred to NIH-Image. The macro analyzed a 512×512 pixel area within each nanopattern (Fig. 4B). This area was tranformed into the frequency space (power spectrum) (Fig. 4C), where a density slice at 175 was performed (this value was chosen after some preliminary testing and was not critical for the result) (Fig. 4C). The frequency space was analyzed by approximating ellipses to the selected area. Major axis, minor axis and the angle of the major axis for each ellips were measured. In each measurement there was a pronounced major axis reflecting the most common frequency. This major axis was chosen for further calculations. The ratio major axis/minor axis, was calculated and indicate the spreading of angles, a high value represents a uniform, highly parallel axon pattern while a low value indicates a more random distribution (1 = totally random). The angle of the major axis, is the orthogonal projection of the main direction that the regenerating axons have, i.e. 90° means perfect alignment.

3. Results

3.1. Nanoimprinted negative pattern

Seventeen different striped patterns with variable distances (pitch) between ridges and grooves were produced, with good reproducibility, in 200×200 μm squares on the resist material (Fig. 2). After 5–7 days in culture, numerous axons had grown across the printed squares (Fig. 2). Most axons (diameter $< \sim 1$ μm) except for the thickest ones (diameter $> \sim 1$ μm) were found to

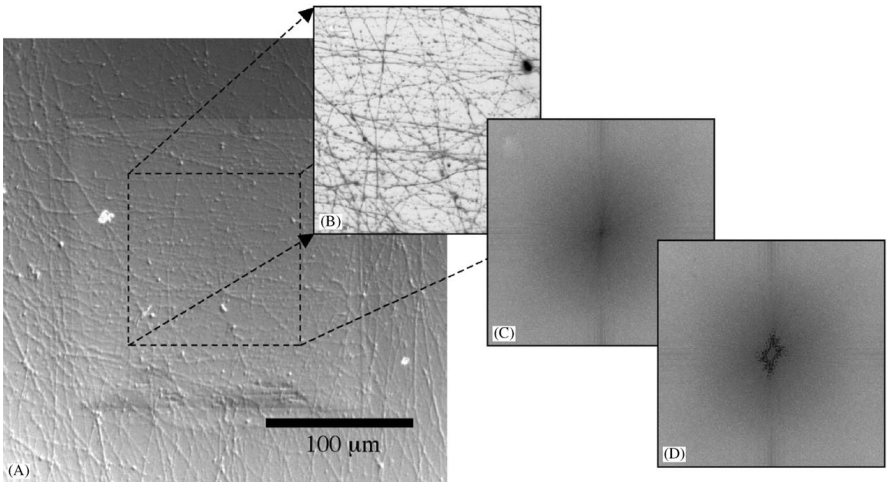

Fig. 4. The major steps in the image FFT analysis of axonal outgrowth (here a pattern with 100 nm width and 300 nm pitch is depicted). The middle part (512 × 512 pixels) of a patterned area is selected from a digital image of axonal outgrowth (A). A fluorescense microscopy image is used in order to delete the influence of the grooved topography (B). When the FFT of the picture (B) is computed, the power spectrum is the result (C). The program approximates ellipses to the power spectrum (D). The largest major axis is used as a measure of the overall axon direction (although orthogonal). The ratio between the major and minor axis reflects the spreading of angles (see also Table 2).

align along the imprinted nanopatterns and consequently turned up to 90° as they entered the second line of squares. The SEM-images of the preparations showed that the axons grew on the ridges of the patterns, and not within the grooves irrespectively of the distance between the ridges (Fig. 5B and C). Orientated growth was observed on all types of patterns, although the 100 nm wide grooves seemed to be somewhat less efficient, as compared to the patterns with larger widths. On narrow grooves/ridges the axons grew on top of several ridges simultaneously, while on wider grooves/ridges the axons were found on single ridges. In some experiments (Fig. 5B and C) DRGs were used to test if guidance by nanopatterns was a general phenomenon and not restricted to autonomic sympathetic nerve fibers. We found that sensory nerve fibers (DRG) were guided by the nanopatterns in the same manner as the axons from autonomic ganglia (SCG).

Spatial resolution for the smallest patterns was 5000 lines per mm and the largest patterns 500 lines per mm, a resolution that is beyond that of a peripheral nerve. The maximum number of axons observed within one square, was around 100 in the present experiments.

3.2. Nanoimprinted positive (inverted) pattern

The axons on the original negative (grooved) pattern were always found on the ridge edges, and not in the grooves. Previous studies have shown that cells prefer negative or zero radius curvature over positive ones, i.e. cells prefer to grow uphill rather than downhill [17]. This may explain why we did not find any axons in the grooves; axons, like cells, thus seem to refrain from turning downwards. To further test this behavior, we made an inverted, positive, nanopattern to see whether the axons stayed down between the ridges, or if they preferred to turn upwards, onto the ridges. On the inverted pattern, we found that axons, after a short growth distance, turned up onto the ridge edges and proceeded to grow along the ridges (Figs. 3 and 6). In fact the guiding influence from the inverted positive pattern was as good, if not better, than the original negative pattern.

3.3. FFT analysis

The FFT analysis indicated that there were differences in axonal alignment between the nanoimprinted patterns. Table 2. shows the average angle of the axons and the homogeneity of the axon population (ratio: major axis/minor axis). It is clear from Table 2, that a good alignment is accompanied by a good homogeneity and vice versa. The analysis showed that in general, patterns with 100 nm widths had lower homogeneity and alignment than patterns with larger widths.

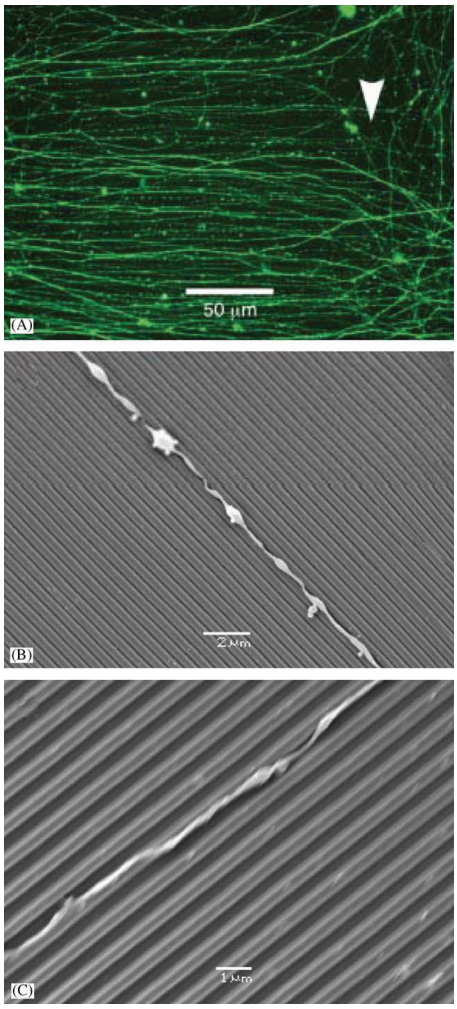

Fig. 5. A: Axons aligning along a horizontally imprinted pattern (200 nm width and 400 nm pitch). The arrow indicates the border of the pattern. The more random growth of axons outside the pattern is clearly visible. Note that the larger axons are not as well guided as the thinner ones. B: (100 nm width and 500 nm pitch) and C: (400 nm width and 800 nm pitch): Scanning electron microscopy pictures showing that the axons grow on the ridge edges, and not in the grooves.

4. Discussion

The physical properties of contact guidance, i.e. how cells respond to the surrounding topography, have been studied in detail using mainly μm-sized patterns, although most studies have been performed using other cells than neurons. Recently also nanoimprinted patterns (pits with diameter of only 35 nm) have been reported to affect the filopodia of fibroblasts [13], showing the extreme sensitivity of these cellular extensions. The present findings that nanopatterns can also serve to guide axons, and that axons grow on top of the nanometer sized ridges, are new.

The results of this study show that axons can be guided by nanosized structures on a polymer surface and that hundreds of axons could be separated within a square of 0.2×0.2 mm. The efficiency of guidance appeared to be related to the diameter of the axons. Large diameter fibers (>1 μm) were more often found to be less affected by the patterns as compared to small diameter fibers (<1 μm). One explanation to this behavior might be that larger growth cones may traverse the grooves, although we found some filopodia of large

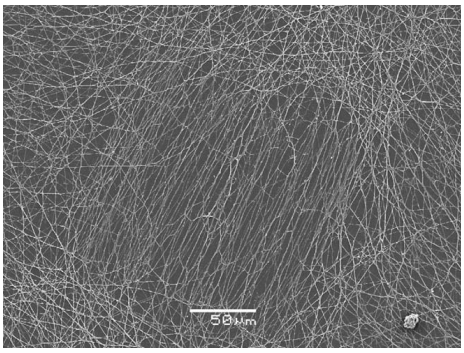

Fig. 6. Scanning electron microscopy image of axons on an inverted nanoimprinted pattern (200 nm wide ridges and 1 μm pitch). The inverted pattern shows good macroscopic guidance, even though some axons can be seen to change ridge. The length of a square side is 200 μm and can easily be detected by the aligned axons.

Table 2
The result of the FFT analysis

Width (nm)	Pitch (nm)	Major/Minor	Angle of major axis (°)
100	200	3.6	80.5
100	300	2.3	78.9
100	500	1.5	25.1
200	400	7.5	88.2
200	600	5.1	90.1
200	1000	3.1	105.8
400	800	4.4	95.2
400	1200	4.7	93.6

The "Major/Minor" column shows the degree of guidance (homogeneity) and the "Angle of major axis (°)" shows the orthogonal projection to the main direction of the regenerating axons.

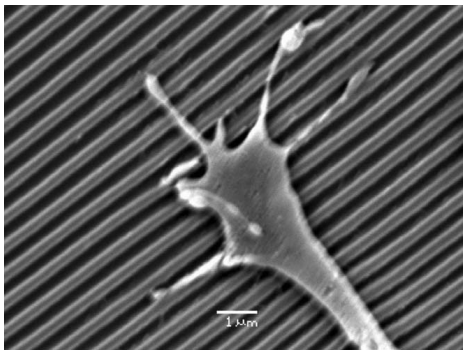

Fig. 7. Scanning electron microscopy image showing a large growth cone with filopodia, extending both perpendicular and parallel to the underlying pattern.

growth cones oriented along the patterns (Fig. 7). In many cases, especially when looking at larger axons, it appeared that the smallest patterns (widths of 100 nm) were not as efficient as the patterns with larger widths. This observation was also supported by the FFT analysis and suggests that structures smaller than 100 nm, may fail to elicit a guidance response in the axons. Interestingly, it has been reported that ordered nanotopography, in the range of our smallest patterns 100 nm, could reduce cell adhesion [4,18]. This may be another clue to why sometimes less contact guidance of axons was found on topographies with grooves/ridges of 100 nm. This effect might also be due to the size dependence, i.e. only the thinnest axons would be guided on these patterns. Furthermore, we found that axonal outgrowth occurred at ridges (most often at the edge of a ridge) in the patterns, not in grooves. This behavior has been reported before, but then for single cells (fibroblasts) on microstructures [19]. The finding that axons and whole cells behave in the same way when guided by substrate topography is interesting and indicates a common mechanism. Hypotheses regarding contact guidance of cells may therefore also apply to axons. If this is true, it gives the opportunity to predict axonal reaction and design substrates accordingly.

Chemical interactions through biochemical patterning can never be excluded, and the question is always raised in studies like this. We believe though, that the imprinting process will give less difference in roughness between the different parts of the substrate, i.e. wall, top and bottom of a groove, as compared to lithographic processes. The reason to this is the isotropic property of the imprinted PMMA combined with the imprinting procedure, where all surfaces are made simultaneous and in the same way. Even if the material is perfectly isotropic there will always be some edge effects due to geometrical restrictions to the polymer, e.g. concentration of charges. By choosing a substrate that minimizes the adsorption of proteins, the chemical influence should be depressed. PMMA has been shown to adsorb proteins 5–10 times less that polystyrene [17].

This study does not give an answer to how the guiding mechanism works, but it is reasonable to assume that the cellular mechanisms underlying axonal guidance are comparable to those responsible for guidance of whole cells and that guidance relies on extra-cellular cues, which through signal transduction mechanisms are transformed into reorganization of the cytoskeleton. Such mechanism of action operates during axonal guidance in embryos where proteins, like semaphorines and ephrins [20], inhibit axons from growing the wrong way. In regenerating nerves, the axons grow along the inside of the basal lamina tubes where laminin through interactions with integrin receptors affects outgrowth. Axons can also be guided by gradients of trophic factors and topographical cues even though little is known about the effects of topography on axonal guidance in vivo. In this study topographical cues were used and, at least initially, there are no adhesion or integrin binding proteins on the nanopatterns. Although we cannot exclude that such proteins later could be released from the ganglion, or the Matrigel® used to glue the ganglion onto the chip surface.

With respect to the construction of a BMI, the present findings offer solutions to three important aspects: spatial resolution, stability of guiding elements and industrial production. Firstly, the state of the art in the area of implanted electrodes (in humans) is the cortical implant BrainGate™ (Cyberkinetics Neurotechnology Systems) [21] and the well-known cochlear implant. In these types of implants the maximum number of electrodes varies between 10 and 100 on an area of a few mm^2 in size [2]. The nano approach could increase spatial resolution substantially. In the present study hundreds of separated axons were found on an area less than $0.04\,mm^2$. Secondly, protein covered e.g. micro-contact printed surfaces can be used for axonal guidance. Such surfaces are, as opposed to topographical cues used here, unstable. Axonal outgrowth is a slow process, why patterns must be maintained for extended periods of time in implanted BMIs. The use of NIL has many advantages for biological purposes since it is cheap and speeds up the substrate fabrication, hence many test surfaces can be produced. The resolution is not dependent on scattering or diffraction; hence patterns smaller than 10 nm are easily reproduced [14]. PMMA is a well-characterized polymer for NIL in our laboratory and an axonal outgrowth pilot study on PMMA, that showed good growth rate for DRG axons, was carried out. Therefore, PMMA was chosen as substrate material. Finally, the fact that imprinting can be used is favorable for fast and cheap fabrication of

nanostructures as compared to EBL, which is a serial, time-consuming and expensive process unsuitable for mass production. It is conceivable that nanoimprinted surfaces may have multiple uses including that of guiding axons on neuro-electronic junctions, which can be used to listen and talk to the nervous system. Nanopatterns, as presented in this study, could also be used for axonal guidance during nerve repair or provide patterned scaffolds for tissue repair.

5. Conclusions

We conclude that nerve cell processes, axons can be guided by imprinted nanosized patterns (grooves and ridges) down to 100 nm on a polymer material. Axons seem to grow on ridges in the pattern rather than in grooves, although groove width affected guidance. The relation of axon diameter and groove/ridge width appeared to be crucial for axonal guidance.

Acknowledgments

The present study was supported from grants from the Swedish Research Council (12712), VINNOVA, the Øresund Academy and the Royal Physiographical Society. Thanks are due to Inger Antonsson and Marie Adler Maihofer for expert technical assistance.

References

[1] Friehs GM, Zerris VA, Ojakangas CL, Fellows MR, Donoghue JP. Brain–Machine and Brain–Computer Interfaces. Stroke 2004;35:2702–5.
[2] Donoghue JP. Connecting cortex to machines: recent advances in brain interfaces. Nature Neurosci Suppl 2002;5.
[3] Curtis ASG, Wilkinson CDW. Topographical control of cells. Biomaterials 1997;18:1573–83.
[4] Curtis ASG. Small is beautiful but smaller is the aim: review of a life of research. Eur Cells Mater 2004;8:27–36.
[5] Flemming RG, Murphy CJ, Abrams GA, Goodman SL, Nealey PF. Effects of synthetic micro- and nano-structured surfaces on cell behaviour. Biomaterials 1999;20:573–88.
[6] Teixeira AI, Abrams GA, Bertics PJ, Murphy CJ, Nealey PF. Epithelial contact guidance on well-defined micro- and nanostructured substrates. J Cell Sci 2003;116:1881–92.
[7] Dalby MJ, Riehle MO, Yarwood SJ, Wilkinson CDW, Curtis ASG. Nucleus alignment and cell signaling in fibroblasts: response to a micro-grooved topography. Exp Cell Res 2003;284:274–82.
[8] Wojciak-Stothard B, Curtis ASG, Monaghan W, MacDonald K, Wilkinson CDW. Guidance and activation of murine macrophages by nanometric scale topography. Exp Cell Res 1996;223:426–35.
[9] Dalby MJ, Riehle MO, Johnstone H, Affrossman S, Curtis ASG. In vitro reaction of endothelial cells to polymer demixed naontopography. Biomaterials 2002;23:2945–54.
[10] Dalby MJ, Riehle MO, Johnstone H, Affrossman S, Curtis ASG. Investigating the limits of filopodial sensing: a brief report using SEM to image the interaction between 10 nm high nanotopography and fibroblast filopodia. Cell Biol Int 2004;28:229–36.
[11] Rajnicek AM, Britland S, McCaig CD. Contact guidance of CNS neurites on grooved quartz: influence of groove dimensions, neuronal age and cell type. J Cell Sci 1997;110:2905–13.
[12] Stepien E, Stanisz J, Korohoda W. Contact guidance of chick embryo neurons on single scratches in glass and on underlying aligned human skin fibroblasts. Cell Biol Int 1999;23(2):105–16.
[13] Dalby MJ, Gadegaard N, Riehle MO, Wilkinson CDW, Curtis ASG. Investigating filopodia sensing using arrays of defined nano-pits down to 35 nm diameter in size. Int J Biochem Cell Biol 2004;36:2005–15.
[14] Chou SY, Krauss PR, Zhang W, Guo L, Zhuang L. Sub-10 nm imprint lithography and applications. J Vac Sci Technol 1997;B15(6):2897–904.
[15] Maximov I, Sarwe EL, Beck M, Deppert K, Graczyk M, Magnusson MH, et al. Fabrication of Si-based nanoimprint stamps with sub-20 nm features. Microelectr Eng 2002;61–62:449–54.
[16] Carlberg P, Graczyk M, Sarwe EL, Maximov I, Beck M, Montelius L. Lift-off process for nanoimprint lithography. Microelectr Eng 2003;67–68:203–7.
[17] Alaerts JA, De Cupere VM, Moser S, van den Bosh de Aguilar P, Rouxhet PG. Surface characterization of poly(methyl methacrylate) microgrooved for contact guidance of mammalian cells. Biomaterials 2001;22:1635–42.
[18] Casey BG, Cumming DRS, Khandaker II, Curtis ASG, Wilkinson CDW. Nanoscale embossing of polymers using a thermoplastic die. Microelectr Eng 1999;46:125–8.
[19] den Braber ET, Jansen HV, de Boer MJ, Croes HJE, Elwenspoek M, Ginsel L A, et al. Scanning electron microscopic, transmission electron microscopic, and confocal laser scanning microscopic observation of fibroblasts cultured on microgrooved surfaces of bulk titanium substrata. J Biomed Mater Res 1998;40(3):425–33.
[20] Cook G, Tannahill D, Keynes R. Axon guidance to and from choice points. Curr Opinion Neurobiol 1998;8:64–72.
[21] http://www.cyberkineticsinc.com.

II

Cell guidance by magnetic nanowires

Fredrik Johansson*, Malin Jonsson, Kersti Alm and Martin Kanje

Department of Cell and Organism Biology, Lund University
Helgonavägen 3b, SE-22362 Lund, Sweden
*Corresponding author. Tel.: +46 46 2229354; fax: +46 46 2224539.
E-mail address: per_fredrik.johansson@cob.lu.se

Abstract
The phenomenon of contact guidance on thin fibres has been known since the beginning of the 20th century when Harrison studied cells growing on fibres from spider's web. Since then many studies have been performed on structured surfaces and fibres. Here we present a new way to induce guidance of cells or cell processes using magnetic nanowires. We have manufactured magnetic Ni-nanowires (200 nm in diameter and 40 μm long) with a template-based electro-deposition method. Drops of a nanowire/ethanol suspension were placed on glass cover slips. The nanowires were aligned in an external magnetic field and adhered to the cover slips after evaporation of the ethanol. When the wires had adhered, the magnetic field was removed. L929 fibroblasts and dissociated dorsal root ganglia (DRG) neurons from mice were cultured on the nanowire-coated cover slips for 24 h and 72 h respectively. The fibroblasts were affected by the aligned nanowires and displayed contact guidance. Regenerated axons also displayed contact guidance on the wires. There were no overt signs of toxicity caused by Ni-wires. Aligned magnetic nanowires can be useful for lab-on-a-chip devices and medical nerve grafts.

Keywords: Nanowire, axon, fibroblast, magnetic, guidance, *in vitro*

1. Introduction

Structurally well-defined magnetic nano-particles (MNP) and nanowires have become increasingly importants tool in biotechnology applications such as drug delivery, imaging and cell manipulation (1-5). For delivery applications, MNPs can be loaded with drugs and moved by externally applied magnetic fields, so that the drugs can be released close to the region of interest, *e.g.* a tumour. Due to the metal core, such particles can also be easily visualized by magnetic resonance imaging. Cell manipulation by external magnetic fields, *i.e.* cell separation, has been made possible using phagocytosed MNPs in cells. Hultgren *et al.* demonstrated that for cell separation, magnetic nanowires have an advantage over spherical particles since they have a stronger magnetic moment and hence may exert a larger force on the cell. The advantages of wires as compared to particles are due to the high aspect ratio (elongated shape), resulting in higher magnetic anisotropy. Furthermore, it is possible to create chemically different functional sequences along the wires (5-7). The use of different metals along the wires combined with linking of specific molecules, such as thiols for functionalization of gold, enables such chemical patterning. Electro-deposition of ferromagnetic metals, *e.g.* Ni, in nano-porous alumina membranes is a very successful method to obtain magnetic nanowires using standard laboratory equipment (8). Such magnetic Ni-

nanowires have typically a width of 200 nm, which corresponds to the pore size of the template, while lengths are determined by the membrane thickness or deposition time. The size of such wires is very suitable for cell interaction applications such as cell separation (1-3), where the wires should be internalized in cells with 10 to 20 µm diameters. Spatial cell organization can also be achieved among cells with internalized nanowires, either spontaneously in an end-to-end fashion, or by using external micro-magnet patterns (9, 10).

For many applications such as tissue engineering and neuronal networks, guidance of cells or cellular processes is important. To this end, mainly two approaches are used, namely chemical patterning of surfaces (11) or topographic patterning. Organized topography, *i.e.* grooves (12, 13), steps (12, 14), fibres (12, 15, 16), or even rows of standing nanowires (17), are among the structures which induce contact guidance for migrating cells and/or outgrowing nerve cell processes, axons. The techniques required to obtain such topographic patterns on cell substrates are fairly cumbersome and involves processes such as e-beam-lithography, UV-lithography and epitaxi.

Most studies are performed on micrometer-sized structures due to technical limitations, but we and others have shown that the phenomenon of contact guidance is valid also for submicron structures (13). On rounded

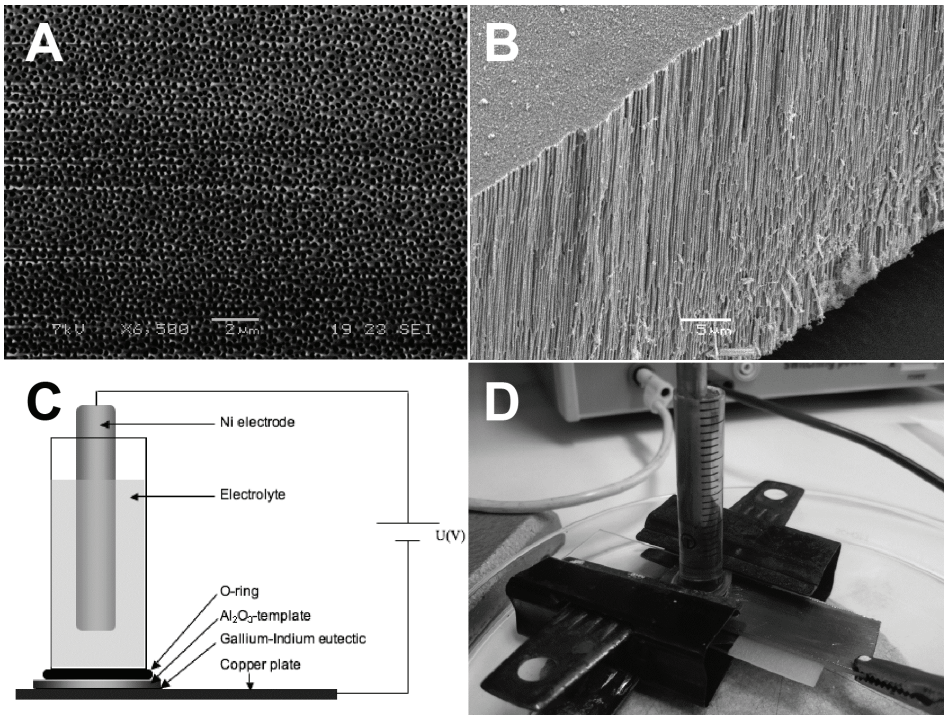

Fig. 1 A. SEM image showing a top view of the pores in an alumina membrane. **B.** SEM image (tilted 45°) of a cracked membrane, revealing the pores of a 60 μm thick alumina membrane. **C.** This simplified sketch shows the electro-deposition setup. **D.** Photograph of the setup used.

surfaces such as fibres, the substrate curvature influences the growth direction of nerve cell processes. It has been demonstrated that thinner fibres (Ø=35 μm) induce a more pronounced guidance than thicker fibres (Ø= 68-500 μm) do (16). From this result, indicating better guidance on thin, small radius, fibres one may expect that fibres such as a Ni nanowire (Ø=200 nm) would induce a clear contact guidance effect if aligned on a surface. Patterns of guiding magnetic nanowires would eliminate the need for any lithographic processing of the substrate to achieve cell patterning and could be valuable for the construction of neuronal networks *in vitro*.

Here, we have studied the guidance of outgrowing nerve cell processes from dorsal root ganglia (DRG), and guidance of L929 mouse fibroblasts on aligned Ni nanowires. The nanowires were produced by template-based electro-deposition in commercially available alumina membranes.

2. Material and methods

2.1. Nanowire synthesis

The synthesis of the Ni nanowires has been described in detail elsewhere (18). In short, commercially available 60 μm thick alumina membranes (Anodisc, Whatman Inc) with Ø=200 nm pores, (Fig. 1A and B) were used as templates to grow the Ni nanowires. One side of the Anodisc filter has a thin layer (~1 μm) of smaller pores (Ø=20 nm) that merge into the larger pores. This side of the membrane was covered with Ga/In eutectic (Alfa Aesar®, Germany) to form a conductive layer that was used as cathode. The filter was placed on a copper electrode with the conducting layer in contact with the electrode. A reservoir, sealed with gaskets and secured by clippers was placed atop of the filter. The reservoir was filled with Ni plating solution (1M $NiCl_2$, pH 1) and a Ni electrode placed in the solution served as anode (Fig. 1C and D). The electrodepositing voltage was held constant at 1.5 V (DC) for 40 min.

After the electro deposition, the Ga/In coating was removed from the Anodisc membrane by the use of a pad of cotton wool soaked in concentrated nitric acid. The filter was then dissolved in 3 M NaOH during 30 min. The free nanowires were rinsed in 96% ethanol five times.

2.2. Substrate preparation

Glass cover slips (18x18 mm), sterilized in 70% ethanol, were put in the constant magnetic field (110-115 mT) of a permanent magnet. A nanowire suspension (wires in 96% ethanol) was gently sonicated for 20 s immediately before a small drop was put on the glass slide. The sonication minimized the aggregation of magnetic nanowires in the suspension. The nanowires aligned instantly in the magnetic field and bound firmly to the glass surface when the alcohol had evaporated. The nanowire-coated cover slips were then stored in sterile 32 mm Petri dishes until use.

2.3. Cell culture

L929 mouse fibroblast cells were used for quantification of contact guidance induced by the nanowires. Two ml of the cell suspension were seeded onto each nanowire-coated cover slip, at a concentration of 35 000 cells/ml in RPMI 1640 medium complemented with 0.5% fetal calf serum and antibiotics (50 IU/ml penicillin and 50 μg/ml streptomycin). The cells were cultured for 24 h at 37°C in an atmosphere of 95.5% O_2 and 4.5% CO_2. The cover slips were then washed twice in prewarmed (20°C) phosphate buffered saline (PBS) and fixed in 4% paraformaldehyde (PFA) for 10 minutes at room temperature. Control cells were grown directly in standard Petri dishes and were fixated as above. To study the axonal guidance, primary neuronal cell cultures

were used. Female mice (NMRI, Möllegård, Denmark) were anaesthetized and killed by heart puncture. The lumbar L6 –thoracic Th10 DRG, were removed by dissection and dissociated in a solution of 0.25% collagenase as previously described (19). The dissociated cells were suspended in serum-free RPMI 1640 culture medium supplemented with nerve growth factor (20 ng/ml), before 2 ml was seeded onto each nanowire-coated cover slips. The cells were cultured for 72 h at 37°C in an atmosphere of 95,5% O_2 and 4,5% CO_2, washed in prewarmed PBS and fixed as described above.

2.4. Actin staining

After fixation, the L929 cultures were washed three times with PBS, before being extracted with 0.1% Triton X-100 in PBS for 3 to 5 minutes. After additional rinsing in PBS containing 1% bovine serum albumin (BSA), 200 µL of fluorescent phalloidin (5 µL, 6.6 μM methanolic stock solution diluted in 200 µL PBS with 1% BSA, Alexa Fluor® 488 phalloidin, Invitrogen - Molecular probes™) was added to each cover slip. The cultures were incubated for 20 minutes at room temperature, washed once with PBS, incubated with bisbenzimide (1 mg/ml in PBS) for 10 minutes for nuclear staining, and then washed again twice with PBS. The preparations were finally mounted on glass slides with glycerol/PBS (1:1).

2.5. Neurofilament staining

After fixation, the dissociated DRG cultures were labelled with a rabbit neurofilament antibody (against the 200 kD subunit, Sigma) diluted 1:200 in PBS with 0.25% BSA and 0.25% Triton X100. The cultures were incubated at 4°C over night. After rinsing in PBS, the secondary antibody (Alexa Fluor 594, goat-anti-rabbit, Invitrogen - Molecular probes™) was added and the cultures were incubated for an additional 2 h at room temperature. The samples were then counterstained with bisbenzimide, as above, and mounted on glass slides with glycerol/PBS (1:1). The actin- and neurofilament-labeled preparations were studied and photographed using a fluorescence microscope (Olympus AX 70 equipped with an Olympus DP50 camera).

2.6. Scanning electron microscopy (SEM)

The cultures for SEM were fixed with 2.5% glutaraldehyde buffered with 0.15 M sodium cacodylate (pH 7.2, 20°C, 1 h). After fixation, the cultures were repeatedly rinsed in cacodylate buffer. The cultures were dehydrated in a graded series of ethanol (50%, 70%, 96% and 100%) prior to critical point drying. The preparations were sputter coated with Au-Pd before examination in the SEM (JEOL JSM-5600 LV).

2.7. Alignment analysis

The quantitative image analysis was conducted on digital images, using the free software "ImageJ" for Mac OS X (http://rsb.info.nih.gov/ij/). Fibroblasts at five randomly chosen areas for each nanowire-coated cover slip were analyzed using the fit ellipse function in ImageJ. This function replace each cell with an ellipse and give the lengths of the major and minor axis in addition to the angle of the major axis. The angle of the major axis was considered as the cell direction and were given from 0° to 180°. The angles of the nanowires and control cells were measured in the same way. Cells with a major/minor axis ratio <1,5 were considered round, and no direction could be measured. Such round cells were omitted in the alignment analysis, although counted.

2.8. Statistics

The absolute angle deviation of the cells from the average nanowire direction, was tested relative the control cells. The experiment was repeated twice and 486 cells were counted in total. A two-tailed t-test was used for the comparison and $p<0,05$ was considered significant.

3. Results

3.1. Nanowires

The Ni nanowires differed somewhat in length. From SEM images, the length of the wires was estimated to 40 ± 10 μm (mean ±SD). The diameter was 200 nm ± 20 nm (mean ±SD), although some irregularities due to defect pores were found (not shown). The overall alignment of the nanowires was found to be very good (Fig. 2) although not perfect. In this study, a high concentration of wires was desirable to ensure cell-wire interaction from many cells. Therefore some aggregation due to magnetic interaction among neighbour wires was inevitable. The nanowires are fixed to the surface by electrostatic and van der Waahls forces (20), and were not moved by the cells. This indicates a strong adhesion of the wires to the naked glass surface.

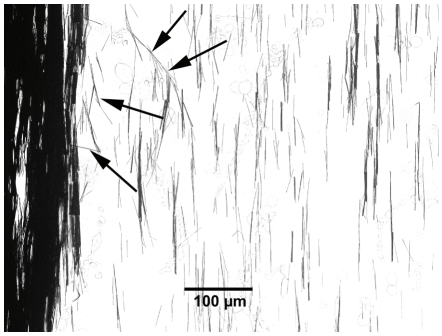

Fig. 2. This brightfield micrograph shows a typical area with magnetically aligned Ni nanowires. The alignment of nanowires, by the external magnetic field, was not perfect. A few wires were not aligned while others had aggregated (arrows).

3.2. L929 fibroblasts alignment

L929 fibroblasts cultured on nanowire-coated cover slips were mostly found on the nanowires and were clearly aligned and elongated along the nanowires (Fig. 3A). Fibroblasts that were not in contact with the nanowires generally had a flattened shape with extensions in different directions, similar to that observed in the control cultures (Fig. 3B and C). The alignment analysis showed a significant ($p<0,001$) difference between cells on nanowires (deviation angle: 23.0° ± 1.9°) and cells on smooth control surfaces (deviation angle: 48.5° ± 2.4°).

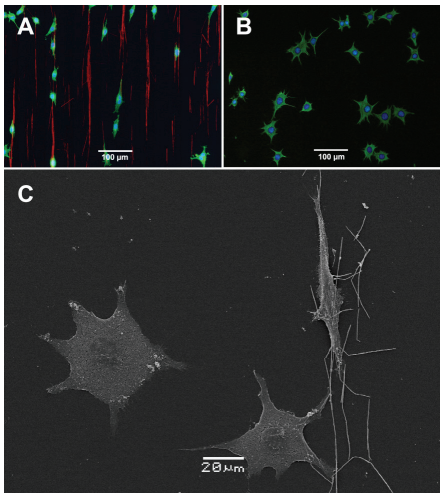

Fig. 3. The images shows L929 fibroblasts cultured on both the nanowire-coated cover slips and smooth plastic control surfaces. **A.** The L929 fibroblasts display contact guidance on the aligned Ni nanowires, and becomes elongated along the wires. **B.** The control cells show no alignment. **C.** The SEM image show fibroblasts both on nanowires and on the smooth glass surface. Note the different morphologies.

This difference was also clear from the polar diagrams where the direction of the fibroblasts coincides nicely with the direction of the aligned nanowires, while the direction of the control cells was more isotropic (Fig. 4). Furthermore, there were more round cells, *i.e.* cells with a major/minor axis ratio <1,5, on the control surfaces than on the nano-coated surfaces, 25% and 48% respectively.

3.3. DRG axon alignment

Regenerating axons from DRG neurons also displayed contact guidance, although the axons often changed nanowire in a wandering fashion. Each single axon may change wire or even ignore to grow along a wire, in a seemingly random outgrowth process (Fig. 5). Even though the contact

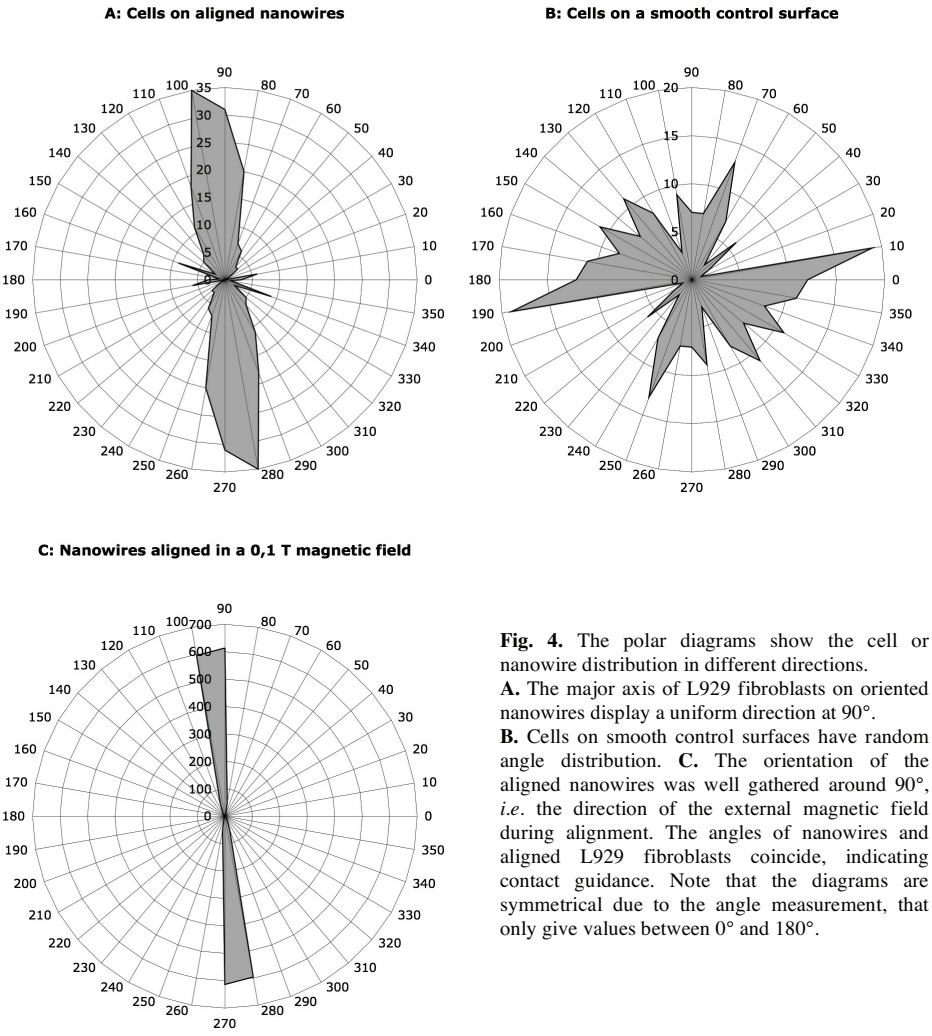

Fig. 4. The polar diagrams show the cell or nanowire distribution in different directions. **A.** The major axis of L929 fibroblasts on oriented nanowires display a uniform direction at 90°. **B.** Cells on smooth control surfaces have random angle distribution. **C.** The orientation of the aligned nanowires was well gathered around 90°, *i.e*. the direction of the external magnetic field during alignment. The angles of nanowires and aligned L929 fibroblasts coincide, indicating contact guidance. Note that the diagrams are symmetrical due to the angle measurement, that only give values between 0° and 180°.

guidance cue from a single nanowire may be questioned, the overall guiding effect is obvious from the images. This supports our previous study on axonal guidance induced by grooves and ridges, where a wandering outgrowth of axons still displayed a high degree of overall guidance (13).

4. Discussion

Previous studies have demonstrated that magnetic Ni nanowires can be used to manipulate cells. After nanowire internalization by phagocytosis, the cells can be moved by external magnetic fields (1-3, 9, 10). Here, for the first time, we demonstrate contact guidance of whole cells (fibroblasts) and cell extensions (DRG axons) induced by aligned magnetic Ni nanowires. Guidance of cells by externally controlled structures could find applications in many different fields, *e.g*.

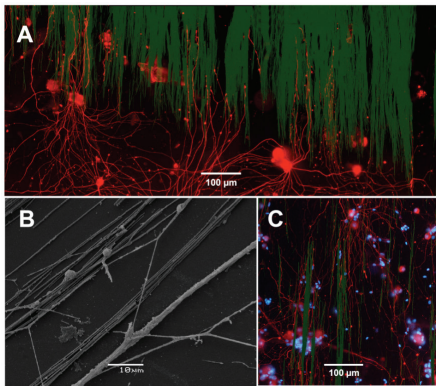

Fig. 5. The images show regenerating axons from dissociated DRG neurons interacting with the aligned nanowires. **A.** The guidance of axons was somewhat less than that found for the L929 fibroblasts, and most clearly detected when an excess of nanowires forming large aggregates, was available. (Fluorescence image: neurons are red, nanowires faint green). Note the randomly growing axons outside the nanowire-coated area. **B.** This SEM image shows axons growing along the nanowires for a while, and their deflection in another direction. At areas with low concentrations of nanowires, the axons often change wire to grow along, as if the guiding cue of one wire is too weak to establish sufficient contact guidance. **C.** This overview of axons on aligned nanowires at low concentration shows that even if the axons occasionally change wire to grow along, the total arrangement display typical contact guidance. (Fluorescence image: neurons are red, nanowires faint green and nuclei blue).

"lab on a chip" devices, medical nerve grafts or for the construction of tissue or organ like structures *in vitro*, including neuronal networks. Furthermore, the possibility to combine different metals along the wire, *e.g*. Au-Ni-Au, and also chemically functionalize the different parts of the wire, makes magnetic nanowires highly interesting for further nanobiotechnology applications (3, 5, 7).

In this study, the contact guidance due to a single wire was obvious in the L929 fibroblast cultures. The axons in the DRG neuronal culture showed a wandering outgrowth from one wire to another, suggesting that more powerful guidance cues (more wires) are needed to induce good guidance. It has been shown that repetitive, symmetrical nanopatterns induce weaker cell adhesion than do single structures (21), an interesting finding that may be related to contact guidance phenomena.

To develop cell-guiding patterns, the alignment of the wires may be improved and alignment parameters have been extensively studied (20, 22). The alignment may be affected by the liquid flow during evaporation, where the drag force exceeds the magnetic force of the external field. Furthermore, an excess of nanowires results in aggregation due to magnetic interactions among the wires, resulting in alignment disturbances. The introduction of micro magnet arrays (5, 10) may facilitate the production of complicated guiding patterns in real time without any predetermined lithographic patterning. This would enable a more dynamic way of testing guidance phenomenon *in vitro* and would be valuable for the production of neuronal networks and cell patterns.

Ni at a high concentration is toxic to cells, and there could be a release of Ni in the culture medium, something that may be crucial for the viability of the cell culture. However, in cell separation studies, using similar wires as here, Hultgren *et al*. found no signs of toxicity for NIH-3T3 mouse fibroblast cultured for 3 days (1, 3). In MC3T3-E1 osteoblasts and marrow stromal cells, Prina-Mello *et al*. reported changes in organelle responses but the viability of the cells was not significantly compromised by the internalization of the Ni nanowires (9). Furthermore, Schedle *et al*. found a dose dependent inhibition of ^{3}H-thymidine incorporation into L-929 fibroblasts when they were exposed to different metal cations. For L-929 fibroblasts, Ni^{2+} was found to affect proliferation less than Au^{3+}, Cu^{2+} and Co^{2+} (an alternative ferromagnetic metal), but more than Zn^{2+}, Pd^{2+} or Cr^{2+} (23). It is also

speculated that insoluble Ni, internalized by phagocytosis may be mutagenic (24). The issue of toxicity must be addressed, but for long time studies, covering the wires with inert biocompatible materials, *e.g*. polymers, may control the release of Ni. Additionally, functionalization with molecules, such as laminin, may also enhance both the biocompatibility and the guiding properties of the nanowires. This would improve the performance of the wires, without affecting their magnetic properties.

We have demonstrated that Ni nanowires that are attached to a surface, induce contact guidance for both fibroblasts and axons. The molecular mechanism by which this occurs remains to be elucidated. However, contact guidance involves rearrangement of focal adhesion points and cytoskeleton elements (25, 26). It has been reported that cells internalize free Ni nanowires via an integrin-mediated phagocytosis (3). Since integrins are involved in both axonal outgrowth and cell adhesion to surfaces, an interesting possibility is that the alignment of the fibroblasts and axons are due to their attempts to phagocytose the firmly attached nanowires. This could be an important guidance mechanism that to our knowledge has not been previously suggested.

5. Conclusion

The present study showed that aligned magnetic Ni nanowires induce contact guidance both for single migrating cells (L-929 fibroblasts) and outgrowing axons from dorsal root ganglion neurons. The construction of patterned substrates for the control of cellular growth opens a new avenue of medical and biotechnological applications for magnetic nanowires.

6. Acknowledgements

This work was supported by the Swedish Research Council. Thanks are due to Inger Antonson for her technical assistance. Thanks are also due to Waldemar Hällström and PhD Per Gustavsson for their valuable input to the study.

7. References

1. Hultgren A, Tanase M, Chen CS, Meyer GJ, Reich DH. Cell manipulation using magnetic nanowires. Journal of Applied Physics 2003;93(10):7554-7556.
2. Hultgren A, Tanase M, Chen CS, Reich DH. High-yield cell separations using magnetic nanowires. Ieee Transactions on Magnetics 2004;40(4):2988-2990.
3. Hultgren A, Tanase M, Felton EJ, Bhadriraju K, Salem AK, Chen CS, et al. Optimization of yield in magnetic cell separations using nickel nanowires of different lengths. Biotechnol Prog 2005;21(2):509-15.
4. Jain TK, Richey J, Strand M, Leslie-Pelecky DL, Flask CA, Labhasetwar V. Magnetic nanoparticles with dual functional properties: Drug delivery and magnetic resonance imaging. Biomaterials 2008;29(29):4012-21.
5. Reich DH, Tanase M, Hultgren A, Bauer LA, Chen CS, Meyer GJ. Biological applications of multifunctional magnetic nanowires (invited). Journal of Applied Physics 2003;93(10):7275-7280.
6. Hernandez-Velez M. Nanowires and 1D arrays fabrication: An overview. Thin Solid Films 2006;495(1-2):51-63.
7. Kim S, Shuford KL, Bok HM, Kim SK, Park S. Intraparticle surface plasmon coupling in quasi-one-dimensional nanostructures. Nano Lett 2008;8(3):800-4.
8. Martin CR. Nanomaterials: A Membrane-Based Synthetic Approach. Science 1994;266(5193):1961-1966.
9. Prina-Mello A, Diao Z, Coey JM. Internalization of ferromagnetic nanowires by different living cells. J Nanobiotechnology 2006;4:9.
10. Tanase M, Felton EJ, Gray DS, Hultgren A, Chen CS, Reich DH. Assembly of multicellular constructs and microarrays of

cells using magnetic nanowires. Lab Chip 2005;5(6):598-605.
11. Gustavsson P, Johansson F, Kanje M, Wallman L, Linsmeier CE. Neurite guidance on protein micropatterns generated by a piezoelectric microdispenser. Biomaterials 2007;28(6):1141-51.
12. Flemming RG, Murphy CJ, Abrams GA, Goodman SL, Nealey PF. Effects of synthetic micro- and nano-structured surfaces on cell behavior. Biomaterials 1999;20(6):573-88.
13. Johansson F, Carlberg P, Danielsen N, Montelius L, Kanje M. Axonal outgrowth on nano-imprinted patterns. Biomaterials 2006;27(8):1251-8.
14. Clark P, Connolly P, Curtis AS, Dow JA, Wilkinson CD. Topographical control of cell behaviour. I. Simple step cues. Development 1987;99(3):439-48.
15. Badami AS, Kreke MR, Thompson MS, Riffle JS, Goldstein AS. Effect of fiber diameter on spreading, proliferation, and differentiation of osteoblastic cells on electrospun poly(lactic acid) substrates. Biomaterials 2006;27(4):596-606.
16. Smeal RM, Rabbitt R, Biran R, Tresco PA. Substrate curvature influences the direction of nerve outgrowth. Ann Biomed Eng 2005;33(3):376-82.
17. Prinz C, Hallstrom W, Martensson T, Samuelson L, Montelius L, Kanje M. Axonal guidance on patterned free-standing nanowire surfaces. Nanotechnology 2008;19(34):-.
18. Bentley AK, Farhoud M, Ellis AB, Lisensky GC, Nickel AML, Crone WC. Template synthesis and magnetic manipulation of nickel nanowires. Journal of Chemical Education 2005;82(5):765-768.
19. Lindwall C, Dahlin L, Lundborg G, Kanje M. Inhibition of c-Jun phosphorylation reduces axonal outgrowth of adult rat nodose ganglia and dorsal root ganglia sensory neurons. Mol Cell Neurosci 2004;27(3):267-79.
20. Hangarter CM, Rheem Y, Yoo B, Yang EH, Myung NV. Hierarchical magnetic assembly of nanowires. Nanotechnology 2007;18(20):-.
21. Curtis AS, Casey B, Gallagher JO, Pasqui D, Wood MA, Wilkinson CD. Substratum nanotopography and the adhesion of biological cells. Are symmetry or regularity of nanotopography important? Biophys Chem 2001;94(3):275-83.
22. Hangarter CM, Myung NV. Magnetic alignment of nanowires. Chemistry of Materials 2005;17(6):1320-1324.
23. Schedle A, Samorapoompichit P, Rausch-Fan XH, Franz A, Fureder W, Sperr WR, et al. Response of L-929 fibroblasts, human gingival fibroblasts, and human tissue mast cells to various metal cations. J Dent Res 1995;74(8):1513-20.
24. Kasprzak KS, Sunderman FW, Jr., Salnikow K. Nickel carcinogenesis. Mutat Res 2003;533(1-2):67-97.
25. Oakley C, Brunette DM. The sequence of alignment of microtubules, focal contacts and actin filaments in fibroblasts spreading on smooth and grooved titanium substrata. J Cell Sci 1993;106 (Pt 1):343-54.
26. Wojciak-Stothard B, Curtis AS, Monaghan W, McGrath M, Sommer I, Wilkinson CD. Role of the cytoskeleton in the reaction of fibroblasts to multiple grooved substrata. Cell Motil Cytoskeleton 1995;31(2):147-58.

III

Nanowire induced activation of macrophages

Martin Kanje[a*], Waldemar Hällström[b], Lars Montelius[b] and Fredrik Johansson[a]

[a] Department of Cell and Organism Biology, Lund University Lund, Sweden
[b] Department of Solid State Physics, Lund Univeristy Lund, Sweden
* Corresponding author
E-mail address: Martin.Kanje@cob.lu.se

Abstract
Resident intraperitoneal macrophages from mouse in explant cultures were exposed to nanowires made of nickel, gold and polystyrene, or gallium phosphide (GaP). The former wires had a diameter of around 200 nm and lengths from 5-60 µm. The GaP wires had a diameter of 50 nm and an approximate length of 2.5 µm.
All types of nanowires activated the explanted macrophages as visualised by changes in morphology and/or an increased expression of binding sites for the plant lectin IB4. However, the degree of activation was different. Ni wires were the most potent. The macrophages tried to engulf the wires and some perished in these attempt reducing the number of macrophages in the exposed cultures and increasing the number cells which accumulated propidium iodide. Plastic wires had no effect on cell death
Injections of the nanowires intraperitoneally increased the number of macrophages, which could be harvested from the animals three days later, a classical sign of activation. The results show that large aspect ratio nanostructures like nanowires cause activation of an inflammatory response both *in vitro* and *in vivo* but the response is dependent on the type of nanowires used.

Key words: Macrophages, nanowires, macrophage activation, gold, nickel, gallium-phosphide, and health hazard.

1. Introduction

Concerns have been expressed with respect to the possibility that nanoparticles and nanostructures may be toxic [1-3]. We are constantly exposed to such particles if we live in an urban environment since these particles arise from vehicle brakes, tyres etc. Indeed, humans have been exposed to nanoparticles during the course of evolution since such particles are formed as a result of volcanic activity [4,5]. It is reasonable therefore to assume that we have developed mechanisms to deal with such particles at least with particles with low aspects ratios, that is particles where the diameter is comparable to the length of the particle. Today nanoparticles with very large aspects ratios including nanowires and nanotubes can be produced in a variety of materials. Since some of these are size wise and structurally similar to asbestos-like needles, a known inflammatory agent and carcinogen [6,7], the question can be raised if these large aspect ratio nanoparticles may pose a treat if inhaled or injected in the body. This question is important considering that attempts are made to construct nanobots that is nano sized robots which should be used to target cancer cells or make repairs at the cellular level possible. There are but a few studies concerning nanomaterials and how they interfere with cells and few has concerned

inflammatory cells like macrophages [8,9]. Macrophages are one of the first lines of defence in the body. These inflammatory cells are derived from monocytes and belongs to the white blood cells and the innate immune system. Macrophages attack foreign bodies and bacteria. They do so by recognizing the surface of foreign body sometimes after opsonisation *i.e.* the binding of certain proteins to the surface of the foreign material [10]. This triggers the macrophages, which destroys bacteria by engulfment and the release of free radicals. If the material cannot be engulfed the macrophages stimulate processes which leads to the encapsulation of the foreign body (for review see Adams [11]). Exposure to asbestos leads inflammation activation of macrophages and the encapsulation of the needle like asbestos structures in the lung tissue.

In the present study we investigated if nanowires made of different materials including polystyrene and metals interfered with intraperitoneal macrophages from mouse and if these structures could activate the macrophages and perhaps kill them.

2. Materials and methods

2.1 Intraperitoneal macrophages *in vitro*

Resident peritoneal macrophages were obtained from NMRI mice weighing around 30 g or a green fluorescent protein labelled mice (GFP mice).
The animals were anaesthetised and decapitated. Then a portion of phosphate buffered saline (PBS) was injected intraperitoneally. Following belly massage during 2 min intraperiotoneal fluid was withdrawn with a syringe. Approximately 1.5 ml could be obtained. The sample was centrifuged for 10 min at 1300 g. The cell-containing pellet was resuspended in 1 ml ice-cold erythrocyte lysis buffer (NH_4Cl 8.3 g/l, $NaHCO_3$ 0.84 g/l and EDTA 29.3 mg/l, pH 7.4) for 5 min. The samples were then centrifuged and washed twice in serum free medium RPMI 1640, 1 ml each time. The sample was resuspended in 1 ml medium and counted in a haemocytometer. For most experiments the samples were the diluted to around 1.5-1 million cells/ml. Samples of this cell suspension (200 µl) was seeded onto 18mm x18 mm glass cover slips (Menzel Gläser, Germany) in plastic Petri dishes. For time-lapse confocal microscopy, 200 µl cell suspension was seeded into plastic Petri dishes with around glass window in the bottom. After two hours non-adherent cells were removed by washing in PBS. Finally 2 ml of RPMI 1640 containing 2 % fetal calf serum was added. The cultures were maintained at 37 ^{o}C in a humidified atmosphere of 6.5 % CO_2 in oxygen.

2.2. Nanowires *in vitro*

After various periods of time usually after over-night culturing, portions of nanowires (20 µl) maintained in PBS at a concentration of around 10^9 wires/ml were then added to the cultures. After an additional 24 h incubation period,
propidium iodide (PI) exclusion was used to assay cell death. PI, which can only enter into cells with a leaky cell membrane, dissolved in PBS was added to a final concentration of 5 µg/ml medium. After 10 minutes the cultures were washed and the cover slips with the macrophages photographed in a fluorescence microscope. PI positive cells were regarded as dead. Their number was determined on the digital photographs taken at randomly selected areas of the cover slips and expressed in percent of the total cell number of cells.

2.3. Nanowires *In vivo*

A total of 12 female NMRI mice (Taconic, Denmark) were used. Each mouse received 10^9 nanowires of either Ni, Au, plastic or no nanowires in PBS as an i.p. injection. Three days later macrophages were prepared from the animals as described above. Cell numbers were determined in a

haemacytometer and macrophage cultures prepared from the lavage.

2.4. Nanowire production

Anodisc filters (Whatman) 200 nm were used as template for nanowire production [12,13]. The polystyrene nanowires were produced essentially as described by Xu et al. 2007 [13]. In short, around 0.5 ml polystyrene Mw=100000 (Alfa Aesar, Germany) dissolved in xylol (5g/15 ml in xylol) was mixed with 40 µl of a DiI solution comprised of a few DiI crystals that had been dissolved in 40 µl xylol. Two drops of this fluorescent polystyrene mixture was put on an objective slide. An Anodisc filter was placed atop of the fluorescent polystyrene. The filter was then covered with the blue filter protection paper and another glass objective slide. Office clamps were used to compress the preparation which was then put into a deaerated exicator over night. The preparation was dismounted and dried in air until there was no smell of xylol. The filter was then dissolved away in 3 M NaOH for 60 minutes, thus leaving densely packed PS nanowires. The plastic wires was washed in water, sprayed with ethanol and allowed to dry. The plastic nanowires were then scraped from the PS into a solution of 3% Triton X in water and the wires were separated by sonication. The wires were then pelleted by centrifugation washed in water and finally diluted in 1 ml sterile PBS. In this manner fluorescently labelled PS nanowires were obtained.

The nickel and gold nanowires were produced by electrodeposition. To this end, one side of the Anopore filter was covered with Gallium/Indium eutectic. The filter was then mounted on a piece of copper clad PCB board. Onto which a thin layer of nickel had been deposited, the filter was attached to the board using an inverted (piston removed) insulin syringe and two office clamps. Electro-deposition was performed in a solution of 1 M $NiCl_2$, pH 1 at 1.5 V for various periods of time using a nickel anode. The filter was then removed treated for a short period in nitric acid to dissolve the eutectic and subsequently dissolved in 3 M NaOH as described. The nickel wires were assembled using a magnet, washed in water, sterilised in ethanol and finally resuspended in 1 ml sterile PBS. The length of the nanowires could be controlled by variation of the electrodeposition time. The gold nanowires were also produced by electro-deposition, using a solution of $HAuCl_4$ 0.02 M and 1 M NaCl in a 1:3 v/v mixture, pH 1.5 and a carbon anode. There was a much larger spread in nanowires length for the gold nanowires that for the more homogenous Ni nanowires. The GaP nanowires were produced by epitaxy as previously described [14].

2.5. Microscopy

2.5.1. Scanning Electron microscopy

A sample of the nanowire suspension was centrifuged and the pelleted nanowires resuspended in ethanol. A drop of this suspension was then applied to a SEM-holder. The preparation was then sputtered with gold/palladium and observed in a scanning electron microscope (SEM). The macrophages for SEM studies were fixed in 4 % paraformaldehyde, washed in PBS, dehydrated in a series of ethanol, critical point dried and sputtered in gold/palladium.

2.5.2. Confocal microscopy

Green fluorescent macrophages from GFP mice and the red fluorescent (DiI) labelled nanowires were used in some experiments and but also GFP labelled macrophages and non-fluorescent metal nanowires.

2.5.3. Phase contrast microscopy

Routine observations and determinations of cell numbers were made in a phase contrast microscope to which a digital camera (Olympus D50, Japan) was attached. The cover slips were photographed and the number of cells

determined on the photographs. These numbers were recalculated and expressed as number of cells/cm^2.

2.6. Immunocytochemistry

The cultured macrophages were fixed for one hour in 4% paraformaldehyde in PBS, washed in PBS and then subjected to staining with either antibodies to F4/80 or with the lectin, IB4.

The F4/80 antibody (Serotech, Sweden) was used at a at a dilution of 1/200 in PBS containing serum albumin and Triton X after over night incubation at 4°C followed by washing the cultures ere treated with a secondary Alexa labelled anti rat antibody (Invitrogen, Sweden) at a dilution of 1/50. The cultures were washed and mounted in PBS/glycerol 1:1. Cover slips for lectin staining were incubated in biotin labelled IB4 followed by Alexa labelled avidin. The nuclei of the cells were stained by the inclusion of bisbenzimide in the final washing solution. The labelled cultures were photographed in an Olympus fluorescence microscope. The free software Image J was used for determination of the total cell area staining for IB4 respectively and also the total nuclear area.

3. Results

3.1. Nanowire properties

Figure 1 is a SEM picture of the different nanowires used. The nanowires produced in the aluminium oxide filters had a diameter of around 200 nm. The length of

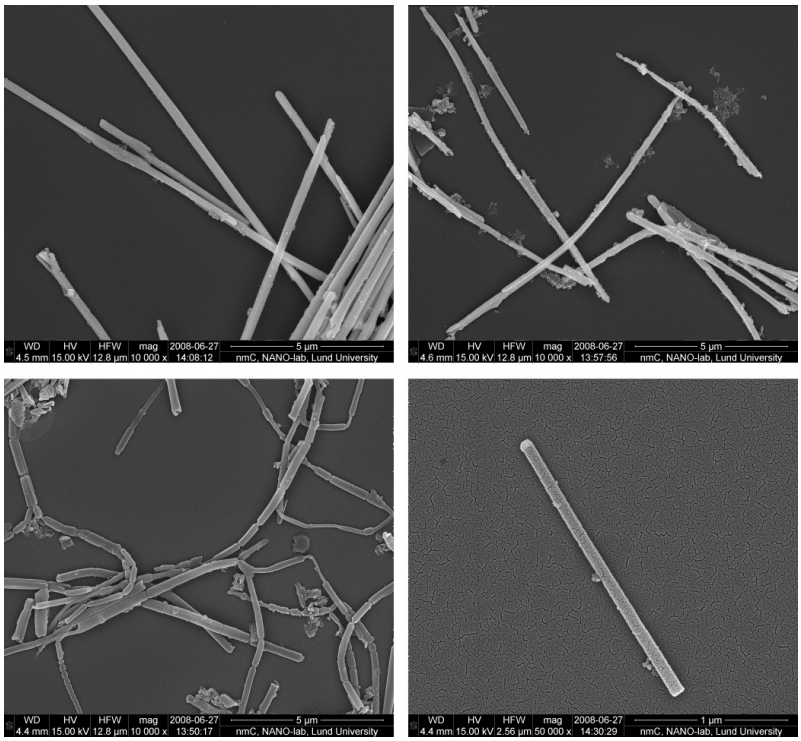

Figure 1 Scanning electron micrograph the nanowires. *Upper left,* Ni wires, *upper right* Au-wires, *lower left,* polystyrene (PS) wires, *lower right,* GaP wires. Note that the GaP wires are shown at a higher magnification. The deformability of the PS wires is obvious.

the metal wires were proportional to the time used for their production. The nickel nanowires produced at 1.5 V for 1 h were around 40 μm long. These wires were also magnetic and did, when diluted, align along the earth's magnetic field (not shown). In denser solutions, they formed larger aggregates. The gold nanowires had a size distribution different from the nickel nanowires. These wires had length between 5-40 μm and they were difficult to produce with as a narrow size distribution as that obtained for Ni-wires. The polystyrene nanowires were more flexible and bendable then both the GaP and the metallic wire perhaps not only because the plastic is softer but also because kinks could be observed on these wires. The flexibility of the plastic nanowires could be observed as the effect of molecular collision (Brownian movement) in the light and fluorescence microscope. The maximal length of the plastic wires was roughly equal to the thickness the Anopore filter (60μm). The GaP nanowires which were produced by epitaxi were shorter or around 2.5 μm and had a diameter of around 50 nm. The aspect ratio (diameter/length) of such wires was 1 to 50 while the plastic and metallic could have an aspect ratio up to 1 to 300.

3.2. Macrophage cultures

Around 90% of the seeded cells that had attached to the glass cover slips after 2h expressed the macrophage marker F4/80 (not shown). At this time point, most of the attached cells (around 75%, see Table V had a round morphology with a large nucleus, a typical monocytes/macrophage morphology (Fig 2.). At 24 h the attached cells had a spindle shaped morphology mostly with two processes. The number of cellular processes increased with time in culture. The number of cells decreased with time in culture so that at 48 h approximately 52 % of the cells that were attached at 2h were still on the cover slip (Table I)

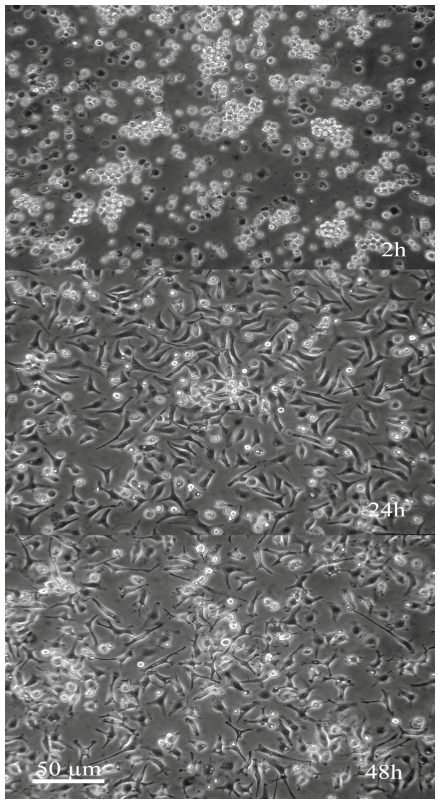

Figure 2 *Mouse macrophages in culture at various periods of time. Photograph of intraperitoneal mouse macrophages as they appear in the phase contrast microscope 2 h (upper-), 24 h (middle-) and 48 h (lower panel) after seeding onto a glass cover slip. Note how the cells spread on the surface and attain a flattened morphology with processes. Scale bar= 50μm.*

3.3. Nanowire addition *in vitro*

After 24 h, the cells in cultures were exposed to nanowires. They then underwent dramatic morphological changes. After a short while many of the cells exhibited extensive vacuolisation. The cells also aggregated around the nanowires and tried to engulf them. This was true for all types of wires. Internalized plastic nanowires are depicted in figure 3. With time there was a decrease in the number of cells in the nanowire treated cultures but significant changes was only

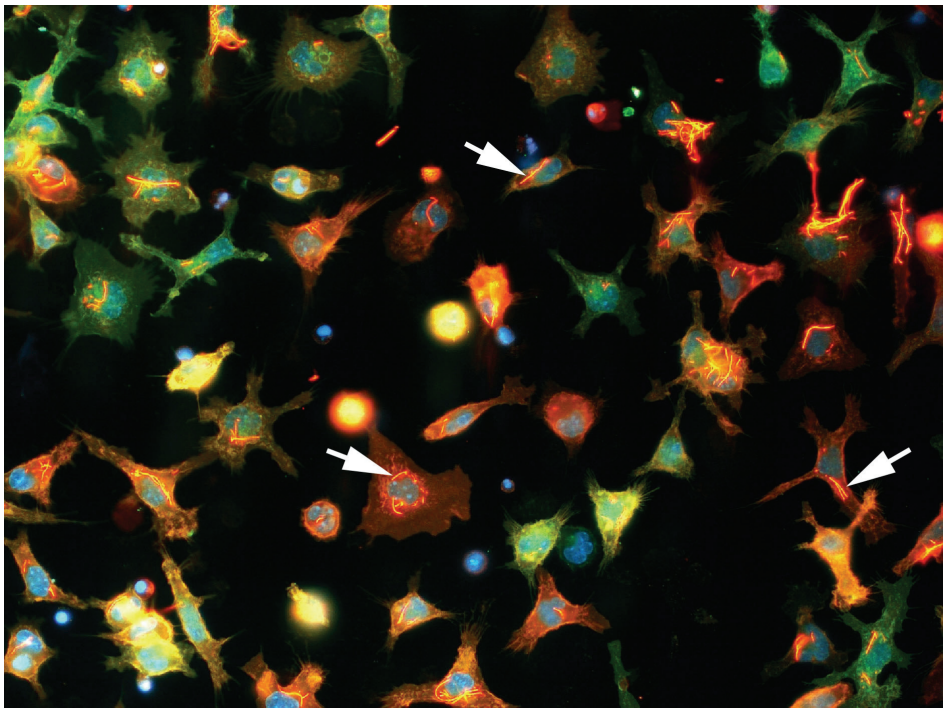

Figure 3. Cells exposed to plastic DiI labelled nanowires. Green IB4 staining, red F4/80, blue bisbenzimide. Fragments of nanowires (yellowish red) are seen within several macrophages (arrows). Macrophages recovered from animals injected with nanowires also contained phagocytosed wires (not shown).

observed in the cultures exposed to Ni and GaP nanowires during the first 24 h (Table II). Addition of all but the plastic nanowires however increased cell death as visualised by propidium iodide staining (Table III). Ni nanowires was the most efficient increasing the number of PI positive cells by 22 %.

Confocal microscopy was used to further study the interaction of the macrophages with the nanowires. In these experiments we first utilised GFP labelled cells and DiI labelled plastic nanowires and time lapse filming. These experiments revealed that the macrophages rapidly attacked the nanowires. Within minutes the cells had started to engulf the wires and shorter nanowires fragments could be observed within the cells.

Similar results were observed when metallic nanowires were used together with GFP labelled macrophages (Fig. 4 and Fig. 5). The stacks slices of the cells obtained with the confocal microscope clearly showed that the wires and part of wires were inside the macrophages.

Fig. 6a and b shows a SEM picture of macrophages, which have engulfed nanowires of plastic and nickel respectively.

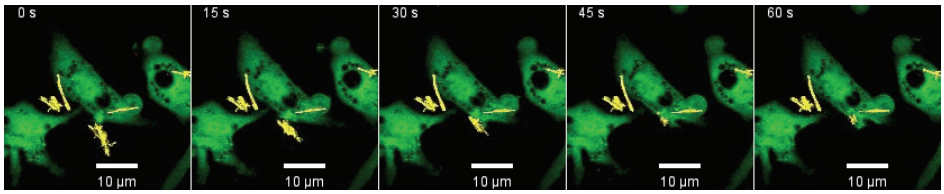

Figure 4. Confocal images from a time series show phagocytosis of gold nanowires as a function of time. The pictures show how nanowires of gold (yellow) are engulfed by a macrophage (green). The wires are engulfed within a 60 s period.

3.4. Macrophage activation

Activated macrophages differ from resident ones in several aspects including the expression of surface markers and morphology. Furthermore, if for instance bacteria is injected intraperitoneally the number of macrophages increase in the lavage.

To test if the nanowires induce macrophage activation *in vivo* we injected suspension of wires intraperitoneally in mice. Three days later macrophages were prepared from these animals. Table IV and Table V shows the results of these experiments.

First the number of cells that could be recovered from the animals had increased in animals injected with plastic gold and nickel nanowires.

Second the number of cells that attached to a glass slide had increased significantly in animals injected with all types of nanowires. Thirdly there was a dramatic change in morphology of the isolated cells, 2 h after plating cells from unprovoked animals mostly had a round morphology and relatively few cells (25%) had spread on the glass surface similar to results observed when macrophages were prepared from naïve animals. The number

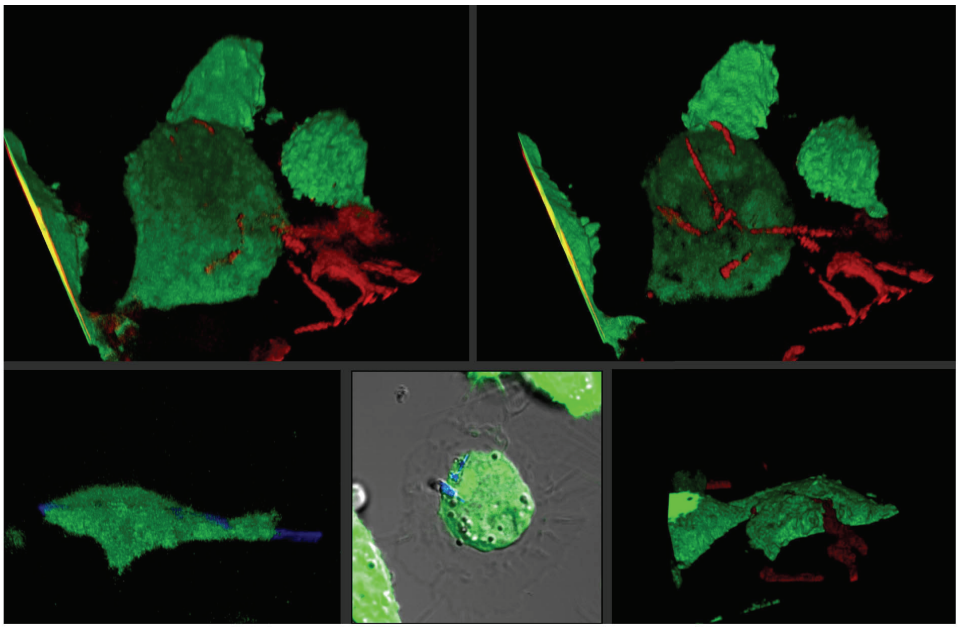

Figure 5. Confocal microscopy, Z-stack showing internalized nanowires of Ni, upper panel and Au, lower panel. As focused is shifted into a plane inside the cells the entire nanowires become visible.

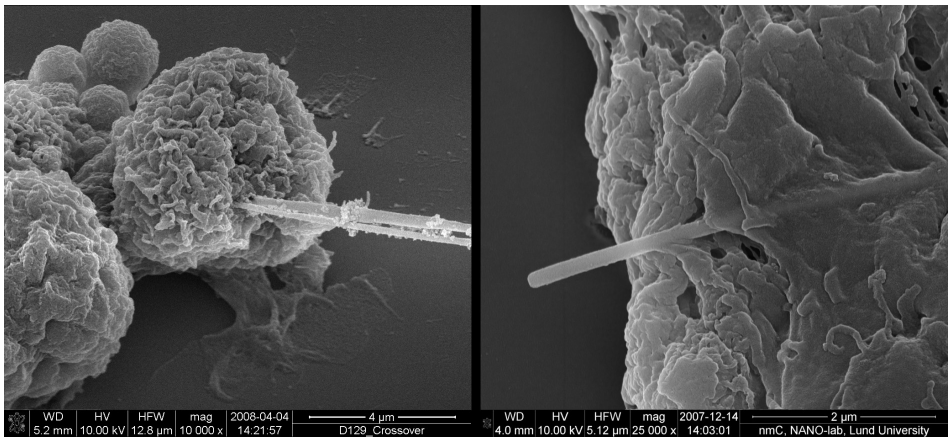

Figure 6. Scanning electron micrograph of macrophages that have engulfed nanowires. *Left,* Ni nanowires protruding from a macrophage. *Right,* polystyrene nanowire partially covered by the macrophage membrane.

of spread cells increased in preparations recovered from animals injected with nanowires even those injected with plastic nanowires Table V.

Immuno-reactivity for IB4 expressed in percent of the total number of cells is shown in Table VI. These numbers had increased in cells from animals injected with gold and nickel nanowires where as the increase observed in animals injected with plastic nanowires was not significant.

Many macrophages isolated from animals injected 3 days earlier with macrophages contained DiI labelled polystyrene nanowires in the cytoplasm. Fewer cells were associated wit the larger nickel wires but the number of cells containing Au nanowires were in between those of nickel and plastic (not shown).

Taken together the macrophages obtained from animals injected with nanowires exhibited classical signs of macrophage activation.

4. Discussion

The main finding in this paper was that nanowires induced activation of macrophages both *in vivo* and *in vitro*. In essence this is not surprising considering that the wires must be regarded as foreign bodies to the innate immune system to which the macrophages belongs [15].

The degree of "activation" was however different. Polystyrene nanowires for instance failed to increase the number of PI positive cells (dead cells) after short term exposure (24h) but it increased the number of macrophages that could be recovered in the lavage 3 days after an i.p. injection in a manner similar to that observed after injection of metallic nanowires. Plastic nanowires, as the metallic ones, also increased the number of cells that spread on a glass surface, another classical sign of macrophage activation.

There are several points which merits discussion in this study, one is the production of the nanowires, and another main point is the way by which activation of the macrophages occurs by the different

nanowires, a third point is if this type of activation may pose a health hazard.

The nickel, gold and plastic nanowires were all made by template assisted synthesis using aluminium oxide filters This is a convenient way of producing massive amount of wires [12,13]. Here, we also introduced a way to make plastic wires visible in the fluorescence microscope by introducing a fluorescent label into the plastic. This feature makes it easy to trace the fate of the nanowires both *in vitro* and *in vivo e.g.* a property, which should prove useful for studies of the distribution of wires inside the animal. Visibility is no problem when metallic wires are used. We also produced nickel nanowires. They are interesting because they are magnetic and they can be manipulated in a variety of ways by external magnetic fields. We have utilised this property to orient nickel nanowires in culture dishes and they act as guides for regenerating nerve fibres (Johansson *et al*. in preparation). A drawback with Ni is that it may be toxic should Ni ions be released. Ni is also an allergen. We therefore used gold nanowires also assuming that these could be more tissue compatible and more inert than the nickel nanowires. Indeed, this appeared to be the case. The Au wires were less efficient as activators of the macrophage. It is conceivable that plastics or glass could be used as a cover to protect wires made of less inert materials than gold should such materials be considered for use in bioimplants.

The nickel nanowires were the most effective in activation of the macrophages. They were also the ones which increased cell death most effectively. It is likely that part of this could be explained if some nickel ions are released from the wires. If this occurs inside the macrophages for instance by lyzosomal activity or if it occurs normally in the medium is not clear. We favour the former explanation since neurons appears not to be affected by high concentrations of guiding nanowires (Johansson *et al*. in preparation). Neurons were also less active in trying to phagocytise the wires in these experiments. Still, the release of metal ions per se cannot be the only cause of macrophage activation since activation occurred also after exposure to plastic nanowires. Which then are the important characteristics responsible for activation of these cells of the innate immune system? *In vivo*, the immune system reacts to the foreign surfaces by covering them with proteins, opsonisation. The surface chemistry and physical properties like topography, charge, elasticity and aspect ratios are factors that needs to be considered when macrophage activation is discussed in this context.

We assume that the stiffness and the aspect ratios could be important. Our finding that the flexible soft plastic nanowires appeared to be less efficient as activators lend support to this assumption. They had no effect on the expression of IB4 and did not induce cell death [16].

After i.p. injections we found that the macrophages that were removed from the animals 3 days later still contained the plastic nanowires and smaller metallic wires they had engulfed.

The wires are thus not easily destroyed and it could be that they could sustain an inflammatory response for extended periods of time. This is an unwanted feature which is exhibited by asbestos fibres [6,7] which are comparable in size the wires we have used in this study. The asbestos fibres provoke macrophages in the lungs and after prolonged exposure this can led to serious health problems. Many countries have also banned the use of asbestos. We have no evidence that the wires used in this study could have similar effects and be a health hazard but their structure and effect on macrophages suggest that attention should be focused on this issue considering the rapid expansion of nanowire use in industry.

5. References

[1] J. W. Card, D. C. Zeldin, J. C. Bonner, and E. R. Nestmann, Am J Physiol Lung Cell Mol Physiol **295,** L400-11 (2008).

[2] Y. Ju-Nam and J. R. Lead, Sci Total Environ (2008).

[3] A. Kroll, M. H. Pillukat, D. Hahn, and J. Schnekenburger, Eur J Pharm Biopharm (2008).

[4] T. R. Martin, G. Ayars, J. Butler, and L. C. Altman, Am Rev Respir Dis **130,** 778-82 (1984).

[5] T. R. Martin, A. P. Wehner, and J. Butler, Am Rev Respir Dis **128,** 158-62 (1983).

[6] L. Greillier and P. Astoul, Respiration **76,** 1-15 (2008).

[7] A. Haegens, A. van der Vliet, K. J. Butnor, N. Heintz, D. Taatjes, D. Hemenway, P. Vacek, B. A. Freeman, S. L. Hazen, M. L. Brennan, and B. T. Mossman, Cancer Res **65,** 9670-7 (2005).

[8] S. Hirano, S. Kanno, and A. Furuyama, Toxicol Appl Pharmacol (2008).

[9] C. A. Poland, R. Duffin, I. Kinloch, A. Maynard, W. A. Wallace, A. Seaton, V. Stone, S. Brown, W. Macnee, and K. Donaldson, Nat Nanotechnol **3,** 423-8 (2008).

[10] D. E. Owens, 3rd and N. A. Peppas, Int J Pharm **307,** 93-102 (2006).

[11] D. O. Adams and T. A. Hamilton, Annu Rev Immunol **2,** 283-318 (1984).

[12] A. K. Bentley, M. Farhoud, G. C. Lisensky, A. B. Ellis, and W. C. Crone, Abstracts of Papers of the American Chemical Society **226,** U259-U259 (2003).

[13] J. H. Xu, M. Li, Y. Zhao, and Q. H. Lu, Colloids and Surfaces a-Physicochemical and Engineering Aspects **302,** 136-140 (2007).

[14] W. Hallstrom, T. Martensson, C. Prinz, P. Gustavsson, L. Montelius, L. Samuelson, and M. Kanje, Nano Lett **7,** 2960-5 (2007).

[15] C. Kantari, M. Pederzoli-Ribeil, and V. Witko-Sarsat, Contrib Microbiol **15,** 118-46 (2008).

[16] D. E. Maddox, S. Shibata, and I. J. Goldstein, Proc Natl Acad Sci U S A **79,** 166-70 (1982).

Tables

Table I CELLS ATTACHED TO THE COVER SLIP

Time (h)	Cells attached
2	100 ± 25 (27)
24	66 ± 17 (27)*
48	52 ± 15 (15)*

Mean value ± SD (N). Values are expressed in percent of the cell numbers attached at 2h (100%). * P<0.05 versus 2 h. Cell numbers were determined from photographs, using an inverted phase contrast microscope equipped with a digital camera.

Table II CELL REMAINING ON THE COVER SLIP

	Percent of cells attached at 2h
PBS (control)	75 ± 13
Polystyrene	65 ± 5
Au-nanowires	80 ± 4
Ni nanowires	55 ± 17*
GaP nanowires	60 ± 18*

Intraperitoneal macrophages cultured over night. Cell numbers were then determined. The same cultures were then exposed to nanowires to a final concentration of 105 wires/ml in PBS or only PBS. After another 24 h incubation the number of cells remaining on the cover slips was determined again and expressed in percent of the cell numbers at 24 h (100%). Values are Mean ± SD (N)* P< 0.05 as compared to the control.

Table III CELL DEATH AS MEASURED BY PROPIDIUM IODIDE

	Propidium iodide positive cells (%)
PBS (control)	18 ± 6 (20)
Polystyrene	20 ± 6 (12)
Au-nanowires	27 ± 5 (12)*
Ni nanowires	40 ± 12 (7)*
GaP nanowires	28 ± 11 (6)*

Intraperitoneal macrophages cultured over night on glass cover slips were exposed to nanowires to a final concentration of 10^7 wires/ml in PBS or only PBS for an additional 24 h. Then the number of cells permeable to propidium iodide (PI) was determined and expressed in percent of total number of cells. Men values ± SD * $P< 0.05$ as compared to the control.

Table IV CELL NUMBER IN LAVAGE

	Cell number (10^6) /ml
PBS (control)	2,2 ± 0,5 (9)
Polystyrene	3.0 ± 0.5 (6)*
Au-nanowires	3.7 ± 0.6 (3)*
Ni nanowires	4,9 ± 0,8 (6)*
GaP nanowires	-

Each animal received an i.p. injection of 109 nanowires. Three days later macrophages were prepared from a lavage and the number of cells determined. Experiments were performed pair wise each time with 3 nanowires injected animals and 3 PBS injected controls. Man value ±SD (N) * $P< 0.05$.

Table V FLATTENED CELLS AT 2h

	Percent of total number of attached cells
PBS (control)	25 ± 8 (10)
Polystyrene	43 ± 11 (8)*
Au-nanowires	44 ± 8 (3)*
Ni nanowires	69 ± 6 (8)*

The number of cells that had a flattened morphology (=did not fit into a circle) encompassing a non-attached cell attached to the cover slips was determined 2h after seeding from digital photographs of the cultures. Values are Mean ±SD (n). *P< 0.05 as compared to the control. The cultures were photographed at 40 x objective magnification highest resolution camera. Cells larger than a circle of 80 pixels were regarded as flattened.

Table VI PERCENT IB4 POSITIVE CELLS

	% IB4 positive cells
PBS (control)	21.1 ± 11.3
Polystyrene	24.7 ± 10.4
Au-nanowires	29.1 ± 10.7*
Ni nanowires	46.0 ± 12.7*

The number of cells that had stained positive for the plant lectin IB4 was expressed as percent of the total number of cells. Values are Mean ±SD (N). *P< 0.05 as compared to the control.

IV

phys. stat. sol. (c) **2**, No. 9, 3258–3262 (2005) / **DOI** 10.1002/pssc.200561135

Guidance of neurons on porous patterned silicon: is pore size important?

Fredrik Johansson[*1], **Martin Kanje**[1], **Cecilia Eriksson**[1], and **Lars Wallman**[2]

[1] Department of Cell and Organism Biology, Lund University, Lund, Sweden
[2] Department of Electrical Measurements, Lund University, Lund, Sweden

Received 26 January 2005, revised 27 January 2005, accepted 27 January 2005
Published online 9 June 2005

PACS 82.45.Vp, 87.68.+z

The paper studies the conditions optimum for the proliferation of neural cells at the surface of porous silicon. The results of this study show that the best results are ahieved with meso-porous silicon. Geometrical properties of the wafers are also important through charge distribution at mask edges, change of hydrophobicity, degree of oxidation, the release of adhesion proteins from regenerating axons, etc.

1 Introduction

The construction of a neuro-electronic junction, a neural interface, which could listen and talk to the nervous system represents a formidable challenge but has enormous potentials since such interfaces could be used to restore deficits in sensory and motor nerve functions including hearing, vision, sensation and mobility.

Such junction, which must be biocompatible, exhibit high spatial and temporal resolutions, are not available for implantation today. However, experimental silicon based neural chips with either metal electrodes or field effect transistors have been used to record neural activity in cell culture. Implantable devices have low resolution and uses metal electrodes mainly for stimulation e.g. pacemakers and cochlear implants.

The quality of the recorded signals from the chip electrodes depends critically on the connection between the neuron and the chip. It is therefore necessary to consider the surface properties of the chip and its electrodes. The nerve-chip contact area should be large, exhibit good seal resistance and be biocompatible. To this end, we speculated that porous silicon might be a suitable surface for good neuron-chip contact and that by virtue of its large surface area and topography, porous silicon could be used to guide outgrowth of nerve cell processes or even be used as an electrode for recordings of electrical activity from neurons or nerve cell processes.

The advantage of increased surface area can be utilised in several ways. For electrodes it is the increased capacitance at the nerve cell contact point, but the increased surface may also be used for binding of proteins that may support axonal outgrowth. This high binding capacity has been used in enzyme reactors [3]. Furthermore porous silicon also elicits less inflammatory response than planar silicon does after implantation [1] and porous silicon has been shown to increase adhesion and survival of cultured nerve cells [2].

These findings together with the fact that neural processes can be guided by topography [4] suggested to us that porous silicon could be used also for guidance of axonal outgrowth either to hot spots i.e. recording area on a chip or to selectively stimulate axonal outgrowth of different types of nerve fibres.

[*] Corresponding author: e-mail: Per_Fredrik.Johansson@cob.lu.se, Tel.: (+46) 46 222 93 54

The purpose of this work was two fold. First to develop techniques to produce porous silicon surfaces compatible with neural cells and their processes and secondly to test if such surfaces could be used to guide nerve cell processes, axons.

2 Material and methods

2.1 Silicon substrate for axonal outgrowth

We initially used silicon dioxide as etch mask for porous etching in a mixture of HF and DMF (Dimethylformamide) [5]. However we found that this porous etch method hampered axonal outgrowth. The etch method was thus modified. One 3" p-doped (1–20 Ωcm) <100> silicon wafer was cut in square pieces (18×18 mm^2). The silicon dies were anodized in a mixture of HF and DMF (1:1) with 5 mA/cm^2 during backside illumination. The dies were etched for 5 minutes. The first sample was fabricated according to above defined process and then put in water (MilliQ). The second sample was put in HF for 2 minutes directly after the anodisation, followed by water (MilliQ).

2.2 Silicon substrate for axonal guidance

An oxidized 3" <100> p-doped (1–20 Ωcm) silicon wafer was spin coated with positive photo resist (Shipley 1813SP15), soft baked in oven at 85 °C for 20 min, exposed, in contact mode, and then developed in Microposit 351. After blow-drying in N_2, the wafer was hard baked in oven at 120 °C for 30 min. To expose the silicon in the defined areas the wafer was submerged in buffered HF to remove SiO_2. After rinsing in water, the photo resist was removed in . The wafer was cut into dies, chips, for different treatment (pore size). Figure 1 shows the layout of the porous pattern, the black areas correspond to porous silicon and white areas to planar silicon

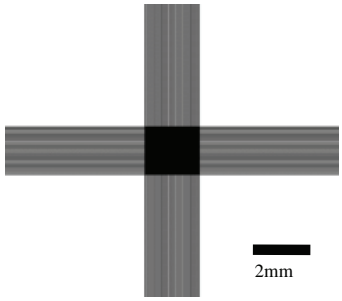

Table 1 Currents and times for the different chips.

Sample	A	B	C
Current (mA/cm^2)	50	20	5
Time (min)	3	5	7

Fig. 1 The porous patterned area had a cross-like shape with a porous square (black) in the center and porous lines departing from the square.

The chips were anodized in a mixture of HF and DMF (1:1) during illumination of the backside (the side with no defined pattern). Three different currents and three different times were used to create different pore sizes (Table 1). The chips were immediately submerged in HF for 5 min to etch away the SiO_2 formerly used as etch mask. After rinsing in water, the dies were stored in water (MilliQ) to avoid breaking of the pore walls and ensuring HF residues to diffuse from the pores.

2.3 Neural cultures

Dorsal root ganglia (DRG) from 3–5 weeks old mice were dissected. The silicon chips were sterilised in 70% ethanol and put in plastic cell culture dishes. The ganglia were attached to the silicon chips using Matrigel®. The ganglia were mounted and left a few minutes to dry (polymerize). Serum free RPMI 1640 medium was added and the dishes maintained in an incubator (with an atmosphere of 93.5% O_2 and 6.5% CO_2) for 7 days at 37 °C.

2.4 Immunocytochemistry

The cultures were fixed in Stefanini´s fixative for two hours (at room temperature) and then rinsed 3 times 5 minutes in phosphate buffered saline (PBS). To visualize axons, the cultures were incubated over night with a primary antibody against neurofilament, Rabbit NF 200 (Sigma, USA) diluted (1:200) in PBS containing 0.1% TritonX and 0.25% albumin. After rinsing in PBS 3 times 5 minutes, the preparations were treated with a fluorescent secondary antibody (goat-antirabbit Alexa 488 Molecular Probes, Eugene USA diluted 1:200 in PBS containing 0.1% TritonX and 0.25% albumin), for 35 minutes at room temperature. The cultures were washed, mounted in glycerol PBS 1:1 and photographed. A fluorescence microscope Olympus AX 70 with exciting wavelength of 488 nm (violet) was used. The camera connected to the microscope was an Olympus DP50.

2.5 Scanning electron microscopy (SEM)

For SEM the preparations were fixed in cacodylate fixative (2% paraformaldehyde, 2% glutaraldehyde 0.15 M Na cacodylate buffer pH 7.2) for two hours and rinsed in cacodylate buffer 3 times 5 minutes. The neurons were then dehydrated in a graded series of ethanol: 40%, 50%, 70%, 96% and abs. alcohol. Drying by the critical point procedure was done prior to sputtering with gold-platinum. The samples were then studied in the SEM (JEOL).

2.6 Evaluation of outgrowth

The SEM-pictures were analyzed every 200th micrometer (from 100 μm to 1500 μm), from the starting point of the etched pattern (Fig. 2). The number of axons on the smooth and porous surfaces was counted respectively at all distances. The percentage on smooth and porous surface was plotted against the distance (Fig. 6). The average distances from the ganglion to the axonal front edge and to the longest axons (Fig. 3) were estimated (±25 μm).

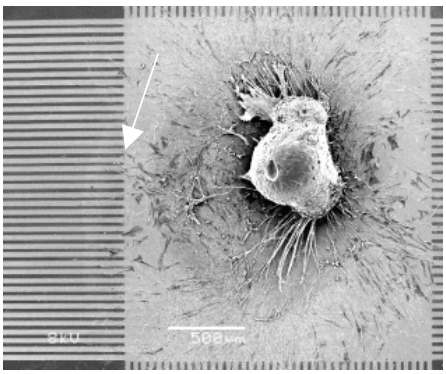

Fig. 2 This SEM picture shows a ganglion on the porous growth plate and the porous / smooth lines. The arrow indicates the ”starting point” of the pattern.

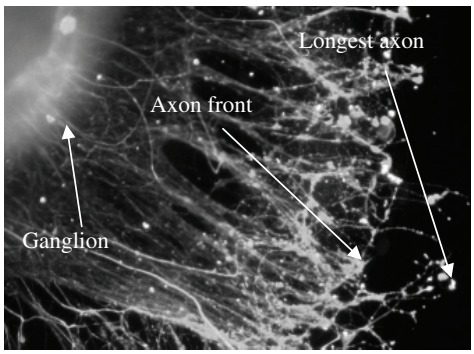

Fig. 3 Picture explaining the length measuring points.

3 Results

3.1 Axonal outgrowth on porous silicon; effects of different fabrication processes

In the first experiment the density and outgrowth distances were measured on Ethanol/HF and DMF/HF etched porous surfaces. When compared, the axonal outgrowth appeared inhibited on surfaces etched with DMF/HF, suggesting that this treatment gave toxic surface properties (not shown). By treating the

chip with HF immediately after the porous etch, the axonal outgrowth could be increased (Fig. 3). This method was then used for the rest of the experiment.

3.2 Axonal outgrowth on porous silicon; effects of pore size

Standard procedure was now: SiO_2 masking, porous etching in DMF/HF (1:1) and HF dip before storing the chips in distilled water for some days. Three pore sizes were achieved: 1–1.5 μm, 0.5–1 μm, and 300 nm (Fig. 4).

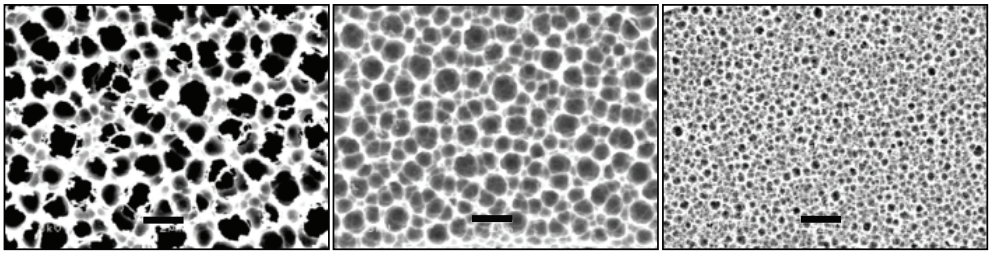

Fig. 4 SEM pictures of the three different porous silicon samples. Pore sizes from left to right: 1–1.5 μm, 0.5–1 μm, and 300 nm. Scale bars 2 μm.

For sample A and B (large pores) no difference in axonal outgrowth between porous and not porous areas could be observed. In contrast, a difference was observed on chips with smaller pores, sample C. Here a larger number of axons were found on the porous areas as compared to the planar areas. Figure 5 show SEM pictures of the axons on sample B and C. Figure 6 shows the quantification of axonal outgrowth on sample C (~0.3 μm pores). The percentage of total axons found on porous silicon is plotted against the distance from the starting point (Fig. 2).

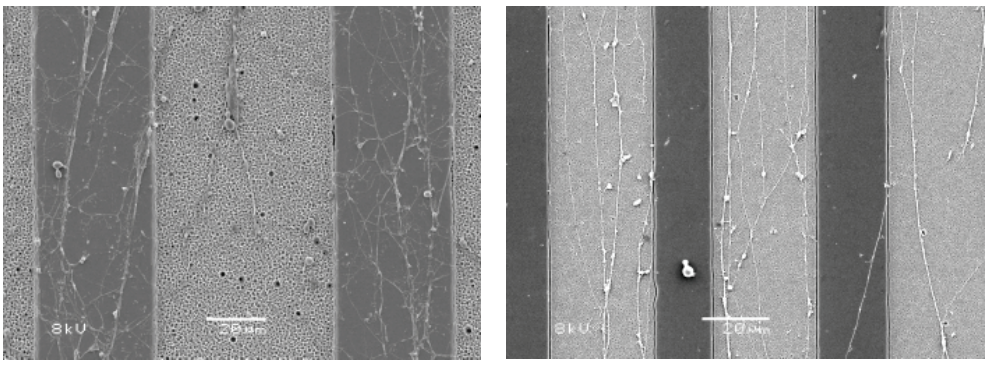

Fig. 5 Left picture shows the random outgrowth on large pore and planar silicon while the right picture shows the axonal preference for small pores (300 nm) over planar silicon.

4 Discussion

Ross G Harrison first demonstrated contact guidance 1911 and several studies have been made since then. Many of these studies shows that cells stay on edges of grooves or ridges. This behaviour may be a clue to why the adhesion of cells to porous silicon is higher than on planar silicon; porous silicon provides regenerating neural processes more edges, which may be preferential.

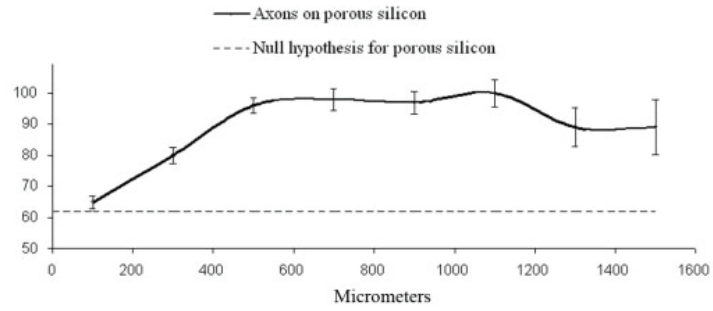

Fig. 6 The diagram shows that after 0.5 mm almost all axons are found on the porous areas.

The present study showed that organ cultured sensory neurons survive and extend their axons on porous silicon and that the porous patterns could be used to guide axonal outgrowth, however the etch method appeared critical. It was also pointed out and that the pore size was a critical parameter for the axonal outgrowth and guidance.

The use of DMF in the etchant makes it easy to mask with SiO_2 since the etchant affect the mask very slowly. This means that the etch time is not crucial and that the mask can be used in several steps i.e. making grooves before the porous etching. The backside of using DMF is the inhibition of axonal outgrowth found in our preliminary experiments. This can be avoided by treating the chip in HF immediately after the porous etch.

In this study the outgrowth and survival of axons on porous silicon with small pores (300 nm) were found to be good and supports previous studies [2]. The mechanism behind good adhesion and preference for porous silicon compared to planar silicon has not yet been explained. The results of this study also show that it is not just the roughness that matters, the geometrical properties are also important. Possible properties giving rise to these phenomena could be: the change from 2D to 3D, charge distribution at edges, change of hydrophobicity, degree of oxidation, the release of adhesion proteins from regenerating axons, the pore size compared to the cytoskeleton and the size of focal adhesions, more experiments are required.

The possibility to guide axons by porous Si opens the door to different Si techniques on the same chip. The less inflammatory response to porous Si also gives hope to the use of Si devices for implantation, even though the results in vitro seldom corresponds directly to in vivo applications. It is although notable that organ culture, like in this study, is a higher level of organisation than dissociated cells in culture.

Porous silicon has several qualities that would make it an excellent choice of material for neuroelectronic interfaces. The possibility to guide axonal outgrowth by patterning is yet another phenomenon in favour of porous silicon

Acknowledgements The study was supported by VINNOVA and the Øresund Academy.

References

[1] A. Rosengren et al., Biomedical Eng. IEEE **49**(4), 392-399 (2002).
[2] S.C. Bayliss et al., Sensors and Actuators A **74**(1-3), 139-142 (1999).
[3] J. Drott et al., JMME **7**, 14-23 (1997).
[4] A. Curtis et al., Biomater. **4**, 1573-1583 (1997).
[5] Izuo et al., Sensors and Actuators A **97/98**, 720-724 (2002).

V

Communications

The Influence of Porous Silicon on Axonal Outgrowth *in Vitro*

Fredrik Johansson, Martin Kanje, Cecilia Eriksson Linsmeier, and Lars Wallman

***Abstract*—Axonal outgrowth on smooth and porous silicon surfaces was studied in organ culture. The pore size of the silicon substrata varied between 100 and 1500 nm. We found that axons preferred to grow and elongate on porous silicon surfaces only when pores of (150–500 nm) are available.**

***Index Terms*—Axon, guidance, porous silicon.**

I. Introduction

Porous silicon (pSi) can be smoothly integrated with electronics and has been shown to be a promising biomaterial, e.g., it increases adhesion and survival of different types of cells, including neurons, to the silicon surface [1]–[4]. A recent work by Sapelkin *et al.* showed that the cell bodies of cells from an immortalized neuronal cell line, preferentially localized to areas of pSi (pore size: 50–100 nm) but not on the smooth Si when cultured on a partly stain etched porous silicon surface [4]. A preliminary study in our laboratory indicated that porous silicon could also be attractive for regenerating nerve cell processes, axons, and not only cell bodies [5]. Potentially, this haptotactic reaction can be used for axonal guidance, a feature that can be utilized in neuroelectric interfaces to guide axons to recording electrodes. When implanted in animals, pSi has been shown to evoke less inflammatory response than smooth Si or Ti [6]. Furthermore, the possibility to chemically modify pSi is a feature that has been explored for cell–surface interactions [7], enzyme reactors [8], and drug delivery systems [9].

Although the number of studies dealing with pSi and cell interaction is growing rapidly, studies on large (pore diameter > 50 nm) macro pSi and its influence on biological systems are rare, and the reaction of cells to these surfaces has not been fully explored. In the present study, we quantified the haptotactic effect of different pore sizes (diameters between 100 and 1500 nm) on axonal outgrowth. To this end, dorsal root ganglia (DRG) explants were cultured on alternating stripes of porous and smooth Si.

Manuscript received October 25, 2006; revised August 30, 2007. This work was supported by VINNOVA and the Øresund Academy. *Asterisk indicates corresponding author.*

*F. Johansson is with the Department of Cell and Organism Biology, Helgonavägen 3b, Lund University, 22362 Lund, Sweden. (e-mail: per_fredrik.johansson@cob.lu.se).

M. Kanje is with the Department of Cell and Organism Biology, Lund University, 22362 Lund, Sweden.

C. E. Linsmeier is with the Department of Cell and Organism Biology, Lund University, 22362 Lund, Sweden, and also with the Department of Experimental Medical Science, Lund University, 221 84 Lund, Sweden.

L. Wallman is with the Department of Electrical Measurements, 221 00 Lund, Sweden, and also with the Department of Experimental Medical Science, Lund University, 221 84 Lund, Sweden.

Digital Object Identifier 10.1109/TBME.2007.912423

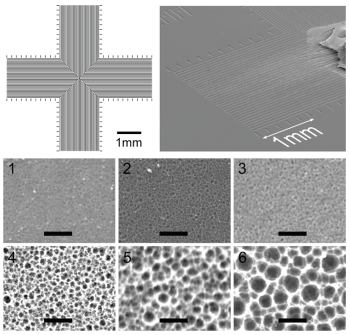

Fig. 1. Top left: Schematic view of the chip, the dark areas (lines) are made porous while the remaining white area is smooth bulk Si. Scale bar 1 mm. Top right: SEM image showing an overview of the pattern after culturing. Bottom: SEM images showing the pore size of the six different porous silicon samples used in this study. Scale bars 2 μm.

II. Materials and Methods

A. Patterning and Anodization of the Si Substrate

Oxidized 3-in $\langle 100 \rangle$ p-doped (1–20 Ω/cm) Si wafers were patterned using standard UV-lithography. The anodization was carried out with backside illumination in a two-chamber setup, containing mixtures of HF and dimethylformamide (Table I). The average pore size of the different silicon chips was estimated over the field of view, from randomly chosen scanning electron microscope (SEM) images (Fig. 1). Concentrated HF was used to remove the SiO_2 mask before thoroughly rinsing in Millipore water. The chips were stored in water for 24 h and sterilized in 70% ethanol before used.

B. Culturing of Dorsal Root Ganglia and Microscopy

The lumbar (L4-L6) DRG from adult female NMRI mice (B&K, Sweden) were dissected and placed in the center of the cross pattern, (Fig. 1). The cultures were incubated for 7 days under conditions described elsewhere [10] before preparation for SEM [12]. All animal-related procedures were conducted in accordance with local ethical guidelines and approved animal care protocols.

C. Quantifying Outgrowth

Three DRGs were cultured on three different patterns for each pore size ($N = 3$). All patterns were studied qualitatively and the pattern with the highest axon densities was chosen for quantification. From the SEM-pictures axons were counted every 200 μm outside the edge of the Matrigel (to assure axon contact with the substrate) to the end of the axonal outgrowth. At each distance, the number of axons on the smooth and the porous areas were counted and expressed as percent axons found on pSi areas. These values, normalized for surface area, are plotted in Fig. 3. A one tailed t-test was performed (using the software "Statview 5.0.1") comparing the initial distribution of axons with that of the mean of all the later distributions on each chip. In other words,

TABLE I
ETCHING PARAMETERS, RESULTING PORE SIZES AND STATISTICAL RESULTS AND AXONAL REACTION. NOTE THAT PORE SIZES BETWEEN APPROXIMATELY 150 TO 500 nm SIGNIFICANTLY ($p < 0,05$) ATTRACTED THE REGENERATING AXONS WHILE THE OTHER PORE SIZES DID NOT. *PERCENTAGE AXONS FOUND ON pSi AT THE FIRST AND THIRD MEASURING POINTS, RESPECTIVELY

Sample number	1	2	3	4	5	6
Etchant ratio HF/DMF	1:1	1:1	1:1	1:1	1:1	1:10
Current density (mA/cm^2)	2,5	5	7,5	10	20	2,5
Etch time (min)	2	2	2	2	2	20
Pore size, diameter (nm)	100	150	200	500	1000	1500
Change* during first 400 µm (%)	52,2-50,4	69,2-78,0	71,6-77,3	72,2-76,8	65,2-65,6	33,3-30,0
Axons significantly on pSi	no	yes	yes	yes	no	no

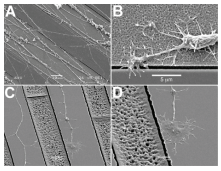

Fig. 2. A: Typical images for medium sized (150–500 nm) pores (sample 2). Bright areas are porous silicon while dark areas are smooth silicon. Note that most axons are found on the porous areas even though the axons may cross the smooth surface occasionally. B: This close up shows a large growth cone that senses the porous-smooth borderline with the well-developed filopodia, but remains on the porous area. Note the trench (due to edge effects during etching) at the borderline and the overall spiky appearance of the growth cone. C: On the largest pores the trend (although not significant) was that the axons grew onto the smooth areas, and followed them as can be seen in this picture. D: This image shows the growth cone from the left picture, sensing a trench and the porous area. Some height difference and edge effects of the etching are easily seen. Note the highly developed lamelopodium of the growth cone.

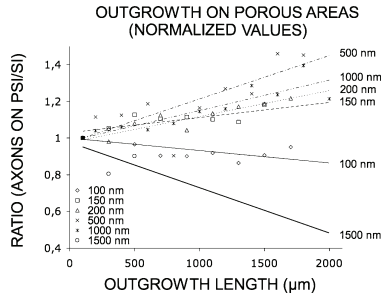

Fig. 3. Diagram shows regression lines for the six different pore sizes (denoted by their estimated average pore sizes). The slope indicate whether the axons grew onto the pSi, (positive slope), or onto the smooth Si (negative slope). Only the smallest and largest pores have negative slope, indicating that those pore sizes may act repellant to regenerating axons. Each point is based on 40–70 different areas (20–35 porous and smooth areas, respectively), resulting in 100–350 axons.

we tested if the distribution at the first point was different from the rest of the chip. $P < 0,05$ was considered significant. Table I shows values from this analysis and data for the first 400 μm of axonal outgrowth.

III. RESULTS AND DISCUSSION

The fabrication of the porous substrates is rather straight forward, using standard techniques that have good reproducibility, resulting in six different pore sizes (Fig. 1). Etching of porous lines, using a mask, resulted in deep trenches (previously described by Föll *et al.* [11]) at the borderlines between porous and smooth Si (visual as black lines in Fig. 2) and also a small difference in height. Axons were frequently found to cross these borderline artifacts; this is why we ignored the influence of contact guidance from these structures.

The results of axonal outgrowth on various chip surfaces are summarized in Table I and can be divided into three main groups due to the pore size and impact on axonal outgrowth.

A. Small Pores

Axons on the sample with the smallest average pore diameter (100–150 nm) showed no preference for any of the surfaces, i.e., the axons were nearly equally distributed between the porous and smooth surface (Fig. 3).

B. Medium Pores

Axons on samples with average pore diameter 150–500 nm showed a significant ($p < 0,05$) outgrowth preference for the porous areas as compared to the smooth areas (Fig. 2(a) and (b) and Fig. 3).

C. Large Pores

Axons on samples with average pore diameter $>$ 500 nm showed no significant preference for the porous areas, and for the largest pore size the trend was rather the opposite, i.e., the axons appeared to prefer to grow onto the smooth Si, and continued to grow on these areas (Fig. 2(c) and (d) and Fig. 3). The outgrowth on the chip with the largest pore sizes was also remarkably shorter than all the others substrates.

The mechanism responsible for the difference in haptotactic response is unknown and open to speculation. On large pore surfaces, there is less edge area available (as compared to surfaces with smaller pores) for protein adhesion (different physical-chemical properties) and therefore fewer axonal attachment points are present. The nonattractive response to the small pores may be due to the fact that these areas are geometrically considered as a flat surface by the regenerating axon. Also, even though a surface with small pores have more edges as compared to a surface with larger pores, this larger edge area may not be available. Large proteins in the same size range as the pores, e.g., laminin (approximately 50–100 nm) [12], may sterically prevent more than a few molecules to adsorb onto the edge of a small pore.

Growth cone morphology on pSi appeared to be different to smooth Si. On smooth Si, a large, highly developed lamellopodia could be seen, while growth cones on porous silicon exhibited a more spiky appearance, with more filopodia and less lamellopodia [Fig. 2(b) and (d)]. Fig. 2(b) also shows that the growth cones can detect and send micro spikes across the trenches at the borderlines between smooth and pSi.

It has previously been shown that cells prefer to grow on pSi (better viability) as compared to smooth Si [1]–[3], but the pore size influence has not been investigated in detail and the majority of studies are made on pores smaller than 150 nm. Interestingly, Sapelkin *et al.* [4] showed that cell bodies of the neuronal B50-cell line showed clear adhesion preference on porous (50–100 nm average pore size) areas as compared to smooth Si surfaces. Our study indicates that axons have no such selectivity in this pore size range. It may therefore be hypothesized that the mechanism that make cell bodies attach to surfaces in an acute adhesion phase differs from the way axons attach during regeneration. Furthermore, Karlsson [13] found a lower activation of adherent neutrophils on Al_2O_3 with 200-nm-wide pores as compared to 20-nm-wide pores, also indicating a lower optimal pore size for cell culturing.

For clinical applications, the pore size range may be revised for human axons since axon diameter may influence the results. In a recent study, we showed that nano-imprinted patterns could guide axons, but frequently, large axons were not guided, indicating an axon-diameter-dependent reaction to topographic cues [10]. For bio-implantation, pSi appears attractive. Axonal guidance and biocompatibility could be enhanced further by incorporate, e.g., growth factors on the surface. Due to the very large area/volume ratio of pSi, large amounts can be incorporated [14], improving neural survival and axonal sprouting. PSi is also suitable for other surface modifications that can promote cell viability and adhesion, although, cell reaction may change not only with surface topography/chemistry, but also with cell type [15]. Furthermore, the increased surface area of pSi makes it suitable as an electrode material with a large chip-cell contact area.

We finally conclude in this study that axons thrive on pSi and exhibit a haptotactic reaction within a certain range of 150–500 nm average pore diameter. This could be utilized to guide axons on chip surfaces.

ACKNOWLEDGMENT

The authors would like to thank I. Antonsson for expert technical assistance and Dr. A. Ressine, P. Gustavsson, and W. Hällström for their valuable discussions regarding pSi and axonal regeneration.

REFERENCES

[1] S. C. Bayliss, L. D. Buckberry, I. Fletcher, and M. J. Tobin, "The culture of neurons on silicon," *Sens. Actuators A*, vol. 74, pp. 139–142, 1999.

[2] S. C. Bayliss, L. D. Buckberry, P. J. Harris, and M. J. Tobin, "Nature of the silicon-animal cell interface," *J. Porous Mater.*, vol. 7, pp. 191–195, 2000.

[3] S. C. Bayliss, R. Heald, I. Fletcher, and L. D. Buckberry, "The culture of mammalian cells on nanostructured silicon," *Adv. Mater.*, vol. 11, no. 4, pp. 318–321, 1999.

[4] A. V. Sapelkin, S. C. Bayliss, B. Unal, and A. Charalambou, "Interaction of B50 rat hippocampal cells with stain-etched porous silicon," *Biomaterials*, vol. 27, pp. 842–846, 2006.

[5] F. Johansson, M. Kanje, C. Eriksson, and L. Wallman, "Guidance of neurons on porous patterned silicon: Is pore size important?," *Physica Status Solidi C*, vol. 9, pp. 3258–3262, 2005.

[6] A. Rosengren, L. Wallman, N. Danielsen, T. Laurell, and L. M. Bjursten, "Tissue reaction evoked by porous and plane surfaces made out of silicon and titanium," *IEEE Trans. Biomed. Eng.*, vol. 49, no. 4, pp. 392–399, Apr. 2002.

[7] A. Angelescu, I. Kleporous silicon, M. Mihaela, M. Simion, T. Neghina, S. Petrescu, N. Moldovan, C. Paduraru, and A. Raducanu, "Porous silicon matrix for applications in biology," *Rev. Adv. Mater. Sci.*, vol. 5, pp. 440–449, 2003.

[8] J. Drott, K. Lindström, L. Rosengren, and T. Laurell, "Porous silicon as the carrier matrix microstructured enzyme reactors yielding high enzyme activities," *J. Micromech. Microeng.*, vol. 7, pp. 14–23, 1997.

[9] L. T. Canham, R. S. Saffie, S. E. Connor, and R. Aston, *Silicon Technology and Pharmaceutics – An Impending Marriage in the Nanoworld*. London, U.K.: Drug Discovery World, 2001, pp. 56–63.

[10] F. Johansson, P. Carlberg, N. Danielsen, L. Montelius, and M. Kanje, "Axonal outgrowth on nano-imprinted patterns," *Biomaterials*, vol. 27, pp. 1251–1258, 2006.

[11] H. Föll, M. Christophersen, J. Carstensen, and G. Hasse, "Formation and application of porous silicon," *Mater. Sci. Eng.*, vol. 39, pp. 93–141, 2002.

[12] E. Engvall and U. M. Wewer, "Domains of laminin," *J. Cell. Biochem.*, vol. 61, pp. 493–501, 1996.

[13] M. Karlsson, A. Johansson, L. Tang, and M. Boman, "Nanoporous aluminium oxide affects neutrophil behaviour," *Microscopy Res. Tech.*, vol. 63, pp. 259–265, 2004.

[14] L. M. Karlsson, P. Tengvall, I. Lundström, and H. Arwin, "Penetration and loading of human serum albumin in porous silicon layers with different pore sizes and thicknesses," *J. Colloid Interface Sci.*, vol. 266, pp. 40–47, 2003.

[15] S. P. Low, K. A. Williams, L. T. Canham, and N. H. Voelcker, "Evaluation of mammalian cell adhesion on surface-modified porous silicon," *Biomaterials*, vol. 26, pp. 4538–4546, 2006.

VI

Porous silicon a potential electrode material in a nerve repair setting - tissue reactions

Fredrik Johansson [a,b]*, Lars Wallman [a,c], Nils Danielsson [a], Jens Schouenborg [a], Martin Kanje [a,b]

[a] Nano Neuro Research Center, BMC F10, Lund University, SE-22184
[b] Department of Cell and Organism Biology, Lund University, Helgonavägen 3b, SE-22362
[c] Department of Electrical Measurements, Lund University, Box 118, SE-221 00 *Corresponding author. Tel.: +46 46 2229354; fax: +46 46 2224539.
E-mail address: per_fredrik.johansson@cob.lu.se

Abstract
Here we compared porous silicon (pSi) with smooth Si as chip-implant surfaces in a nerve regeneration setting. Silicon chips can be used for recordings of neural activity and are potential nerve interface devices. A silicon chip with one smooth and one porous side inserted into a tube was used to bridge a 5 mm defect in the rat sciatic nerve. Six or twelve weeks later, new nerve structures surrounded by a perineurium like capsule had formed on each side of the chip. The number of regenerated nerve fibers did not differ on either side of the chip as shown by immunostaining for neurofilaments. However, the capsule that had formed in contact with the chip was significantly thinner on the porous side than on the smooth side. Cellular protrusions had formed on the pSi side and the regenerated nerve tissue was found to attach firmly to this surface, while the tissue did hardly attach to the smooth silicon surface. We conclude that a pSi surface, due to its large surface area, diminished inflammatory response and firm adhesion to the tissue, should be a good material for the development of new implantable electronic nerve devices.

Keywords: Silicon, Surface roughness, Nerve regeneration, Immune response, In vivo test.

1. Introduction

The biocompatibility of implanted electronic devices in the nervous system is a pivotal issue. Such devices must be non-toxic. They should also be physically stable and function during several years. An ideal implant should therefore not provoke extensive inflammatory reactions since this result in embedding and poor signal pick up.
Many soft materials e.g. hydrogels and biodegradable polymers, have good biocompatibility but are so far unsuitable as long-term electrodes due to electronic or physical short comings, including poor conductivity. The choice of electrode materials is therefore limited mainly to metals or semiconductors yielding stiff rigid implants, which may evoke a foreign body reaction. Many mechanisms are believed to trigger this reaction (1). One such mechanism is micro-movements, i.e. the implants are moving relative to the surrounding tissues, giving rise to shear forces (2). Shear forces are created due to the mobility of the organism i.e. breathing, heartbeat, walking etc. Micro-movements can be minimized by the design of the implant, avoiding unnecessary stretching forces, “untethered” implant (3) and by manipulating the surface of the implant

(chemically or physically) so that the tissue can integrate smoothly with the artificial material.

Surface modifications have been intensively studied for implants in both soft tissue (e.g. in the abdominal wall of different species), and hard tissue (e.g. dental implants and bone replacements). For implants in soft tissue both ordered (4) and random roughness (5, 6) have been studied. Porous materials have been shown to be superior to smooth surfaces both in vitro (7, 8) and in vivo (6, 9, 10) if the pores are within a certain size. In vivo, surface topography of 1 to 2 microns allow direct fibroblast attachment to the surface and has been shown to produce a minimal connective tissue response to the implant and prevent or diminish the presence of inflammatory cells at the implant/tissue interface. If the pores are larger than 3.3 μm, inflammatory cells can invade the pores, i.e. infiltrate the surface. Interestingly, the composition of the implant seems to be of secondary interest as compared to the surface structure (10). The change from bulk material to porous structure also changes the mechanical properties, i.e. the Young's modulus, resulting in a somewhat "softer" material (11).

For chronically implanted electrodes we have suggested that biocompatibility could be improved by nano/micro-modifications of the electrode surfaces (7). An increased surface area due to nanostructures may not only help to anchor the electrode in the tissue (and thereby minimize the micro movements), it may also improve signal recordings due to closer contact and larger contact area to the cells of interest.

We have previously demonstrated that nerve cell processes, emanating from regenerating organ cultured peripheral ganglia change haptotaxic response depending on the pore size of porous silicon (pSi) (7). PSi is manufactured by electrochemical etching and the pore size can be tuned from a few nanometers up to some micrometers (12). This flexibility in morphology and increase in surface area, together with the compatibility to standard micro electro mechanical system (MEMS) techniques from the silicon industry makes it a suitable, and affordable, candidate for long term implanted electrodes.

In this study, we investigated how regenerating peripheral nervous tissue react to an implant with a rough, pSi surface as compared to a smooth surface. The pore size was approximately 1 micrometer and the pSi chip was tested in a tube nerve repair setting (13). To this end, a rectangular silicon chip with one planar and one porous side was used inside the tube to bridge and repair a defect in the rat sciatic nerve.

2. Material and Methods

2.1. PSi chips

A Si 3" wafer (<100>, p-doped, 1-20 Ω/cm, Siltronix) was mounted with gaskets between two home-made Teflon chambers containing a mixture of a 1:1 (v/v) mixture hydrofluoric acid (HF) and dimethyl-formamide (DMF). One electrode was placed in each chamber and a 100 W lamp was positioned ten cm from the chip to illuminate the backside (enhancing the number of diffusible charge carriers i.e. electrons and holes) (figure 1).

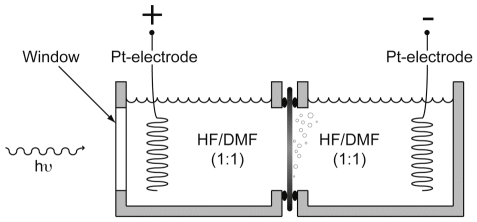

Fig. 1. Overview of the electrochemical etching set up. The two Teflon chambers are filled with HF/DMF (Dimethylformamide) etchant and the Si wafer is hold between the chambers by two gaskets. A window in one of the chambers allows backside illumination (for creating more charge carriers) and two Pt-electrodes provide the voltage needed for the etching to take place.

The etching time was 20 min at 10 mA/cm^2 and the average pore size was determined from scanning electron microscope images. After the electrochemical etching, the wafer was submerged in HF for 5 min to remove DMF residues that may have stuck to SiO_2. After extensive rinsing in distilled water, followed by ethanol, the wafer was dried under a flow of N_2 and diced into (2×5 mm) chips. The resulting chips were further rinsed in acetone and ethanol prior to implantation.

2.2. Implantation and dissection

All animal related procedures were approved by the Malmö/Lund Animal Ethics Committee on Animal Experiments. One pSi chip (5×2 mm) was placed in the center of a 9 mm long silicone tubes with an inner diameter of 2 mm. Thus, a two compartments chamber was obtained (figure 2 and 3). In this way a porous and a smooth silicon surface could be presented to the same regenerating nerve.

Female Sprague Dawley rats, weighing around 200 g (Taconic, Denmark) were anaesthetized by a 0.25 ml intraperitoneal injection of a mixture of sodium pentobarbital (60 mg/ml), diazepam (5 mg/ml) and 0.9% sodium chloride in a 1:2:1 volume proportion) and the sciatic nerve was exposed and cut. The cut ends of the nerve were inserted 2 mm into the silicone tube, in contact with the chip edges, and then secured to the tube by sutures (figure 2). The wound was closed using wound clips, and the rats (n=10) were left for 6 or 12 weeks before being killed by an i.p. injection of sodium pentobarbital (0.6 ml, 60 mg/ml), followed by heart puncture. As controls for activating transcription factor 3 (ATF3) (n=5) the nerve was repaired in a similar manner but without any pSi chip in the tube. The implants together with several mm of the nerve, distal and proximal to the silicone tube were dissected by cutting the sciatic nerve a few mm from the tube ends. Dorsal root ganglia (DRG) L4 and L5 were removed bilaterally.

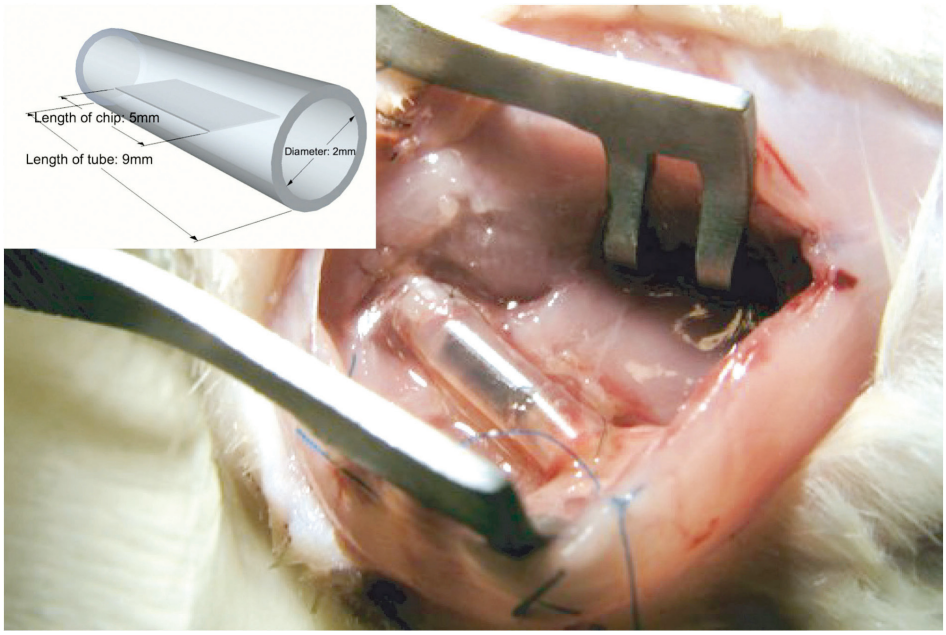

Fig. 2. Photograph showing the chip containing silicone tube during implantation on the sciatic nerve. Insert: The silicone tube was divided in two compartments by the silicon chip. The regenerating tissue could thereby grow on both side of the chip.

2.3. Immunohistochemistry

The dissected tubes and tissue were placed in Stefanini's fixative (2% formaldehyde and 15% of a saturated aqueous picric acid solution in 0.1 M phosphate-buffer, pH 7.2) for 2 h. The silicone tube was then carefully removed in order to facilitate the penetration of the fixative. The explants were washed 3x5 min in phosphate buffered saline (PBS) and the tissue was carefully separated from the chips to be able to sectioning the tissue. The free tissue was immersed in sucrose before sectioning (10 μm thick cross sections) in a cryostat (Leitz). The sections were washed 3x5 min in PBS before incubation with the primary antibodies (rabbit anti-tubulin III (Santa Cruz Biotech. Inc., USA) and anti-ED1 (Serotech Ltd., England) diluted 1:400 in PBS with 0.25% Triton-X and 0.25% bovine serum albumin (BSA)) over night in a refrigerator. The sections were washed and incubated with the secondary antibodies diluted 1:400 (Alexa goat-anti-rabbit (A11034) and goat-anti-mouse (A11029) Invitrogen Molecular Probes™) respectively for 2h in room temperature. The cell nuclei were counterstained with bisbenzimide (1 μg/ml). The sections were mounted in glycerol and PBS (1:1).

The dissected DRGs were fixed in Stefanini´s fixative, sectioned (10 μm) in a cryostat and immuno-stained for ATF3 using a rabbit anti-ATF3 antibody (Santa Cruz Biotech Inc. USA), diluted 1:400 followed by a secondary Alexa labeled antirabbit IGg antibody as above. The transcription factor ATF3 is up regulated in response to nerve injury (14, 15). All antibodies used in this study have been used previously in our lab, and the specificity have been tested and confirmed (14).

2.4. Electron microscopy

2.4.1. Scanning electron microscopy

After 6 or 12 weeks the pSi chips were fixed in 2.5% glutaraldehyde in 0.15 M sodium cacodylate buffer (pH 7.2, for 1h at room temperature), dehydrated in a series of alcohol (50%, 70%, 90%, 95% and 100% ethanol) and critical point dried (Bal-Tec CPD 030) before sputtering (~12nm thick layer) with gold/palladium. The porous structure with some remaining tissue (residues from chip-tissue separation) after the implantation was then studied in the scanning electron microscope (JEOL JSM-5600 LV).

2.4.2. Transmission electron microscopy

One explant (6 weeks) was fixed in 2% glutaraldehyde for 5h. After fixation, the tissue was separated from the chips as described above, post fixed in 2% osmiumtetroxide for 1h and thoroughly rinsing in cacodylate buffer. The tissue was dehydrated in a series of alcohol and finally in acetone. The tissue was embedded in resin, trimmed and finally sectioned on a microtome. The sections were mounted on copper grids and studied in the transmission electron microscope.

2.5. Image analysis

All quantitative image analyses were made on digital photographs from the fluorescently labeled, 10 μm thick sections, using the free software "ImageJ" for Mac OS X (http://rsb.info.nih.gov/ij/). For counting the cells within the DRGs, an automatic cell counter plug in (ICTN - http://rsb.info.nih.gov/ij/plugins/index.html #acq) was used.

2.5.1. Capsule thickness

The implant delineated by a capsule of fibroblast like cells, reminiscent of a perineurium, surrounded the tissue containing regenerating nerve cell processes, axons. The distance from the axon containing tissue, to the implant surface and tube, was considered a capsule. The thickness of this capsule was measured at three positions facing the chip and three positions facing the tube: in the center and 200 μm out from the center (figure 3).

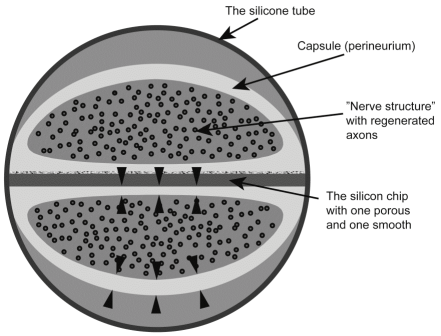

Fig. 3. The drawing shows the structures inside the tube after 6 weeks. The arrowheads indicate the positions of capsule measurements (at the two chip surfaces and towards the silicone tube). After 12 weeks the entire tubes were usually completely filled with tissue.

2.5.2. ED1 positive cells

The interface area defined as the area within 40 μm from the implant surface, were analyzed for ED1 positive cells (invading macrophages) by measuring the immuno-stained area. Cell structures with intensities five standard deviations above the background were considered positive. The immuno positive area was expressed in percent of the total analyzed area.

2.5.3. Percent nerve tissue

The immunostained tubulin area was used as a measure of the number of axons within the "endoneurium", i.e. the area surrounded by the tissue capsule. The immuno-stained, and total area was measured (using ImageJ) by manually outlining the "endoneurium". The percent axon containing tissue was then calculated.

2.5.4. ATF3 positive cells (regenerating marker)

The total number of nerve cells within the ganglion sections was measured semi automatically by the ICTN plug-in. The ATF3 positive cells, easily detected by their intensively green nuclei, were counted manually, and the percent positive cells were calculated (figure 4).

2.6. Statistics

Statistical validation of the measurements, were done using the software "Statview" for Macintosh. A two-tailed ANOVA was used to compare the tissue reaction to the two different surfaces exposed to the regenerated tissue and at the two different time points. P-values <0.05 were considered significant.

3. Results

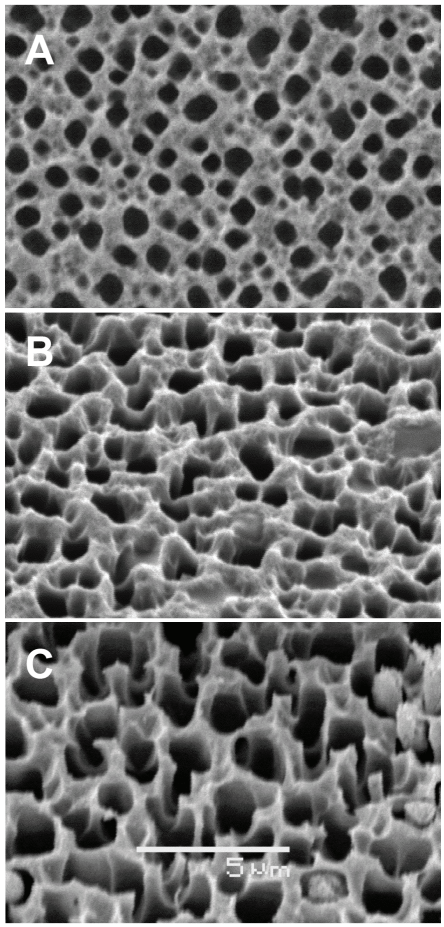

Fig. 4 A: top view of the porous surface before implantation, **B:** tilted view (30°) of the porous layer before implantation and **C:** tilted view (30°) of the explanted porous layer 12 weeks after implantation. Note the changed morphology of the surface.

3.1. PSi

Figure 4a shows the pSi surface, manufactured by electrochemical etching. This procedure resulted in an approximately 5μm thick surface layer with a spongy morphology and micrometer sized pores (figure 4b). The surface morphology of chips, implanted for 12 weeks, appeared slightly changed with somewhat sharper pore edges as compared to surfaces prior to implantation (figure 4c). The smooth surface showed no such changes (not shown).

3.2 Regenerated tissue on the implant

At six weeks, two nerve structures, containing both myelinated and unmyelinated axons, had formed inside the tube, one on each side of the chip and he chip was incorporated in the nerve. Figure 5a shows the nerve structure and the chip after 6 weeks of indwelling with the silicone tube still in place, and figure 5b shows it with the tube removed. In most cases, the tissue did not fill the tube, but rather formed a dome on the implanted chip surface (figure 3). The size (volume) of the regenerated tissue on the porous and smooth side of the chip differed in some cases due to misplacement of the cut nerve end during implantation (i.e. the nerve end had slid over mainly on one side of the implant). In the analysis, this was compensated for by calculating ratios (percent) of labeled cells out of the total number of cells found on each side.

The regenerated neuronal tissue was surrounded by fibroblast like cell layers, a perineurium like structure, here referred to as the capsule (figure 3). The whole structure looked like a normal nerve fascicle, although partly flat, with an endoneurium containing nerve fibers, Schwann cells and blood vessels (figure 5 c and d).

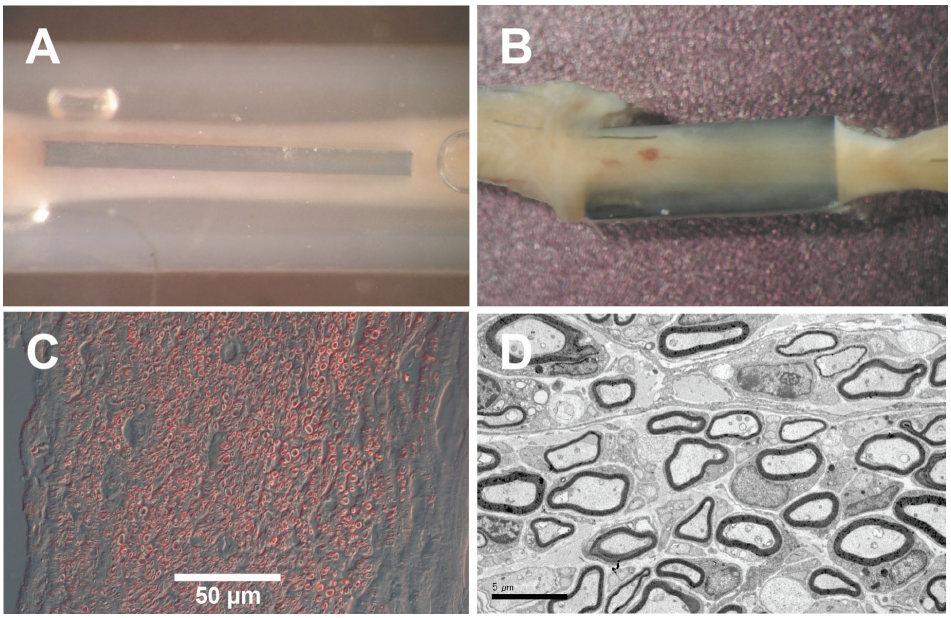

Fig. 5 A: The chip inside the silicone tube after 6 weeks. The regenerated tissue, including blood vessels are obvious on the chip surface. **B:** The chip without the silicone tube, note the remaining sutures that were used to secure the tube to the nerve. **C:** Phase contrast micrograph of a cross section reveals regenerated myelinated axons and blood vessels. **D:** This TEM picture shows both myelinated and unmyelinated axons with normal morphology.

After 12 weeks the chip structure was totally embedded in the nerve tissue and many tubes were filled with regenerated tissue. The overall morphology and cellular composition did not differ from the 6 weeks implants.

3.3. Good adhesion on pSi

The regenerated tissue attached strongly to the highly porous Si and protruded into the pores, demonstrating good surface interaction (figure 6) at both 6 and 12 weeks. On the smooth silicon side, the tissue had not attached strongly to the surface and could be removed after fixation with little resistance. After removal of the newly formed nerve tissue, the implant surfaces were studied in SEM and fluorescence microscope. On the smooth side few occasional cells were found, while on the porous side, a few patches some cell layers thick could be observed on the porous surface.

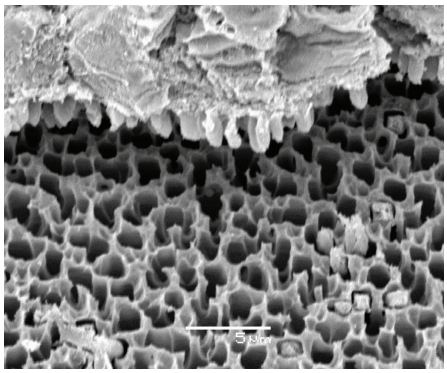

Fig. 6. SEM image. The tissue has adhered to the pSi and protruded into the pores resulting in a very firm attachment to the porous surface.

3.4. Capsule thickness

For both 6 and 12 weeks, the chip-facing capsule was significantly thinner at the porous surface as compared to the smooth surface. The thickness of the chip-facing capsule also decreased over time (from 6 to 12 weeks) for both the porous: from 27.8 μm to 20.5 μm and the smooth: 30.9 μm to 25.6 μm surfaces, although the change was only statistically significant ($p<0.05$) for the porous surface (figure 7a).

On the side facing the silicone tube (figure 3), the capsule was found to be significantly thicker than the corresponding capsule facing the implanted chip surface for both porous ($p<0.001$), and smooth ($p<0.01$) surfaces. Furthermore, the thickness of the tube-facing capsules decreased significantly over time on the smooth side of the chip, while on the porous side the thickness increased ($p<0.001$).

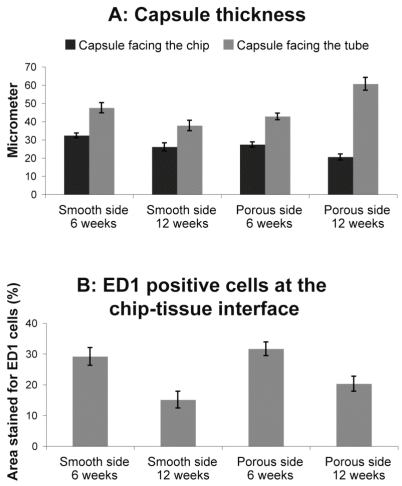

Fig. 7 A: Diagrams showing the capsule thickness at 6 and 12 weeks at different places. **B:** ED1 positive cells. The density of ED1 positive cells (immuno positive area) was the same on both side of the chip, and decreased over time. The values are presented as mean ± SEM.

3.5. ED1 positive cells

By immuno-staining for macrophages (ED1), a foreign body reaction was observed mainly within the 40μm thick interface layer. The percentage immuno-positive area, i.e. proportionally to the number of macrophages, decreased over time (from 6 to 12 weeks), but no significant difference between the porous and smooth side was found at any time (figure 7b). There were also macrophages outside the interface area, although to a much lesser extent (figure 8).

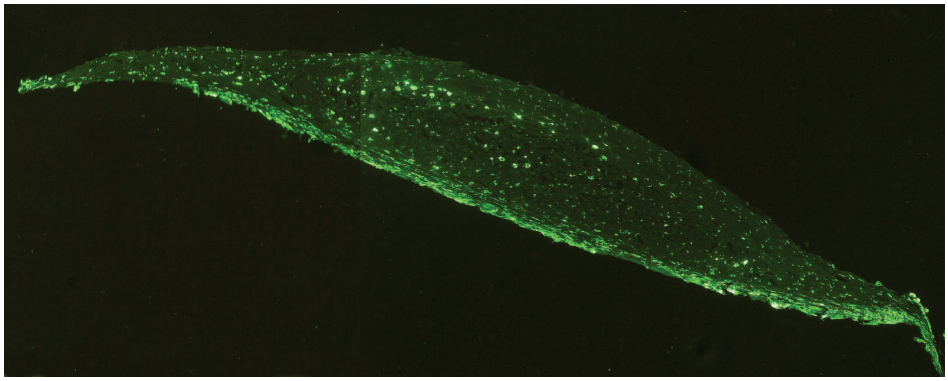

Fig. 8. Fluorescently labeled ED1 positive cells (invading macrophages) are concentrated to the chip-tissue interface, but are also present within the whole regenerated tissue, although at a lower density.

3.6. Nerve tissue

The nerve structures, i.e. the sectioned area containing β(III)-tubulin axons, occupied approximately equally large areas of the total tissue regarding both time points and implant side. The percent nerve tissue on the smooth Si at 6 weeks was 53,2% ±1,7, and at 12 weeks 59,4% ±4,2 as compared to the pSi with 59,4% ±1,7 and 54,9% ±2,3 respectively. There was no statistical difference.

3.7. ATF3 positive cells

The expression of a survival and regeneration related transcription factor (ATF3) was visualized in the cell bodies of the sensory neurons that had regenerated through the tube (figure 9). The percent ATF3 positive cells in sectioned DRGs did not differ regarding pSi implant, empty silicone tube controls, or time points (6 or 12 weeks).

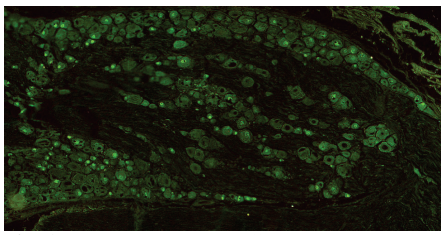

Fig. 9. ATF3 expressing cells in a DRG after 6 weeks are easily detected and quantified by immunohistochemistry.

4. Discussion

This is the first report describing a pSi chip in a nerve repair setting. PSi is, due to its large surface area, a new potential electrode material, but as we discuss below, it also has other properties, which may be advantageous for an implantable neuroelectronic interface.

After implantation on the sciatic nerve, we found that two new fascicles had formed in the tube divided by the silicon chip. The regenerated nerve structures on either side of the chip contained myelinated and unmyelinated axons, blood vessels and were surrounded by a perineurium. They were thus similar to the new nerve structure observed following entubulation repair (15, 16). Furthermore, the expression of ATF3, a survival indicator, was not different from that observed after repair of a transection nerve injury (15). Therefore the regeneration process as such does not seem to be affected by the implanted silicon chip, indicating that neither smooth nor pSi is neurotoxic.

There are several major aspects, which warrant discussion with respect to the possibility of using pSi for recording or stimulation of neural activity. One is embedding of the material or capsule thickness, which in turn is related to the

foreign body reaction and inflammation. A third interesting topic is the surface related properties of pSi including its support of axonal outgrowth in vitro (7), its electrode properties (17), its use for anchoring (this paper) and drug release (18).

It has been suggested that the capsule thickness around an implanted device is partly dependent on shear forces and the friction that arises due to movements of the organism (2). If the tissue can move along with the implant, shear and friction forces decrease and the capsule thickness would become less pronounced. In this study, the capsule was found to be thinner on the porous side of the chips as compared to the smooth side. This is a main finding since it means that pSi can be used to anchor an implant in the tissue, thus reducing micro movements and encapsulation. It is in accordance with studies where it has been shown that structured surfaces implanted under the skin evoke less inflammatory responses and encapsulation (9, 10). When comparing the capsule thickness at the silicone tube interface i.e. opposite to the chip surface, the one on the porous side of the chip was found to be thicker than the one on the smooth side. This difference could be due to the immobility of the nerve structure on the porous side (firm adhesion) as compared to the mobility of the nerve structure on the smooth side. The shear and friction forces may therefore be larger against the tube on the porous side than on the smooth side resulting in a thicker capsule. The idea of a relation between micro-movements and encapsulation is also in line with the finding that the thickness of the capsule facing the tube significantly increased over time (between 6 and 12 weeks) on the porous side of the chip. On the smooth side of the chip, the much lower adhesion resulted in a more “untethered” like situation. Our results suggest that it is favorable to use pSi for anchoring electrodes since it evokes less encapsulation which is an advantage when electrical recordings are considered.
As expected, the amount of inflammatory cells (ED1 positive) decreased over time. Such a decrease is also observed in other implant studies and is a typical development for a foreign body reaction (1). This reaction includes an acute inflammatory phase, with a large recruitment of macrophages, followed by an increased encapsulation and decreased number of inflammatory cells. Interestingly, the surface structure had no effect on the number of ED1 positive cells. There is therefore no simple correlation between the number of macrophages and the resulting capsule thickness.

The percent regenerated tissue occupied by axons did not significantly differ between smooth and porous surfaces or time points, demonstrating an even and isotropic growth, during the regeneration of the nerve. However, the area of the regenerated axons (i.e. number of axons) showed a trend that there are more axons relative to the total tissue area, on the porous side after 6 weeks than after 12 weeks and vice versa for the smooth side. One could speculate that initially the porous surface favors axonal outgrowth by its ability to promote adhesion and adhere more growth stimulatory proteins than smooth silicon. Later, the surface is hidden by the capsule yielding no advantage for the pSi over smooth Si resulting in an equal distribution of axons after prolonged periods.

PSi has, as mentioned, a large surface area which is suitable for electronics and the longitudinal arrangement of the chip in this study may also, allow stacking of chips within the tube creating good flexibility for electrode designs. PSi can also be utilized for the slow release of drugs (18). The possibility to integrate this feature on an electrode surface for anti-inflammatory drug release, in order to depress the acute

inflammatory response, is tempting to peruse, as suggested by Moxon (6).

We observed a slight change in the surface topography over time when the chips were examined in the SEM after indwelling. It has been found that pSi may degrade in the highly corrosive environment in vivo (19). However, the residues of the dissolved Si are harmless (19, 20), and therefore a slight dissolution of a pSi implant may be acceptable. Still, the long-term consequences this slight instability of the pSi surface at the nano level (18) warrants further investigations. Still, the combination of a large surface area and biocompatibility, make pSi an interesting candidate for implantable devices such as electrodes for the nervous system, where electronics and biocompatibility must work side by side. The present results show that Si is not toxic in a nerve repair setting. Furthermore pSi is superior to smooth silicon, since it promote anchoring and firm adhesion thereby forming both a better electrical and physically stable contact.

5. Conclusion

Nerve structures form on each side of an implanted Si chip having one porous and one smooth surface following entubulation nerve repair. At 6 and 12 weeks, the chips were encapsulated and there were no overt signs of abnormal tissue reaction or toxicity due to the Si chip. The nerve tissue interacted strongly with the pSi surface. The encapsulation was found to be less for the pSi as compared to both smooth Si and the surrounding silicone tube.
Our results suggest that the pSi surface is a suitable material for tissue integration. The nerve structure appears to attach firmly to the porous surface resulting in a very large contact area, a promising feature for further bioelectronic applications.

6. Acknowledgements

This work was supported by The Royal Physiographic Society in Lund, Knut and Alice Wallenberg foundation (project number: KAW 2004-0119) and a Linné grant (project number: 600012701) from the Swedish Research Counsil. Thanks are due to Marie Adler Maihofer and Rita Wallén for their technical assistance.

7. References

1. Rosengren A. Tissue reactions to biomaterials. PhD-thesis, Lund University 1997.
2. Picha GJ, Drake RF. Pillared-surface microstructure and soft-tissue implants: effect of implant site and fixation. J Biomed Mater Res 1996;30(3):305-12.
3. Biran R, Martin DC, Tresco PA. The brain tissue response to implanted silicon microelectrode arrays is increased when the device is tethered to the skull. J Biomed Mater Res A 2007;82(1):169-78.
4. den Braber ET, Ruijter, J.E. de, Jansen, J.A. The effect of a subcutaneous silicone rubber implant with shallow surface microgrooves on the surrounding tissues in rabbits. Journal of biomedical materials research 1997;37:539-547.
5. Parker JATC, Walboomers XF, Von Den Hoff JW, Maltha JC, Jansen JA. Soft-tissue response to silicone and poly-L-lactic acid implants with a periodic or random surface micropattern. Journal of Biomedical Materials Research 2002;61(1):91-98.
6. Moxon KA, Hallman S, Aslani A, Kalkhoran NM, Lelkes PI. Bioactive properties of nanostructured porous silicon for enhancing electrode to neuron interfaces. J Biomater Sci Polym Ed 2007;18(10):1263-81.
7. Johansson F, Kanje M, Linsmeier CE, Wallman L. The influence of porous silicon on axonal outgrowth in vitro. IEEE Trans Biomed Eng 2008;55(4):1447-9.
8. Bayliss SC, Buckberry LD, Harris PJ, Tobin M. Nature of the silicon-animal cell interface. Journal of Porous Materials 2000;7(1-3):191-195.
9. Rosengren A, Wallman L, Danielsen N, Laurell T, Bjursten LM. Tissue reactions evoked by porous and plane surfaces made

out of silicon and titanium. IEEE Trans Biomed Eng 2002;49(4):392-9.
10. Campbell CE, von Recum AF. Microtopography and soft tissue response. J Invest Surg 1989;2(1):51-74.
11. Bellet D, Lamagnere P, Vincent A, Brechet Y. Nanoindentation investigation of the Young's modulus of porous silicon. Journal of Applied Physics 1996;80(7):3772-3776.
12. Foll H, Christophersen M, Carstensen J, Hasse G. Formation and application of porous silicon. Materials Science & Engineering R-Reports 2002;39(4):93-141.
13. Zhao Q, Lundborg G, Danielsen N, Bjursten LM, Dahlin LB. Nerve regeneration in a 'pseudo-nerve' graft created in a silicone tube. Brain Res 1997;769(1):125-34.
14. Lindwall C, Dahlin L, Lundborg G, Kanje M. Inhibition of c-Jun phosphorylation reduces axonal outgrowth of adult rat nodose ganglia and dorsal root ganglia sensory neurons. Mol Cell Neurosci 2004;27(3):267-79.
15. Kataoka K, Kanje M, Dahlin LB. Induction of activating transcription factor 3 after different sciatic nerve injuries in adult rats. Scandinavian Journal of Plastic and Reconstructive Surgery and Hand Surgery 2007;41(4):158-166.
16. Danielsen N, Vahlsing HL, Manthorpe M, Varon S. A 2-Compartment Modification of the Silicone Chamber Model for Nerve Regeneration. Experimental Neurology 1988;99(3):622-635.
17. Persson J, Danielsen N, Wallman L. Porous silicon as a neural electrode material. J Biomater Sci Polym Ed 2007;18(10):1301-8.
18. Zhang K, Loong SL, Connor S, Yu SW, Tan SY, Ng RT, et al. Complete tumor response following intratumoral 32P BioSilicon on human hepatocellular and pancreatic carcinoma xenografts in nude mice. Clin Cancer Res 2005;11(20):7532-7.
19. Mayne AH, Bayliss SC, Barr P, Tobin M, Buckberry LD. Biologically interfaced porous silicon devices. Physica Status Solidi a-Applied Research 2000;182(1):505-513.
20. Reffitt DM, Jugdaohsingh R, Thompson RP, Powell JJ. Silicic acid: its gastrointestinal uptake and urinary excretion in man and effects on aluminium excretion. J Inorg Biochem 1999;76(2):141-7.